EXPERIMENTAL AND NUMERICAL INVESTIGATIONS OF CONTINUOUS COMPOSITE GIRDERS REINFORCED WITH CFRP

BY

MOHAMMAD ABDUL RAHMMAN SAMAANEH

A Dissertation Presented to the

DEANSHIP OF GRADUATE STUDIES

KING FAHD UNIVERSITY OF PETROLEUM & MINERALS

DHAHRAN, SAUDI ARABIA

In Partial Fulfillment of the
Requirements for the Degree of

DOCTOR OF PHILOSOPHY

In

CIVIL ENGINEERING

MAY, 2015

KING FAHD UNIVERSITY OF PETROLEUM & MINERALS

DHAHRAN- 31261, SAUDI ARABIA

DEANSHIP OF GRADUATE STUDIES

This dissertation, written by **MOHAMMAD A. SAMAANEH** under the direction of his dissertation advisor and approved by his dissertation committee, has been presented and accepted by the Dean of Graduate Studies, in partial fulfillment of the requirements for the degree of **DOCTOR OF PHILOSOPHY IN CIVIL ENGINEERING**.

Prof. Alfarabi M. Sharif
(Advisor)

Dr. Omar A. Al-Swailem
Department Chairman (A)

Prof. Muhammed Baluch
(Co-Advisor)

Prof. Salam A. Zummo
Dean of Graduate Studies

عمادة الدراسات العليا
DEANSHIP OF GRADUATE STUDIES

Prof. Abul Kalam Azad
(Member)

7/6/15
Date

Prof. Husain J. Al-Gahtani
(Member)

Prof. Abul Fazal M. Arif
(Member)

IN THE NAME OF ALLAH, THE MOST GRACIOUS, THE MOST MERCIFUL

Dedicated

To

My Beloved Parents and Wife

ACKNOWLEDGMENTS

All praise be to ALLAH Subhanahu wata'ala for bestowing me with health, opportunity, patience and knowledge to complete thesis research. May the peace and blessing of ALLAH (S.W.T) be upon prophet Mohammad (PBUH), his family and his companions.

I would like to thank my parents, wife, sisters and all of my family for their continuous love, encouragement, prayer, emotional and moral support throughout my life. Words fall short in conveying my gratitude towards them. A prayer is the simplest way I can repay them – May ALLAH (S.W.T) give them good health and give me ample opportunity to be of service to them throughout my life.

I would like to acknowledge KFUPM for the support extended towards my research through its remarkable facilities and for providing me the opportunity to pursue graduate studies.

I acknowledge, with deep appreciation, the inspiration, encouragement, remarkable assistance and continuous support given by my thesis advisor Prof Alfarabi M. Sharif. His valuable suggestions made this work interesting and a great learning experience for me. I am deeply indebted to my committee members, Prof. Mohammed Baluch, Prof. Abul Kalam Azad, Prof. Husain Al-Gahtani, and Prof. Abul Fazal Arif for their constructive support and encouragement.

I would like to acknowledge my friends at KFUPM, Palestine, and everywhere for their support and love.

LIST OF CONTENT

TABLES

FIGURES

THESIS ABSTRACT

NAME: **MOHAMMAD ABDUL RAHMMAN SAMAANEH**
TITLE: **EXPERIMENTAL AND NUMERICAL INVESTIGATIONS OF CONTINUOUS COMPOSITE GIRDERS REINFORCED WITH CFRP**
Major Field: **CIVIL ENGINEERING**
Date of Degree: **MAY 2015**

Continuous composite steel-concrete girders composed of cast-in-place concrete slab and steel girders are widely used in bridges and buildings. In design, the concrete slab at the negative moment region is ignored for composite action because of tensile stress, and the steel girder is assumed to either act alone or compositely with the longitudinal slab reinforcement. The inactiveness of slab in composite action at negative moment regions diminishes the full composite action of the girders, resulting in its reduced strength and stiffness.

This research presents experimental and numerical investigations on the use of Carbon Fiber Reinforced Polymer (CFRP) to maintain the composite action at the negative moment region of continuous composite girders. This is achieved by bonding CFRP sheets to the top of concrete slab at the negative moment region. A total of six two-span continuous composite girders were tested. The girders were designed to have full composite action between the concrete slab and steel girder. The experimental results confirmed effectiveness of CFRP sheets to maintain the composite action at negative moment region under service load. The use of CFRP also improved strength and stiffness of the continuous composite girders.

Three-dimensional Finite Element (FE) model of continuous composite girder was developed using commercial software ABAQUS and validated with the experimental results. The developed model was used to investigate the proper thickness and length of CFRP sheets to achieve the full plastic capacity of composite girders and avoid premature failure of CFRP and epoxy adhesive. The model results were used to obtain the required number of shear connectors to develop full composite action between steel beam and concrete slab at negative moment zone. Experimental and numerical results were used to develop simplified design approach to compute the required thickness of CFRP sheets to strengthen continuous composite girder.

DOCTOR OF PHILOSOPHY

KING FAHD UNIVERSITY OF PERTOLUEM AND MINERALS
Dhahran, Saudi Arabia

THESIS ABSTRACT (ARABIC)

ملخص الرسالة (باللغة العربية)

الاســــــــــم: محمد عبد الرحمن سماعنه

عنوان الرسالة: نمذجة الكمرات المستمرة المركبة والمسلحة جزئيا باستخدام البوليمير المدعم بألياف الكربون

التخصـــــص: هندسة مدنية (إنشاءات)

تاريخ التخـرج: شعبان 1436هـ (الموافق مايو 2015)

تستخدم الكمرات المستمرة المركبة من العقدات الخرسانية ومقطع فولاذي في أنظمة البناء والجسور بشكل شائع. يتضمن تصميم الكمرات المستمرة إهمال العقدة الخرسانية في منطقة عزم الدوران السالب بسبب أحمال الشد، بينما يعتبر المقطع الفولاذي مؤثراً بشكل منفصل أو بشكل مركب مع حديد التسليح الطولي. إن عدم فعالية العقدة الخرسانية في منطقة عزم الدوران السالب يتسبب في إنهاء التأثير المركب للكمرة مما يتسبب في تقليل من قدرة تحمل الكمرة وجساءتها.

يقدم هذا البحث دراسة تجريبية وعددية لإستخدام صفائح البوليمر المدعم بألياف الكربون من أجل الحفاظ على التأثير المركب في منطقة عزم الدوران السالب في الكمرات المركبة المستمرة. تم تحقيق هذه الدراسة من خلال إلصاق صفائح البوليمر المدعم بألياف الكربون على السطح العلوي للعقدة الخرسانية في منطقة عزم الدوران السالب. تم إجراء البرنامج التجريبي على ما مجموعه ستة كمرات مركبة والتي تم تصميمها حتى تمتلك تأثيراً مركباً تاماً بين المقطع الفولاذي والعقدة الخرسانية. أكدت النتائج التجريبية فعالية استخدام صفائح البوليمر المدعم بألياف الكربون للحفاظ على التأثير المركب في منطقة عزم الدوران السالب تحت تأثير الأحمال الخدماتية، كما ساهمت صفائح البوليمر المدعم بألياف الكربون في تحسين قدرة تحمل الكمرات المستمرة المركبة بالإضافة إلى تحسين جساءتها.

تم تطوير نموذج ثلاثي الأبعاد باستخدام برنامج العناصر المحددة (ABAQUS) لتمثيل الكمرات المستمرة والمدعمة بصفائح البوليمر المدعم بألياف الكربون، كما تم التحقق من نتائج هذا النموذج باستخدام النتائج التجريبية. تم استخدام هذا النموذج من أجل إيجاد السماكة الأفضل ومقدار الطول المناسب للكمرات المركبة وتمكين الكمرات أن تصل للقوة القصوى ومنع أي فشل مفاجئ في ألياف البوليمر المدعم بصفائح الكربون أو فيالمادة اللاصقة. كما تم استخدام النتائج النهائية للنموذج لحساب عدد الوصلات الميكانيكية اللازمة لتحقيق التأثير المركب التام والمناسبة لقوى الشد داخل صفائح البوليمر المدعم بألياف الكربون.بالإضافة إلى ذلك، فقد تم استخدام نتائج البرنامج التجريبي والنمذجة للحصول على معادلات مبسّطة لحساب السماكة المطلوبة من صفائح البوليمر المدعم بأليف الكربون.

درجة الدكتوراه
جامعة الملك فهد للبترول والمعادن
الظهران ، المملكة العربية السعودية

CHAPTER ONE

INTRODUCTION

1.1 GENERAL

The composite steel-concrete girders composed of cast-in-place concrete slab and steel beam are commonly used in bridges and buildings. The composite action formed using mechanical shear connectors, headed studs which are welded to the top flange of the steel beam. The use of composite steel-concrete structures reduces the construction cost and efficiently utilizes materials properties, considering the high compressive and tensile strength of concrete and steel, respectively. Composite steel-concrete girders have some advantages such as reducing the weight of steel section, in addition to the increasing of floor stiffness which gives opportunity to increases the span length of the member [1].

For continuous composite steel-concrete girders, the concrete slab at the negative moment region will be under tension and consequently loses its contribution to the composite action. In design, the concrete slab at the negative moment region is ignored for composite action because of tensile stress, and the steel girder is assumed to either act alone or compositely with the longitudinal slab reinforcement. The inactiveness of slab in composite action at negative moment regions diminishes the full composite action of the

girders, resulting in its reduced strength and stiffness. This work is intended to maintain the composite action between the concrete slab and steel girder at the negative moment region by bonding Carbon Fiber Reinforced Polymer (CFRP) sheets to the top of concrete slab. The concrete slab will be considered fully composite with the steel section while the bonding between the concrete slab and CFRP sheet will take into account the property of the adhesion. This new approach will maintain the composite action at the negative moment region and consequently improves the strength and stiffness of the continuous composite girder. This research will be conducted in three stages, including experimental, numerical, and then using the results to obtain simplified design approach.

1.2 NEED FOR THE RESEARCH

The composite action between steel and concrete in bridges has a lot of advantages in reducing cost, materials, and depth of the members. In simple span, the concrete slab under compression, where the compression capacity of the concrete is high. Continuous spans have many advantages in reducing the deflection of the member, long spans and economical sections. The negative bending moment over the interior supports in the continuous spans put the concrete in tension. Therefore the composite action lost and the capacity of the section is reduced. Including the composite action at the negative moment region leads to more economical girders with longer spans and less depth.

In view of the limited published work on the use of CFRP to strengthen composite girders at the negative moment zone, an experimental work undertaken to evaluate the effectiveness of CFRP in providing composite action at the negative moment zone. The aim of this work is to present the findings of the experimental investigation of the proposed construction to maintain the composite action at the negative moment regions of continuous composite girders. CFRP sheet will be bonded to the top of concrete slab at the negative moment region for two-span continuous composite girders and structural performance will be evaluated up to failure. A three dimensional Finite Element (FE) model will be developed for the composite girder using ABAQUS which will be verified with the experimental results. The model will be used to conduct a parametric study for different girders. Finally a simplified design approach will be developed to help engineers design the composite girder with proper CFRP thickness.

Continuous Composite girders will be prepared and adequate number of shear connectors will be provided to insure full composite action between the concrete slab and steel section .The steel section will be designed to eliminate all second order effects. CFRP sheets will be bonded to top of concrete slab, and the length of CFRP sheets (L_{CFRP}) covers the whole negative moment region in addition to an adequate development length to gradually develop the strength of CFRP. Each girder will be tested to failure and its data will be compiled and analyzed to prepare the experimental results.

1.3 OBJECTIVES OF THE STUDY

The objective of this research is to study the behavior of continuous composite girders with CFRP bonded to the top of concrete slab at the negative moment region. Following are the main objectives of this work:

1. Undertake a planned experimental work to evaluate the performance of continuous composite girders with CFRP sheets bonded to the top of the concrete slab at the negative moment region. The testing will assess the effectiveness of CFRP to maintain the composite action.
2. Develop a three dimensional FE model for the continuous composite girder with CFRP using commercially available software. The model will consider full composite action between the concrete slab and the steel section. However, the bonding between the concrete slab and CFRP sheets will be modelled taking into account the adhesion properties.
3. Develop a simplified mechanistic approach for design to help engineers design continuous composite girders with the proper thickness of CFRP.

1.4 RESEARCH PROGRAM

This research will include three main parts as follows:

1. The experimental program will be conducted by testing continuous composite girders with and without CFRP sheets to study the effectiveness of CFRP in maintaining the composite action. CFRP thickness will be varied to evaluate its contribution throughout the loading history of the girders.

The mechanical properties for concrete, steel reinforcement, structural steel and CFRP will be evaluated according to the ASTM standards. The bond strength of epoxy adhesive between concrete slab and CFRP sheets will be evaluated using single pull-out shear test whereas two way push-out shear test will be conducted to find the shear capacity of shear studs.

A total of six composite girders will be designed, prepared, and tested in this study. Adequate number of 19 mm diameter shear connectors will be welded to top flange of steel section to insure full composite action between the concrete slab and steel section. The steel section will be designed to eliminate all second order effects such as local buckling, lateral torsional buckling and effect of concentrated load on the web. CFRP sheets will be bonded to top of concrete slab and the length of CFRP sheets (L_{CFRP}) covers the whole negative moment region plus adequate development length to gradually develop the strength of CFRP.

Strain gauges will be installed at several locations on the composite girders to measure the interaction and compatibility between the different materials. Strain gauges will be fixed to all composite girder components at mid-span and over the interior support.

2. A three dimensional nonlinear FE model will be developed for the continuous composite girder with CFRP sheet bonded to top of concrete slab at the negative moment region using available commercial software. The interaction between concrete slab and steel section will be adapted using proper surface contact between shear studs and surrounded concrete, while the interaction between CFRP and concrete slab will take into account the adhesion properties. The model results will be verified with the experimental results.

Surface-surface contact will be used to present the interaction between concrete slab and steel section. However, the adhesion between CFRP sheet and concrete slab will be represented by cohesive contact to simulate the adhesion properties. Both material and geometric nonlinearities will be considered in the study.

3. The results obtained from the experimental and modeling programs will be utilized to develop a simplified design approach. This study investigated the composite behavior of continuous steel-concrete girders reinforced with CFRP sheet that bonded to the top of concrete slab at the negative moment region.

A simplified design approach will be developed to help engineers design continuous composite girders with proper thickness of CFRP sheets. The approach will be based on limit state at failure, considering strain compatibility and equilibrium conditions. The experimental and numerical results will help in developing the simplified method.

CHAPTER TWO

LITERATURE REVIEW

2.1 USE OF CFRP TO STRENGTHEN CONCRETE

Strengthening of structures using advanced materials is a contemporary research in the field of Structural Engineering. During past two decades, much research were carried out on flexural strengthening of beams using different types of fiber reinforced polymers and adhesives. Life span of Reinforced Concrete (RC) structures may be reduced due to many reasons, such as deterioration of concrete and development of surface cracks due to ingress of chemical agents, improper design and unexpected external loads such as wind or seismic forces acting on a structure, which are also the reasons for failure of structural members. The superior properties of polymer composite materials like high corrosion resistance, high strength, high stiffness, excellent fatigue performance and good resistance to chemical attack etc., has motivated the researchers to use the composite polymers in the field of rehabilitation of structures. Extensive research were conducted on use of CFRP to strengthen concrete structures. This section is highlighting several researches that conducted in this area.

Aravind et al (2013) reviewed fourteen articles on rehabilitation of reinforced concrete (RC) beams. It included the different properties of Glass Fiber Reinforced Polymer

(GFRP) and Carbon Fiber Reinforced Polymer (CFRP) composites and adhesives, influence of dimensions of beams and loading rate causing failure. The paper proposed an enhanced retrofitting technique for flexural members and developed a new mathematical model [2].

Finite element software ANSYS was used by Ibrahim and Mahmood (2009) to model reinforced concrete beams reinforced externally with FRP laminates. Smeared cracking approach was used to model concrete and 3-D layered elements to model FRP composites. Experimental results of six beams with different conditions were used to verify the results obtained from ANSYS [3]. The FE load-deflection curves showed agreement with the experimental results in the linear range, but the FE result was slightly stiffer than that of experimental results. Change in the failure mechanism was observed by using additional FRP reinforcement.

Miller et al. (2001) verified that CFRP cover plates could be used to restore reasonable losses of stiffness and strength in deteriorated bridge girders. "10-37% increasing in stiffness achieved for the corrosion-damaged bridge girders. The development length was found to be on the order of 100 mm. The results indicated 11.6% increase in flexural stiffness due to the retrofitting" [4]. The results showed good agreement with estimated values found using transformed sections.

Experimental work conducted by Quantrill and Hollaway (1998) on the structural behavior of beams strengthened by advanced fiber-reinforced composite plates. The prestressing technique was developed and refined on smaller-scale (1.0 m) length specimens before being applied to larger 2.3 m length beams. Comparisons were made with beams externally reinforced with a plate unstressed at the time of bonding. The main conclusions drawn from the work were indicated that the technique of prestressing advanced composite plates prior to bonding to reinforced concrete beams had the potential to provide more efficient solution to strengthening problems [5].

Theoretical model was proposed by Lau et al. (2006) to estimate shear and peel-off stresses. The research considered the axial stresses in concrete beam strengthened by FRP including variation in FRP plate fiber orientation. Theoretical predictions using FE model validated the experimental results. The results showed that maximum shear and peel off stresses were at the end region of the plate. The maximum shear stress increased by increasing the amount of fibers aligned in the beam's longitudinal axis, the modulus of adhesive material and the number of laminate layers. Whereas, increasing layer thickness of adhesive material decreased the maximum peel-off stress [6].

Experimental program was conducted by Akbarzadeh and Maghsoudi (2011) to study the behavior of RC two-span beams strengthened with hybrid carbon and glass reinforced polymer sheets (HCG). Due to linear stress–strain characteristics of FRP up to failure, the ductility of plated members and their ability to redistribute moment was less than that of un-plated RC beams. Hybrid FRP laminates, which consist of a combination of either

carbon or glass fibers, changed the behavior of the material to a non-linear behavior. The program included total of six continuous beams with overall dimensions equal to 250×150×6000 mm. The test results showed that using the HCG for strengthening the continuous RC beams caused significant increase of bearing capacity, ductility and moment redistribution ratio compared to strengthened beams with CFRP or GFRP [7]. Experimental results showed that stiffness after yielding load was significantly increased by strengthening RC continuous beams with HCG compared to the strengthened beams with CFRP or GFRP. Behavior of the beams strengthening with HCG by increasing applied load tended to become non-linear compared to the strengthened beams with CFRP. Use of the HCG was needed for ensuring of minimum moment redistribution for continuous beams. Assuming that an index value of 3 represents an acceptable lower bound to ensuring the ductile behavior of RC continuous beams strengthened with FRP sheet, use of the HCG is a way for ensuring the minimum ductility.

Analytical, numerical (FE model) and experimental investigations of beams that strengthened with FRP composite were studied by Kasimzade and Tuhta (2012). The effect of FRP wrapping to the maximum load and moment capacity was evaluated. Paper presented applications of strengthening structures using CFRP [8].

Experimental study conducted by Sobuz et al. (2011) to investigate the flexural behavior of reinforced concrete beams strengthened with CFRP laminates attached to the bottom of the beams. A total of five beams having different CFRP laminates configurations were tested to failure in four-point bending over a clear span 1900mm. Four beams were strengthened by changing the levels of CFRP laminates whereas the last one was not strengthened with FRP and considered as a control beam. Test results showed that the

addition of CFRP sheets to the tension surface of the beams demonstrated significantly improvement in stiffness and ultimate capacity. The response of control and strengthened beams were compared and efficiency and effectiveness of different CFRP configurations were evaluated. It was observed that tension side bonding of CFRP sheets with U-shaped end anchorages was very efficient in flexural strengthening. The paper also highlighted the beams failure modes due to the different level of strengthening scheme [9].

Balamuralikrishnan and Jeyasehar (2009) investigated the flexural behavior of CFRP strengthened reinforced concrete beams. For flexural strengthening of RC beams, total ten beams were cast and tested over an effective span of 3000 mm up to failure under monotonic and cyclic loads. The beams were designed as under-reinforced concrete beams. Eight beams were strengthened with bonded CFRP fabric in single layer and two layers which are bonded parallel to the beam axis at the bottom under virgin condition and tested until failure; the remaining two beams were used as control specimens. Static and cyclic responses of all the beams were evaluated in terms of strength, stiffness, ductility ratio, energy absorption capacity factor, compositeness between CFRP fabric and concrete, and the associated failure modes. The theoretical moment-curvature relationship and the load-displacement response of the strengthened beams and control beams were predicted by using FE software ANSYS. The results showed that the strengthened beams exhibited an increase in flexural strength, and flexural stiffness [10].

Siddiqui (2010) studied the efficiency and effectiveness of different practical FRP schemes for flexure and shear strengthening of RC beams. For this purpose, 6 RC beams were cast in two groups, each group containing 3 beams. The specimens of first group were designed to be weak in flexure and strong in shear, whereas specimens of second group were designed just in an opposite manner i.e. they were made weak in shear and strong in flexure. In each group, out of the three beams, one beam was taken as a control specimen and the remaining two beams were strengthened using two different Carbon FRP strengthening schemes. All the beams of two groups were tested under similar loading. The response of control and strengthened beams were compared; efficiency and effectiveness of different schemes were evaluated. It was observed that tension side bonding of CFRP sheets with U-shaped end anchorages was very efficient in flexural strengthening; whereas bonding the inclined CFRP strips to the side faces of reinforced concrete beams were very effective in improving the shear capacity of beams [11].

2.2 USE OF CFRP TO STRENGTHEN STEEL STRUCTURES

Deterioration of steel structures due to corrosion, climate condition, and temperature variations reduces the strength and stiffness of beams. The rehabilitation of steel girders using advanced composite materials offered a smart solution for short-term retrofit or long-term rehabilitation. CFRP offers an attractive way for strengthening steel structures because of high tensile strength and long-life serviceability. This section presented representative samples of studies conducted by researchers on use of CFRP to strengthen steel beams.

Behavior of beam strengthened with CFRP plate in addition to the effect of strengthening length was investigated by Majid Kadhim (2012). FE Software ANSYS was used to model simply supported steel beam using an experimental work data. Comparison between modeling and experimental result showed that ANSYS is capable of modeling and predicting the actual deformation behavior for steel beam [12].

Galal et al. (2011) investigated the effectiveness of using CFRP in retrofitting deteriorated steel beams. The study included using of two thicknesses of CFRP; 0.27 mm and 1.4 mm. The study showed that the post-yield carrying capacity was increased for deteriorated steel beams retrofitted with bonded CFRP. Sudden failure due to either peeling off CFRP or CFRP rupture were the observed failure mode of retrofitted steel beams. The results indicated that adhesive material had a slight influence on the yielding

load, but it had a significant effect on the ultimate flexural capacity in addition to mode of failure of the CFRP retrofitted beams [13].

Experimental and numerical investigations on use of CFRP for flexural strengthening of steel I-beams had been presented by Narmashiri et al (2011). Eight steel beams were selected with the same length and different types and thicknesses of CFRP plates. Both experimental test and numerical simulation were employed. In the experimental test, the gradual static loading in four-points bending method was utilized. In numerical simulation, ANSYS software in the three dimensional (3D) modeling case and nonlinear static analysis method were employed. Results showed that different types and thicknesses of CFRP plates influenced the failure modes, load capacities, and strain distributions on the CFRP plates. Experimental and numerical results showed that flexural behaviors of steel I-beams were improved using CFRP strips. The application of different thicknesses and types of CFRP plates used in strengthening steel I-beams caused change in the CFRP failure modes, load bearing capacity, and strain on CFRP plates. One of the most efficient approaches to increase the strength of beam against the below load splitting was by increasing the CFRP thickness. Applying a thicker CFRP plate caused significant increment in the load bearing capacity, but the CFRP showed brittle behavior, and premature end de-bonding occurred. Application of the IM-CFRP plates caused considerable increment in the load bearing capacity, due to the larger elasticity modulus [14].

2.3 USE OF CFRP TO STRENGTHEN COMPOSITE GIRDERS

CFEP sheets and plates could be used to increase the strength and stiffness of composite girders. For simple span composite girders, CFRP is bonded to the bottom steel flange and therefore increase strength of composite girder. Researchers have been discussed using of CFRP for simple-span composite structures and investigated the ultimate strength and modes of failure as will be presented in this section.

Liu et al. (2001) discussed strengthening and repairing of corroded steel members of composite girders using (FRP) material. The experimental results showed that an improvement in stiffness and plastic load of corroded steel members were achieved by applying CFRP laminates to the tension flange of corroded steel members. The peeling of FRP laminates was the observed failure mode of the retrofitted girders. This was due to high stress concentrations near the girders mid-span [15].

CFRP sheets and steel plates were used to increase the capacity of composite steel-concrete beam (simple span beam) by Sallam et al. (2010). Two different patterns of CFRP sheet were used. The experimental results showed an increase in capacity was achieved by using CFRP sheets and steel plates. CFRP sheet participated in increasing the capacity of the beam significantly after yielding of the bottom steel flange [16].

The ultimate capacity of a composite steel-concrete girder can be enhanced significantly by bonding CFRP laminates to its' tension flange. Tavakkolizadeh and Saadatmanesh (2003) conducted a study on the behavior of steel-concrete composite girders strengthened with CFRP sheets under static loading. "Three composite girders made of A36 steel beam and 75 mm thick by 910 mm wide concrete slab were prepared and tested. Different number of CFRP layers were used in the specimens" [17]. The results showed that bonding CFRP sheet increased the ultimate strength of composite steel-concrete girders and traditional methods could be used to predict the behavior conservatively.

Schnerch et al (2005) conducted feasibility study using large scale members which strengthened with unstressed and prestressed CFRP strips using intermediate and high modulus fibers. Fibers had a tensile modulus up to three times that of steel. The behavior of strengthened steel-concrete composite beams had investigated under conditions of overloading to determine the significance of shear lag. The experimental results indicated that the use of high modulus CFRP materials can greatly reduce the overloading damage due to overloading conditions, in comparison to strengthened beams loaded to similar stress conditions [18].

2.4 MAINTAINING OF COMPOSITE ACTION FOR CONTINUOUS COMPOSITE GIRDERS

The inactiveness of slab in composite action at negative moment regions diminishes the full composite action of the girders, resulting in its reduced strength and stiffness. Researchers have used internal and external prestressing techniques to overcome the loss of composite action at negative moment regions for continuous composite girders. This section is presented main works that conducted in this field.

Experimental and analytical evaluations of the behavior of continuous composite steel-concrete girders prestressed at the negative moment region were investigated by Basu et al. (1987). This study evaluated the effect of using prestress tendons on concrete cracks at the negative moment region. The concrete slab was partially prestressed at that region for two-span continuous composite girders. The concrete slab was cast in two stages. In the first stage the slab was cast at the negative moment region. Then prestressing force was directly applied to the concrete slab so that the slab would act compositely with the steel girder. In the second stage, the rest of the concrete slab covering the positive moment regions was cast. The behavior of a two-span a 18 ft composite beam, consisting of a concrete slab connected to a steel beam using shear connectors and prestressed near the central support region, was studied experimentally. The results were compared with predicted values. The advantages of partial prestressing of composite beams in terms of performance under service loads and economy were further established. The load carrying capacity increased by 20%, so that, expected that the resulting savings in the size of the beams may offset the extra cost of prestressing [19, 20].

The predicted linear and nonlinear response of the two-span partially prestressed composite beam up to collapse showed reasonable agreement with the experimental results, despite the premature local buckling of the bottom flange of the tested beam near the interior support. The problem of cracking of the concrete slab and the resulting partial loss of composite action and stiffness in the negative moment regions of a continuous composite beam was effectively eliminated by using the proposed partial prestressing technique. The test results gave strain values at a section that became nonlinear as the section yielded. The nonlinearity became more pronounced near the central support with the onset of the local buckling phenomenon in the bottom flange.

Experimental investigation was carried out by Elremaily and Yehia (2006) for composite continuous girders prestressed with external prestressed tendons in order to understand the behavior of the composite steel girders under negative moment. Three half-scale test specimens consisting of continuous (two-span) composite girders were tested to the ultimate capacity [21]. The ultimate load carrying capacity increased by 15% whereas deflection decreased, as well as an increase in the elastic limit compared to a non-prestressed girder. The elastic limit increased by effective use of the prestressing technique. The results also showed that prestressing continuous composite girders reduced stresses in steel beam and increased the load level whereas the beams started to buckle close to ultimate. The use of strands to prestress steel girders provided flexibility of varying the required profile to optimize the strength of the steel girder.

Chen et al. (2009) investigated experimentally two and three span continuous composite girders. Each group had one non-prestressed girder and another prestressed one with external tendons. The cracking behavior, local buckling and the ultimate strength of the

beams were investigated experimentally. Type of failure was concrete crushing at the mid-span and web local buckling over the support. The study showed that a significant increasing in the cracking moment resistance was achieved for composite beam prestressed with external tendons. The yielding moment at the negative moment region of the beam was not increased for all cases. Lateral, distortional and local buckling occurred in the compression flanges and web of two span composite girders, whether prestressed or non- prestressed [22].

The study considered the full composite section up to the first crack appeared in the concrete. The first crack in the two-span girder occurred transversely across the concrete slab over the interior support in the non prestressed beams, and subsequent cracks were developed immediately adjacent to the first crack. Distortion in the web and lateral buckling occurred in the bottom flange and significant web buckling and bottom flange buckling were noted after crushing of concrete. The prestressed continuous beams had similar behavior but with much higher load than non-prestressed one. Girder achieved full plasticity at the mid-span section in spite of lateral or distortional buckling occurred in the hogging moment region. In addition to that, higher sagging moment was achieved by the prestressed beam compared to that of non-prestressed beam at the mid-span. For three-span composite girders, lateral torsional buckling and local buckling was initiated in the web and in the compression flanges. Plastic hinges were developed at the mid-span and the internal support section in the hogging moment regions as two span girders. A design proposal based on moment redistribution to evaluate the ultimate capacity of continuous composite girders prestressed using external tendons was proposed in the study [22].

Nie et al. (2011) carried out a loading capacity analysis for prestressed continuous steel-concrete girder. The cracking, yielding, and ultimate capacity of continuous prestressed composite girder under concentrated loads were presented and extended to general cases. Also, nonlinear behavior of prestressed continuous composite beams was simulated by finite element model using finite element software. Materials and geometrical nonlinearities were considered in the numerical model. The model reflected the complexity in the behaviors of prestressed two-span composite girders during the loading process. The increment of tendon forces, slip effect, curvature distribution, formation of plastic hinges, redistribution of internal forces, and the stress distribution were the most complexities in the model. Comparisons between experimental, analytical, and numerical results showed that the analytical method provided reliable and convenient method for a routine design practice. Finite element model provided excellent numerical simulation for the nonlinear behavior of prestressed continuous composite girders [23].

External post-tensioning strengthening is an effective technique to restore the ultimate load carrying capacity of many types of bridges. Choi et al. (2008) expressed a systematic procedure of external post-tensioning technique for strengthening or rehabilitation of existing bridges. Virtual work principle was used for derivation of analytical expressions for the increment of the initial tendon force in the study. Choi introduced a new rating equation for bridges considering the initial tendon force in addition to its increment [24]. Systematic procedures could be used to find number of strands in external tendons in addition to the initial tendon force using the proposed rating equation. Experiments results and finite element analysis were used to verify the analytical expressions for the increment of a tendon force and showed good agreement. The results of the study showed

that the proposed method is suitable for strengthening of existing bridges with external post-tensioning technique. More economical design may be feasible by considering the increment of tendon force.

CHAPTER THREE

DESIGN OF CONTINUOUS COMPOSITE GIRDERS

Design of continuous composite steel-concrete girder and steel-concrete girder bonded with CFRP at negative moment region are presented in this chapter. The design of continuous composite girder was conducted included both; designing steel-concrete section at positive moment region and at negative moment region which included girders with or without CFRP. The following design of the composite girders was conducted based on designed materials and several assumptions as will be discussed in this chapter.

3.1 DESIGN CRITERIA

Composite steel-concrete girders designed based on the following criteria in order to satisfy the research objectives:

a) The composite girders were designed to fail under flexure.
b) Shear failure of steel section was eliminated using proper thickness of web.
c) Local buckling was eliminated using proper width/thickness ratio of steel plates.
d) Lateral torsional buckling was eliminated using proper cross section, providing lateral support at the interior support

e) The highest ultimate capacity of all girders with CFRP should not exceed the ultimate capacity of lab facilities (Loading cells, loading jack, Frame).

3.2 MATERIALS AND GEOMETRY

Two-span continuous composite girder shown in Fig. 3-1 was designed using compressive strength of concrete, f'_c =28MPa, and yield strength of steel section, f_y =248MPa (Gr. 36), whereas the yield strength of steel reinforcement, $f_{y\ S.R}$=420MPa. CFRP used was Grade 230 Nitowrap FRC of 0.131 mm thickness. The ultimate design tensile strength, σ_u= 3480 MPa, and the design strain of CFRP, ε_u= 0.015. The composite girders cross section is shown in Fig. 3-2.

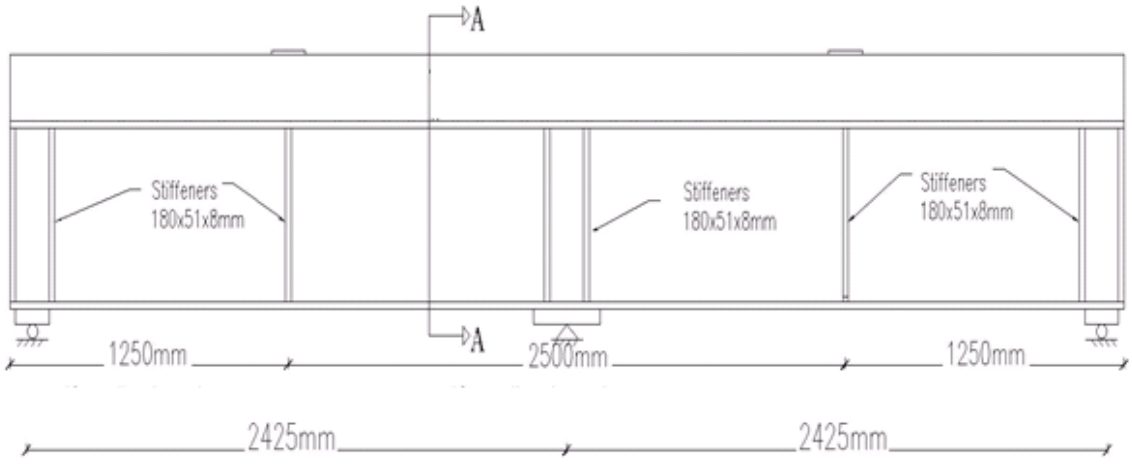

Fig. 3- 1 Details two-span continuous composite girder

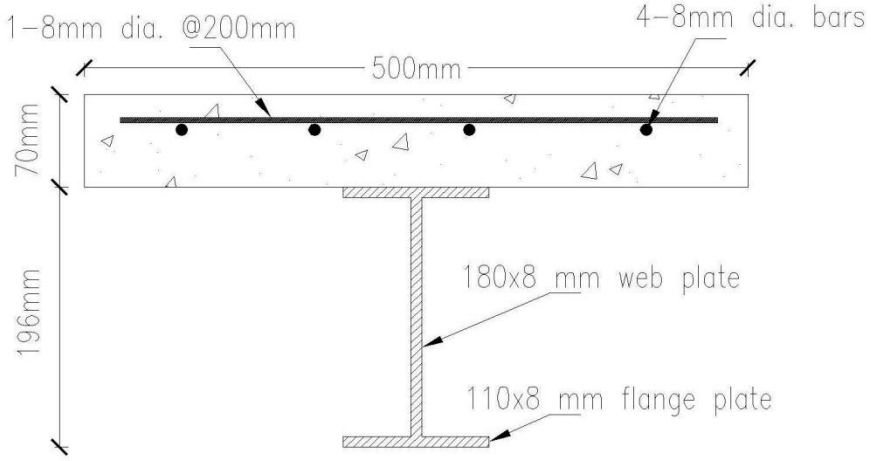

Fig. 3- 2 Section A-A, steel-concrete cross section

3.3 FLEXURAL STRENGTH

3.3.1 Section Capacity at Positive Moment Region:

The neutral axis (N.A) was assumed in the concrete slab as shown in Fig. 3-3. Then the depth of compression block (a) was calculated using equilibrium.

$C_c + C_{S.R} = T_{st}$ Equ. (3.1)

Where

C_c is the compression of concrete

$C_{S.R}$ is the compression of steel reinforcement

T_{st} is the tension of steel.

$0.85\ f'_c\ b\ a + A_{S.R}\ F_{y\ S.R} = A_{st}\ F_{y\ s}$ Equ. (3.2)

Where

f'_c is the compressive strength of standard concrete cylindrical at 28 days

b is the width of the concrete slab

$F_{y\ S.R}$ is the yield strength of steel reinforcements

$F_{y\,s}$ is the yield strength of steel plates

$A_{S.R}$ is the area of steel reinforcement =201mm^2

A_{st} is the area of steel section =3200mm^2

0.85 f'$_c$ (500a)+201x420=3200x248

a= 60.0mm < 70 mm OK

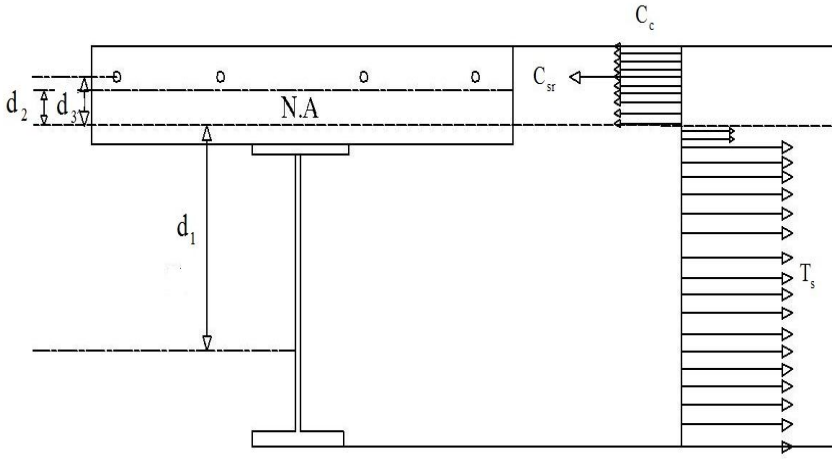

Fig. 3- 3 Stress distribution at the positive moment region at ultimate load

The moment capacity at the positive moment region could be calculated using the following equation:

$M_{+ve} = T_s\,(d_1) + C_c\,(d_2) + C_{S.R}\,(d_3)$ Equ. (3.3)

Where

$d_1 = d + t - c$

$d_2 = c - a/2$

$d_3 = c - d_c$

M_{+ve} is the moment capacity at the positive moment region

c is the depth of compression = a/0.85 = 70 mm

d_c is the cover of concrete

t is the slab thickness

d is the depth of steel section

M_{+ve}==0.85 f'$_c$ x 500x (60)(45)+ 201x420x(70-35)+3200x248x96

M_{+ve}=112 KN.m

3.3.2 Section Capacity at Negative Moment Region without CFRP

Concrete is assumed to be cracked at the negative moment region, so that the location of the shifted N.A is assumed to be in the steel section as shown in Fig. 3-4. The location of the N.A was calculated using the following equilibrium equation:

$T_s + T_{S.R} = C_s$ Equ. (3.4)

Where

C_s is the compression force in the part of steel section subjected to compression.

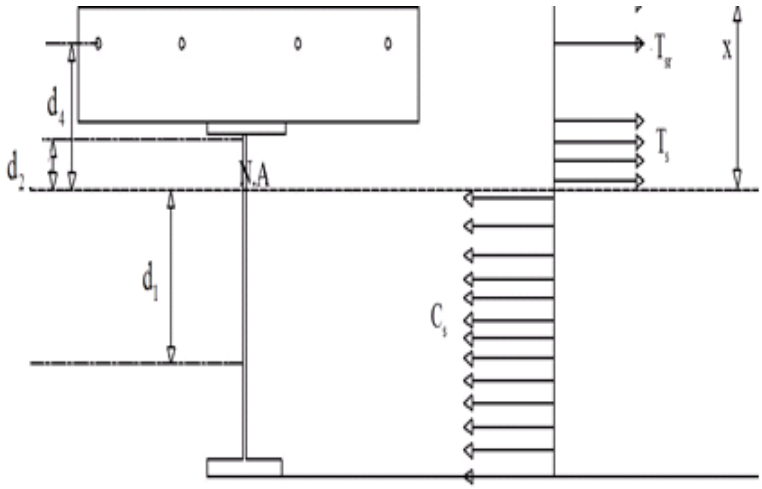

Fig. 3- 4 Stress distributions at the negative moment region without CFRP

The moment capacity at the negative moment region of girders without CFRP could be evaluated using the following equation:

M_{-ve} =C_s (d_1)+ T $_{S.R}$ (d_4)+ T_s (d_2) Equ. (3.5)

Where

M_{-ve} is the moment capacity at the negative moment region

d_1 is the distance between center of compression steel and N.A

d_2 is the distance between center of tension steel and N.A

d_3 is the distance between CFRP and N.A

d_4 is the distance between steel reinforcement and N.A

M_{-ve} =(110x8.0+112x8.0) x81x248 + 201x420x115 +(110x8.0+72x8.0) x 64x248

M_{-ve}=70 KN.m

3.3.3 Section Capacity at Negative Moment Region with CFRP

The ultimate capacity of composite steel-concrete section bonded with CFRP top of concrete slab could be calculated using the following steps:

a) Assume level of strain in CFRP.

b) Assume location of N.A in steel web.

c) Using strain compatibility to find strain in steel flanges, steel reinforcement.

d) Use strain values to find compression and tension equilibrium.

e) Revise assumptions if equilibrium not satisfied.

Using the above steps, the ultimate capacity of section at negative moment region could be estimated. However, the assumptions of level of strain in CFRP and location of N.A should be used based on the following:

1) The level of strain in CFRP should ensure yielding of both steel flanges. This assumption is to ensure reach plastic capacity at ultimate load.

2) The level of strain in CFRP should be limited to a certain value to avoid premature rupture or de-bonding failures of CFRP, and ensuring that this level could be achieved.
3) The assumed location of N.A should be upward the N.A of section without CFRP.

The above steps and assumptions were applied to the designed girders. The design was conducted assuming the maximum planned number of CFRP layers. It assumed that composite steel-concrete girder bonded with THREE layers of CFRP. The strain was assumed 33% of the ultimate strain of CFRP and the N.A location is 168 mm from the bottom flange, then forces in all components of composite girder shown in Fig. 3-5 are:

T_{CFRP} = 228 KN

T_s = 255 KN (strain is 0.00145, steel is yielded)

$T_{S.R}$ = 84.4 KN (steel reinforcement is yielded)

C_s = 540 KN

Check equilibrium using the following equation:

$T_{CFRP} + T_s + T_{S.R} = C_s$ Equ. (3.6)

Tension = Compression (OK)

Where

T_{CFRP} is the tension force in CFRP

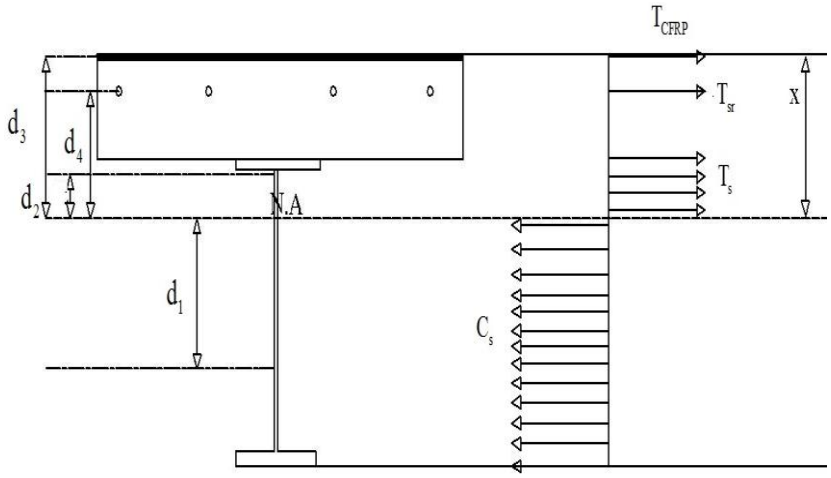

Fig. 3- 5 Stress distribution at the negative moment region with CFRP at ultimate load

The moment capacity at the negative moment region of girders with CFRP could be evaluated using the following equation:

$M^*_{-ve} = C_s\,(d_1) + T_{S.R}\,(d_4) + T_s\,(d_2) + T_{CFRP}\,(d_3)$ Equ. (3.7)

M^*_{-ve} =(110x8.0+160x8.0) x114x248 + 201x420x63 +(110x8.0+20x8.0) x 21x248

+(0.005x232000x0.131x3x500)x98

M^*_{-ve} = 95 KN.m

3.4 ULTIMATE LOAD BASED ON PLASTIC ANALYSIS

The girders were loaded at both mid-spans by a concentrated load (P). At collapse load, plastic hinges will form over the internal support followed by another plastic hinge at mid-span as shown in Fig. 3-6. Assuming that capacity of section at mid span, αMp (Mp is the plastic moment), and over the interior support, Mp, then the ultimate load at plastic moment could be calculated as follows:

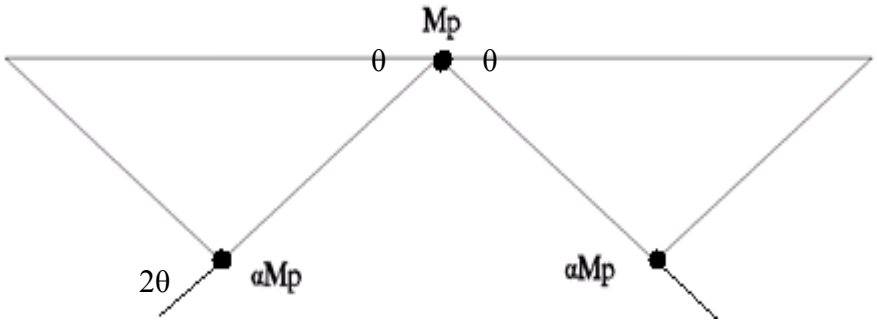

Fig. 3- 6 Failure Collapse mechanism

Using equation of internal work and external work done by the virtual displacement θ for either span.

$$Mp\,\theta + \alpha Mp\,(2\,\theta) = P\,\frac{L\,\theta}{2} \qquad \text{Equ. (3.8)}$$

a) For girder without CFRP at the negative moment region

$\alpha = M_{+ve}/M_{-ve} = 1.6$

$$P = \left(\frac{2(2\alpha+1)Mp}{L}\right) \qquad \text{Equ. (3.9)}$$

P =242KN (expected ultimate load of girder without CFRP)

b) For girder with CFRP at the negative moment region

$\alpha = M_{+ve}/M^{*}_{-ve} = 1.18$

P =264 KN (expected ultimate load of girder with three layers of CFRP)

3.5 DESIGN OF SHEAR CONNECTOR

The concrete slab was designed to be fully composite with the steel section, therefore proper number of shear studs was provided to ensure the full composite action. At positive moment region, 19 mm (3/4'') diameter shear studs were used as indicated in Fig. 3.7. Number of shear studs at the positive moment region calculated according to the AISC manual [25] using the following equation:

Number of shear studs = $\frac{T_S \ or \ C_C + C_{S.R}}{Q}$ Equ. (3.9)

Where

Q is the shear capacity of shear stud

The N.A in the concrete slab, then the compression strength of concrete slab (C_c) is

Cc =0.85x28x500x60/1000 =713KN

The compression strength of steel reinforcement (C_{SR}) is

$C_{S.R}$=201x420/1000 = 85 KN

Total compression is 793 KN

Tension strength of steel section (T_s) is

T_s= 3200x248/1000 =793 KN

Shear stud should resist this load (793KN)

For 19 mm shear studs, Q=105 KN [25], then number of shear studs = (793/105) = 7.6

Use 8 shear studs of 19 mm diameter equally spaced between the point of maximum positive moment and zero moment as shown in Fig. 3-8.

At the negative moment region, the shear studs should resist lateral shear force between steel and concrete. This force is the total tension force in CFRP and steel reinforcement. 19 mm shear studs were used also to resist shear force due to steel reinforcement, and three layers of CFRP (33% of ultimate stress)

$T_{S.R}$=201x420/1000 = 85 KN

T $_{CFRP}$ = (0.005 x 232000 x 3 x 500 x0.131)/1000 = 228 KN

Number of shear studs = $\frac{T_{CFRP} + T_{S.R}}{Q}$ Equ. (3.10)

Number of shear studs = (85+228)/105 = 3.0

Conservatively, use 6 shear studs of 19 mm diameter.

Since the distance between the maximum negative moment to the zero moment, and zero moment to the maximum negative moment will vary depending on the level of loading, so conservatively use the same spacing as shown in Fig. 3-8 (critical).

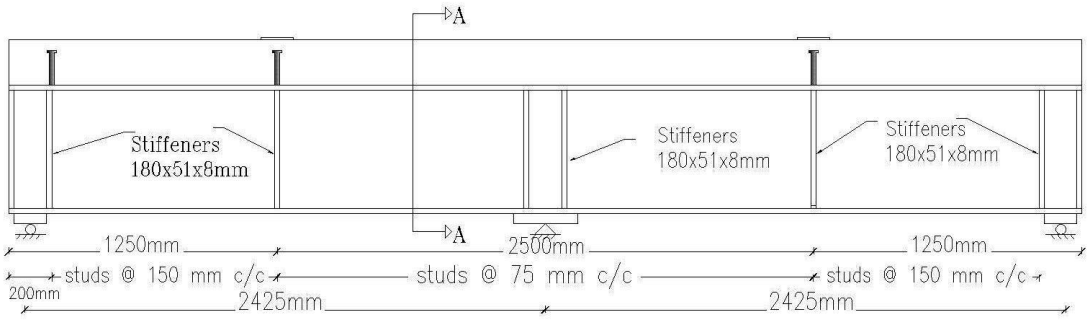

Fig. 3- 7a distribution of shear studs along girders

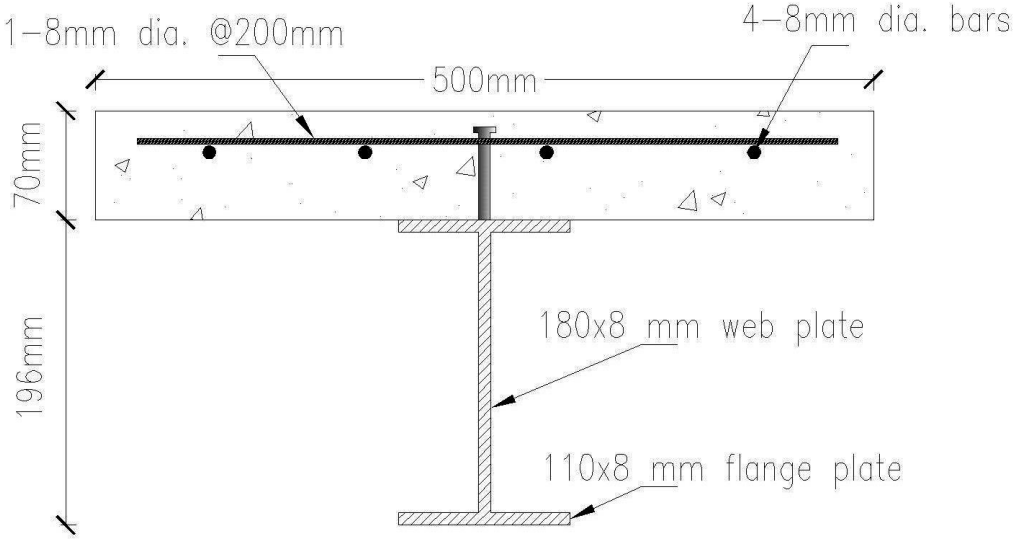

Fig. 3- 7b cross section A-A

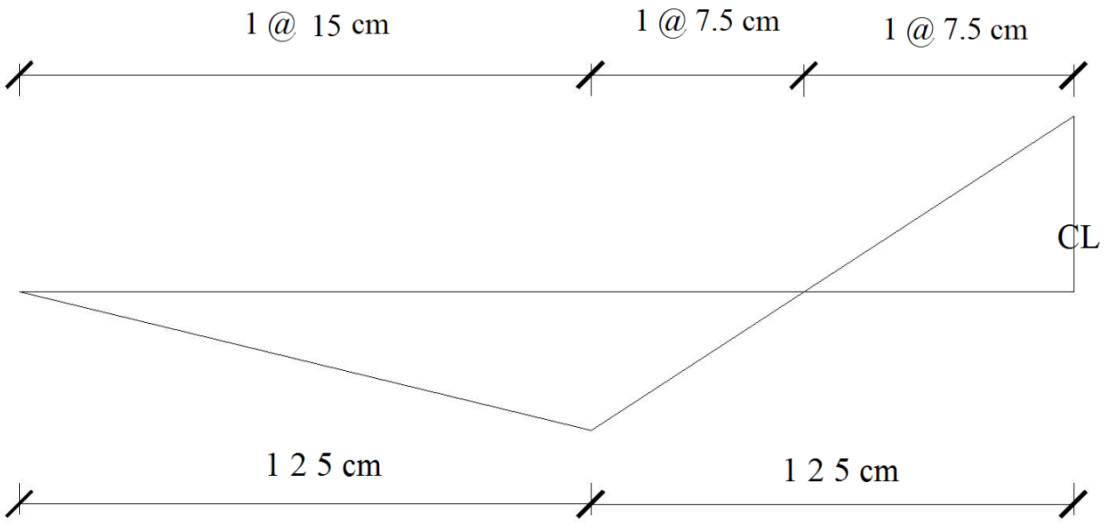

Fig. 3- 8 Distribution of shear studs according to the moment diagram

3.6 CHECK LOCAL BUCKLING AND LATERAL TORSIONAL BUCKLING

3.6.1 Check Local Buckling

Calculation of local buckling were conducted according to AISC manual [25]

For flange

$\frac{110/2}{8} = 6.88 \ < 0.38\sqrt{\frac{E}{Fy}}$ OK

For web

$\frac{184}{8} = 23 \ < 2.5\sqrt{\frac{E}{Fy}}$ OK

3.6.2 Check Lateral Torsional Buckling

At the positive moment region, the slab provided the required lateral support for the compression flange. However, at the negative moment region, lateral support is needed for the compression flange. The first plastic hinge at the interior support should have sufficient rotational capacity so that the second plastic hinge at mid-span could form. The maximum unbraced length to achieve the plastic capacity was calculated using the following equation which provided by AISC.

$$Lpd = \left(0.12 + 0.076\frac{M1}{M2}\right)\frac{E}{Fy}\, r_y \qquad \text{Equ. (3.11)}$$

L_{pd} = 2400 mm

r_y is the radius of gyration about y-axis

So that, only one lateral support is need at interior support

3.7 DESIGN OF WELDING

3.7.1 Design of Flange to Web Welding

The steel beam was designed as built up section, so proper welding according to the AISC manual should be provided to prevent failure of plate connections.

Plate thickness = 8.0 mm

AISC16.1.96: the maximum size of fillet weld edge of material > 6mm

Use 6 mm fillet weld E70

$$\emptyset R_{nw} = 0.75\left(0.707\left(\frac{a}{25.4}\right)\right)0.6xF_E \qquad \text{Equ. (3.12)}$$

$$\emptyset R_{nw} = 0.75\left(0.707\left(\frac{6}{25.4}\right)\right)0.6x70 = 5.26\frac{k}{in} = 922\ N/mm$$

For two faces, and for the critical distance of 570 mm between maximum negative moment and zero moment:

Max capacity = 922x2x570/1000 =1055 KN

Max shear = 0.85x28x500x70 + 110x8.0x248 =1050 <1055 KN OK

Use 6mm E70 for full length

3.7.2 Welding of Shear Connectors

Welding of shear connectors was designed for the full capacity of shear connectors. The full capacity of shear connectors is 105 KN.

Try 12mm fillet weld E70

$$\emptyset R_{nw} = 0.75\left(0.707\left(\frac{12}{25.4}\right)\right)0.6x70 = 10.52\frac{k}{in} = 1842\ N/mm$$

Max capacity = 1842 x2x π x 9.5 =110 KN > 105 OK

3.8 CHECK CONCENTRATED LOAD

Steel plates were needed over supports and under the point load to prevent web local buckling and web crippling.

Web local buckling was checked according to the AISC manual [25]

$$\emptyset Rn = (5k + N) f_{rw} t_w \qquad \text{Equ. (3.13)}$$

$(5x0.3346 + N)36x\ 0.3346 = \frac{500}{4.45(1.5)}$ Assume P_{ult} = 450 KN conservatively

Use plates of N= 30 cm for internal support and 11 cm width

Use plates of N= 15 cm for external support and 11 cm width

Use 16 mm plate thickness for both internal and external supports

Note: web local yielding controls, web crippling is not the critical

3.9 CHECK SHEAR DESIGN

Shear diagram at ultimate plastic load is shown in Fig. (3-19). The capacity of section (web) to resist shear force, V_{steel}, calculated according to the AISC manual [25] as follows:

V_{steel}= 0.6 x(248x8.0x200)= 238 KN > V_{ult}

$V_{ult\ (plastic)}$ = 150 KN (Maximum point load is 265 for girder with 3 layers of CFRP)

The capacity of steel section for shear is higher than ultimate shear, and safe to carry higher load in case that experimental ultimate load is higher than calculated one.

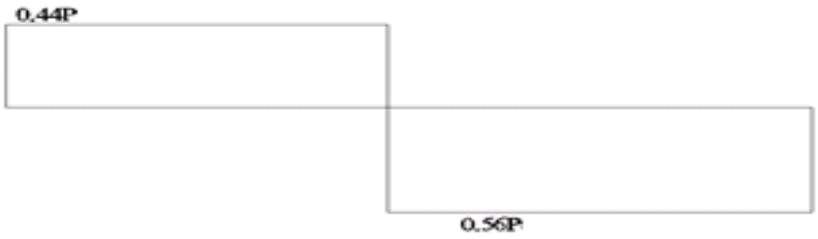

Fig. 3- 9 Shear diagram at full plastic load (one span in view)

CHAPTER FOUR

EXPERIMENTAL INVESTIGATION

4.1 INTRODUCTION

Two-span continuous composite girders were investigated experimentally in this study. This chapter presents a detailed description of testing the composite girders. The experimental investigation included testing of mechanical properties of materials, and shear strength of the interface elements. It included also all preparation and instrumentation steps that conducted to prepare the composite girders, and testing of girders up to failure. The experimental program included the following:

1. Mechanical properties of Materials.
    a. Mechanical properties of concrete.
    b. Mechanical properties of structural steel and steel reinforcement.
    c. Mechanical properties of CFRP.
    d. Shear strength of CFRP epoxy.
    e. Shear strength of shear studs.
2. Full-scale continuous composite girders testing.

4.2 MECHANICAL PROPERTIES OF MATERIALS

4.2.1 Mechanical Properties of Concrete

Three tests were conducted for concrete according to ASTM specifications [26] .The three tests are

1. Compression test.
2. Indirect tensile test.
3. Three points bend test.

4.2.1.1 Concrete compression test

Cylindrical specimens were prepared and tested according to ASTM C39 standard to get the compressive strength of concrete. 75 X 150 mm cylinders (ratio of height to diameter is 2) were cast and cured for 28 days as shown in Fig. 4-1 and Fig. 4-2. Sulfur capping was applied to get smooth surface before testing of cylinders. Two types of compression test were conducted:

a. Normal Compression test to find the ultimate strength, stress-strain diagram, poissons' ratio, and modulus of elasticity of concrete (6 cylinders).
b. Loading-unloading compression test to get plastic strain (2 cylinders).

Fig. 4- 1 Preparation of concrete cylinders for compression test

Fig. 4- 2 Hardened concrete cylinders for compression test

Two longitudinal and two transverse strain gauges were fixed to each cylinder to obtain the mechanical properties of concrete as shown in Fig. 4-3. The first six cylinders were loaded at a rate of 0.1 mm per min (displacement control) up to the failure as shown in Fig. 4-4.

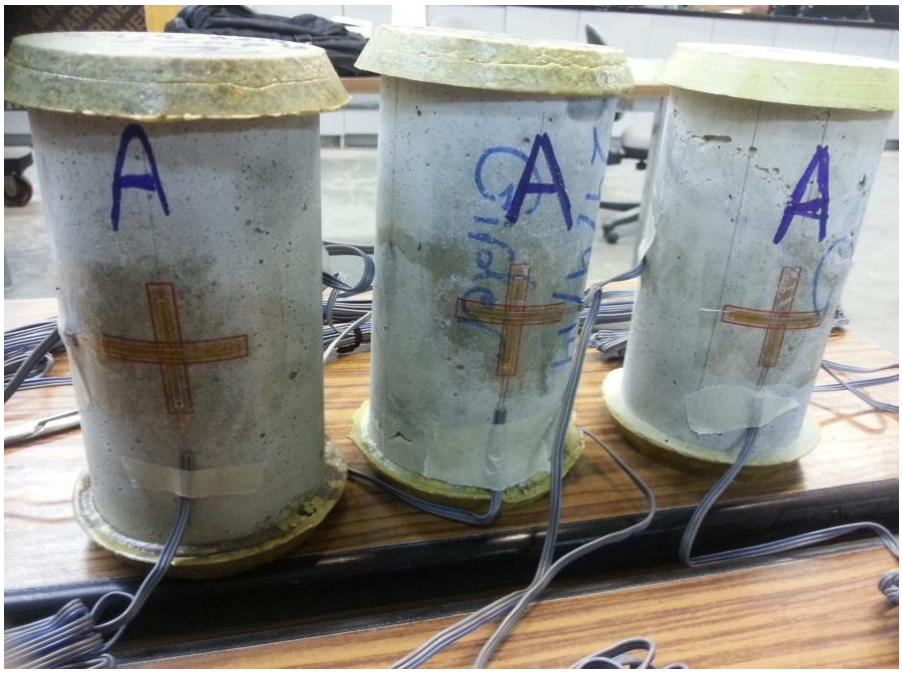

Fig. 4- 3 Fixing strain gauges on concrete cylinders

Fig. 4- 4 Concrete failure under compression test

The readings of strain gauges were used to obtain the stress-strain diagram of concrete as illustrated in Fig.4-5. The obtained mechanical properties of concrete are summarized in Table 1, and the design properties are summarized in Table 2 based on average and standard deviation.

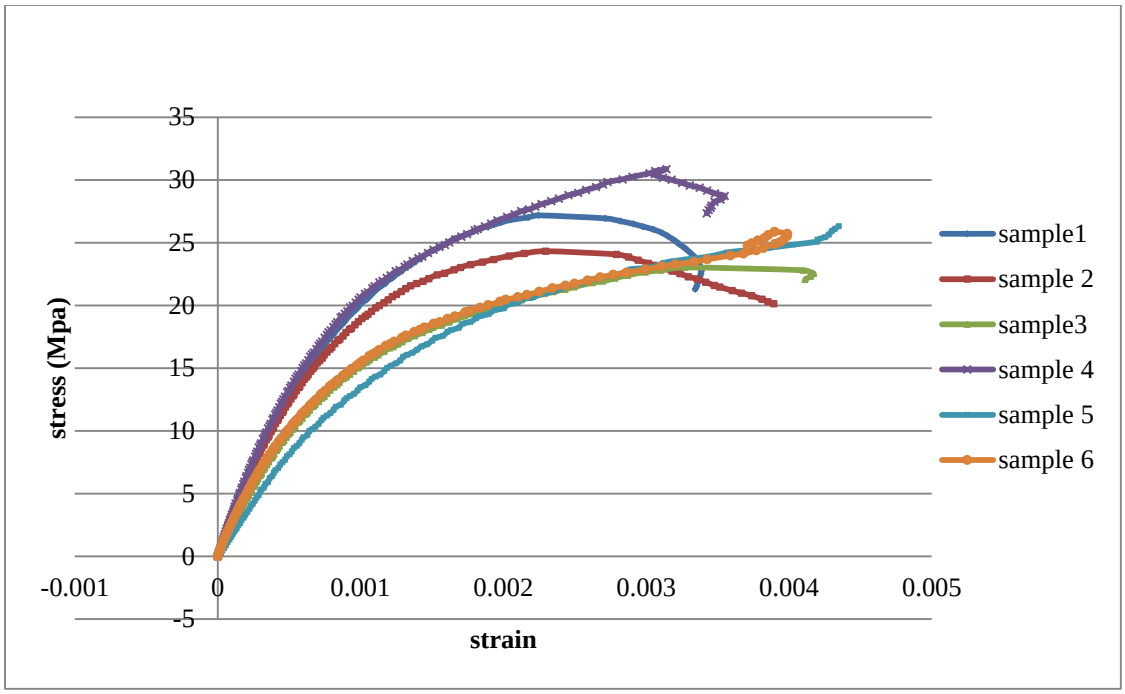

Fig. 4- 5 Stress-strain diagram of concrete

Table 1 Mechanical properties of concrete

Specimen	Ultimate strength (MPa)	Poissons'ratio	Modulus of elasticity (MPa)
Specimen 1	27.2	0.206	28347
Specimen 2	24.4	0.207	28194
Specimen 3	23.1	0.182	20292
Specimen 4	30.9	0.191	30144
Specimen 5	26.8	0.190	17090
Specimen 6	25.9	0.217	21638

Table 2 Design properties of concrete

Mechanical property	**Design value**
Ultimate strength (MPa)	26.4
Modulus of elasticity (MPa)	23800
Poissons' ratio	0.2
Strain at ultimate load	0.0028
Strain at failure	0.0037

The volumetric strain calculated to measure the dilatation of the concrete. Fig. 4-6 shows the volumetric change of concrete. Volumetric strain could be calculated as follows:

$$\varepsilon_{\upsilon} = \frac{\Delta V}{Vo} = \varepsilon_{\alpha} + 2\,\varepsilon_{l} \qquad \text{Equ. (4-1)}$$

Where:

ε_{α} is the axial strain

ε_{l} is the lateral strain

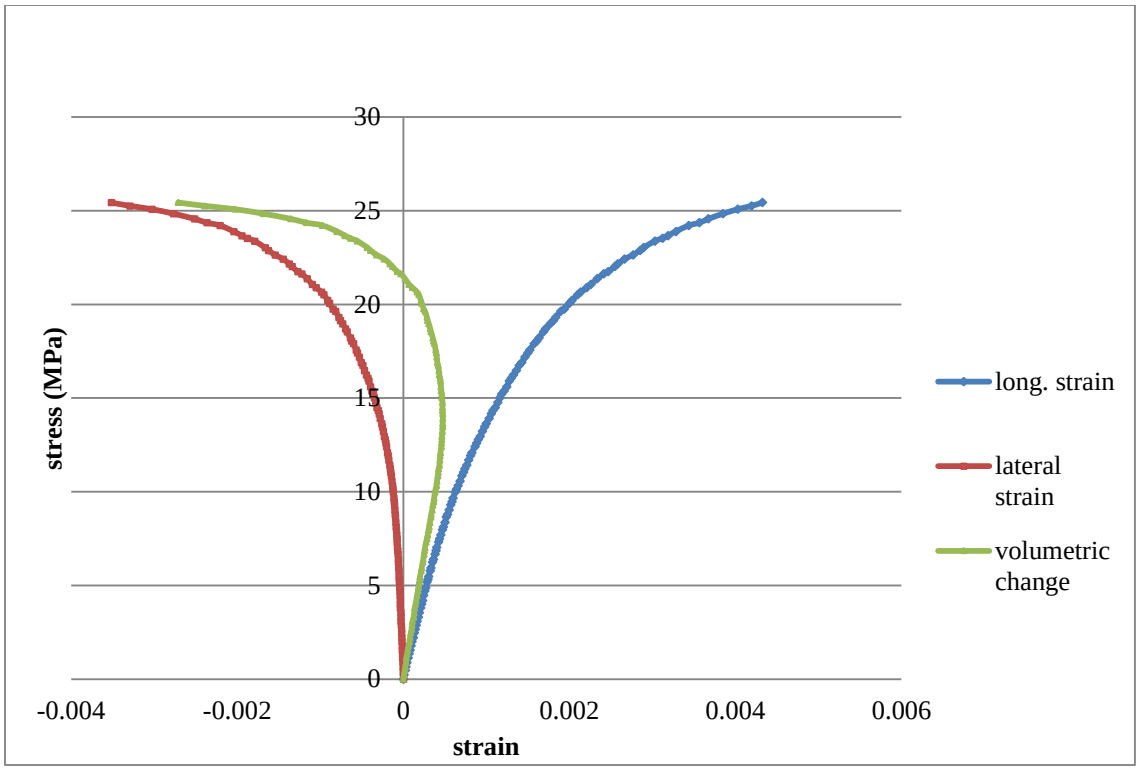

Fig. 4- 6 Volumetric change of concrete

Loading and un-loading compression test was carried out to find the plastic strain as stress in concrete increases. This will help to investigate level of plastic strain at failure point of girders as well as used in FE modeling. Fig. 4-7 shows the stress-strain diagram of concrete under loading-unloading compression test.

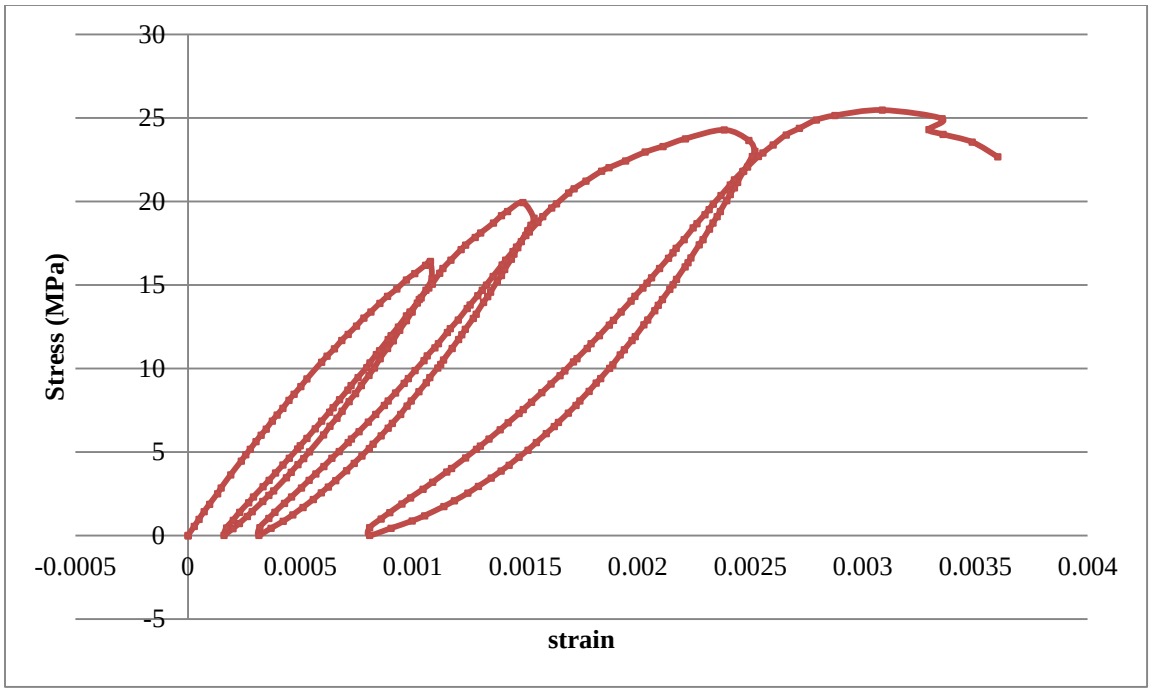

Fig. 4- 7 Loading-unloading compression test

4.2.1.2 Indirect tensile test

Indirect tensile test was conducted to find the tension capacity of concrete. This will be combined with a tension model to be used in FE modeling. This test conducted according to ASTM C496 standards. Three 150 X 300 cylinders were tested to find the tension strength of concrete. The split test conducted using universal ELE compression testing machine. The load was applied at a rate of 0.5 KN/s. Table 3 summarizes the results and tension capacity of concrete. Fig. 4-8 shows schematic view of in direct tension test.

Table 3 Results summary of indirect tension test of concrete

Cylinder	Force (KN)	Indirect tension strength (MPa)
Cylinder 1	53.9	3.05
Cylinder 2	56.7	3.21
Cylinder 3	53.8	3.10
Average		3.12

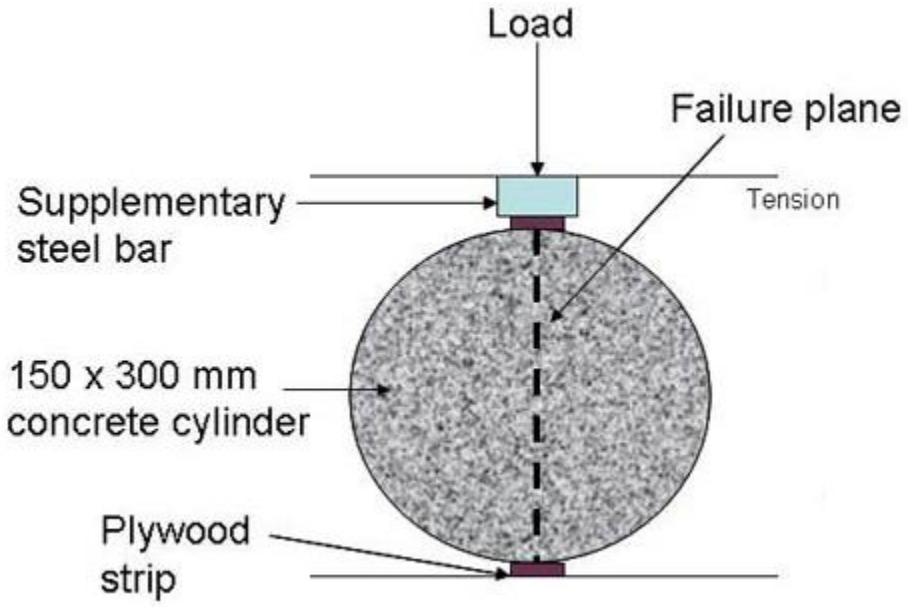

Fig. 4- 8 Schematic view of indirect tension test of concrete cylinder

4.2.1.3 Three points bend test

Three points bend test used to find the flexural strength of concrete as well as modulus of ruptured. Six specimens of 40X40 mm cross section and 160 mm length were prepared, cured, and tested according to ASTM C293 specifications. Fig. 4-9 shows profile set-up whereas testing of specimens is shown in Fig. 3-10. The effective span was taken as 110 mm.

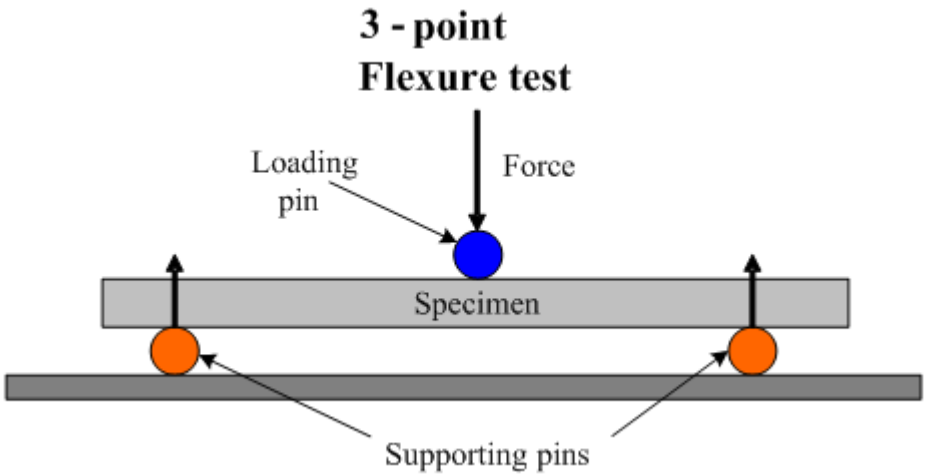

Fig. 4- 9 Three points bend test

Fig. 4- 10 Testing of concrete under 3-point bend test

Data logger used to record loads and displacements up to specimen rupture. Those information were used to find flexural strength and modulus of rupture based on the following formulae. Final results are summarized in Table 4.

$$ft = \frac{M\,Y}{I} \qquad \text{Equ. (4-2)}$$

$$E_t = \frac{PL^3}{48\,I\,\delta} \qquad \text{Equ. (4-3)}$$

Where:

ft is the modulus of Rupture

M is the applied moment

Y is the distance from the neutral axis to the extreme tension

I is the moment of inertia

P is the applied load

L is the beam length

E_t is the tensile elastic modulus

δ is the deflection under the point of load

Table 4 Summary results for 3-point bend test

Specimen	Modulus of Rupture (f_t) (MPa)	Tensile Elastic Modulus (E_t) (MPa)
Beam 1-1	4.84	13684.65
Beam 1-2	4.26	12895.91
Beam 1-3	64.72	20425.23
Beam 1-4	6.44	15624.17
Beam 1-5	5.45	14427.65
Beam 1-6	5.90	20159.82
Average	5.72	16203.1

4.2.2 Mechanical Properties of Structural steel and steel Reinforcement

The tensile strength and stress-strain diagram of steel are important to visualize behavior of composite girder as well as ultimate strength. Steel coupons were prepared and tested according to the ASTM standards. ASTM A770 standards were followed for testing the steel plates. Two orthogonal strain gauges were fixed to the necked part of the plates to measure the longitudinal and lateral strain of steel. Steel plates were loaded up to the failure point. Fig. 4-11 shows profile and testing of steel plates.

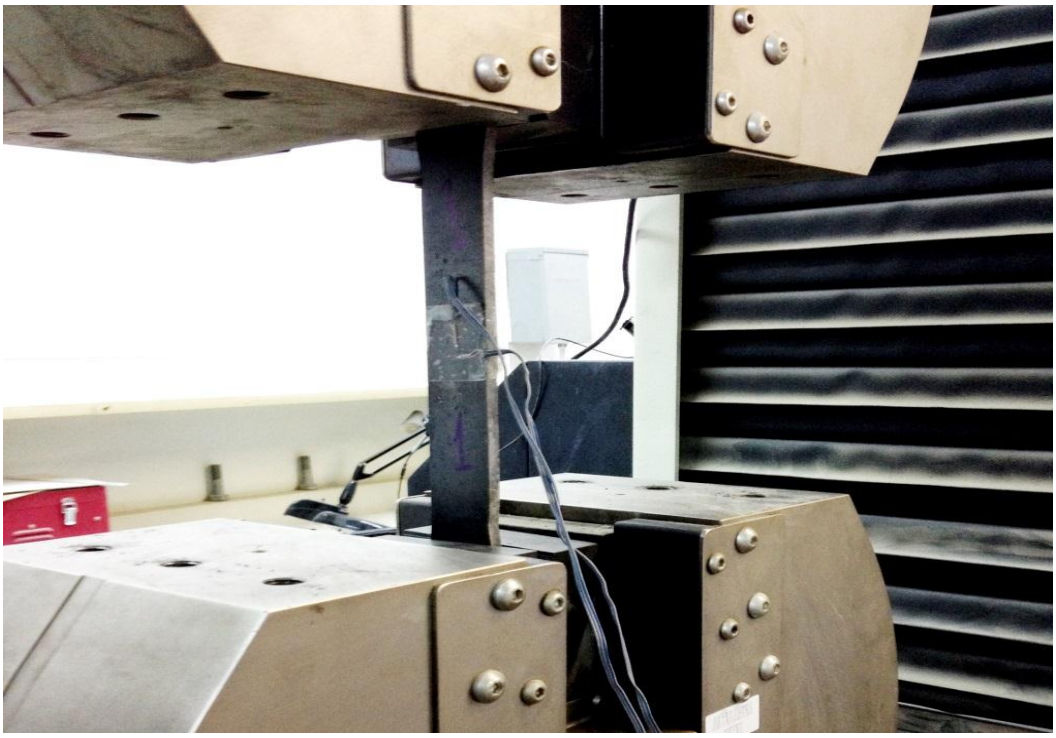

Fig. 4- 11 Tensile test of steel plate

The obtained values of loads and strains were used to plot stress-strain diagram of steel. Fig. 4-12 shows stress-strain diagram of steel which used to find the yielding strength, ultimate strength, and modulus of elasticity of structural steel. Table 5 summarizes mechanical properties of structural steel and Fig. 4-13 shows longitudinal and lateral strain as well as volumetric change of steel.

Table 5 Summary of tension test results for steel plates

plate	Yield strength (MPa)	Ultimate strength (MPa)	Yield strain	Modulus of elasticity (GPa)	Poissons' ratio
Plate 1	284.4	434	0.00142	202	0.29
Plate 2	281.5	428	0.00141	205	0.292
Plate 3	268	430	0.00135	208	0.2898
Average	278.0	430.7	0.0014	205	0.29

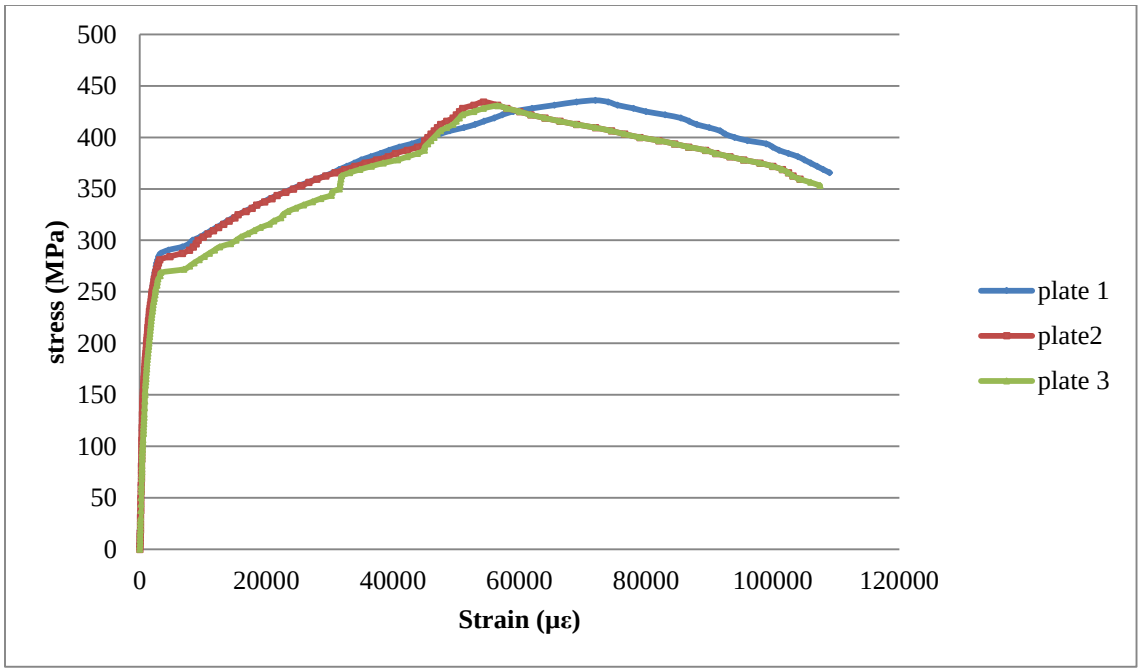

Fig. 4- 12 Stress-strain diagram of structural steel

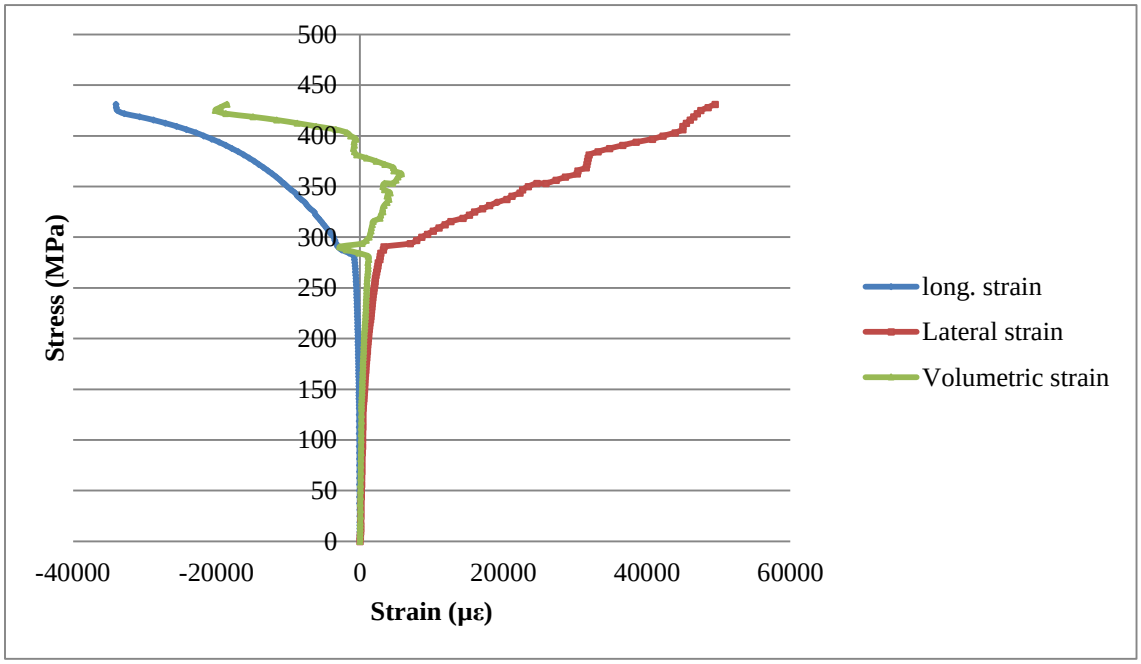

Fig. 4- 13 Volumetric change of structural steel

Steel reinforcement bars of 8 mm diameter were used as longitudinal and lateral reinforcement in concrete. Mechanical properties of steel reinforcement were obtained by preparing and testing steel reinforcement specimens according to the ASTM standards. ASTM A615 standards followed for testing the steel bars as shown in Fig. 4-14. Two orthogonal strain gauges were fixed to measure the longitudinal and lateral strain of steel reinforcement. Caliber used to measure the exact diameter of bars as summarized in Table 6. Mechanical properties obtained from the test are tabulated in Table 7.

Table 6 Diameter and cross sectional area of the tested steel bars

Steel bar	Bar diameter (mm)	Area (mm^2)
Sample 1	7.5	44.16
Sample 2	8.0	50.4
Sample 3	8.0	50.4

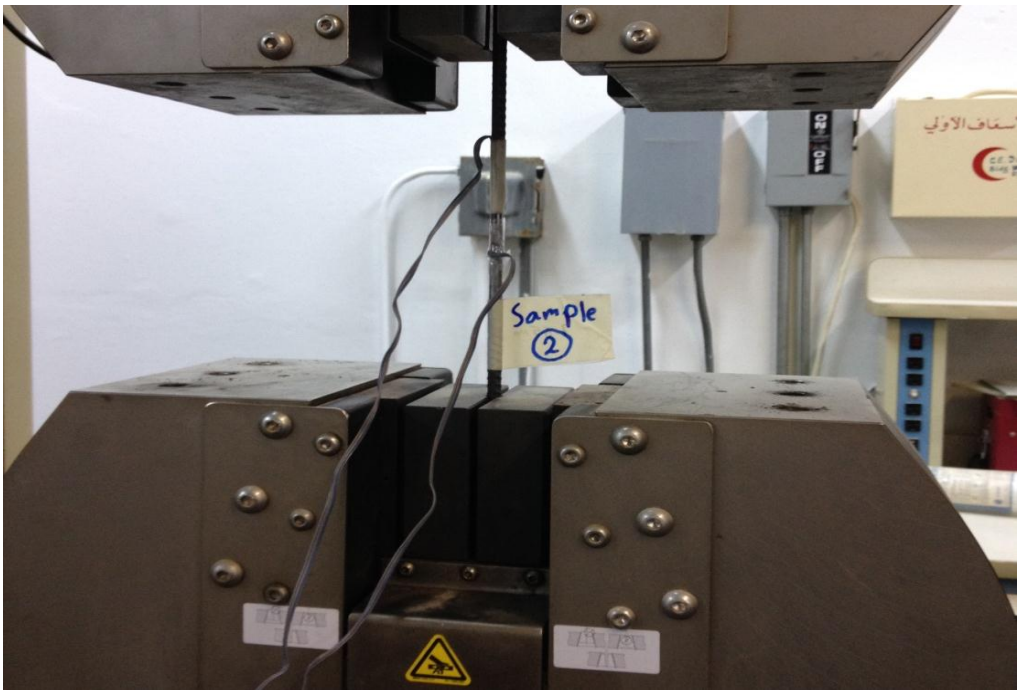

Fig. 4- 14 Tensile test for steel reinforcement bar

The stress-strain diagram of steel bars was obtained as shown in Fig. 4-15, then it used to obtained properties and tensile strength of bars, and will be used in FE modeling.

Table 7 Summary results of tension test of steel reinforcement bars

Steel bar	Yield strength (MPa)	Ultimate strength (MPa)	Yield strain	Poissons' ratio	Modulus of elasticity (GPa)
Sample 1	416	601	0.00203	0.305	209
Sample 2	437	585	0.00214	0.299	204
Sample 3	400	618	0.00196	0.298	201
Average	**417.7**	**601.3**	**0.00205**	**0.30**	**205**

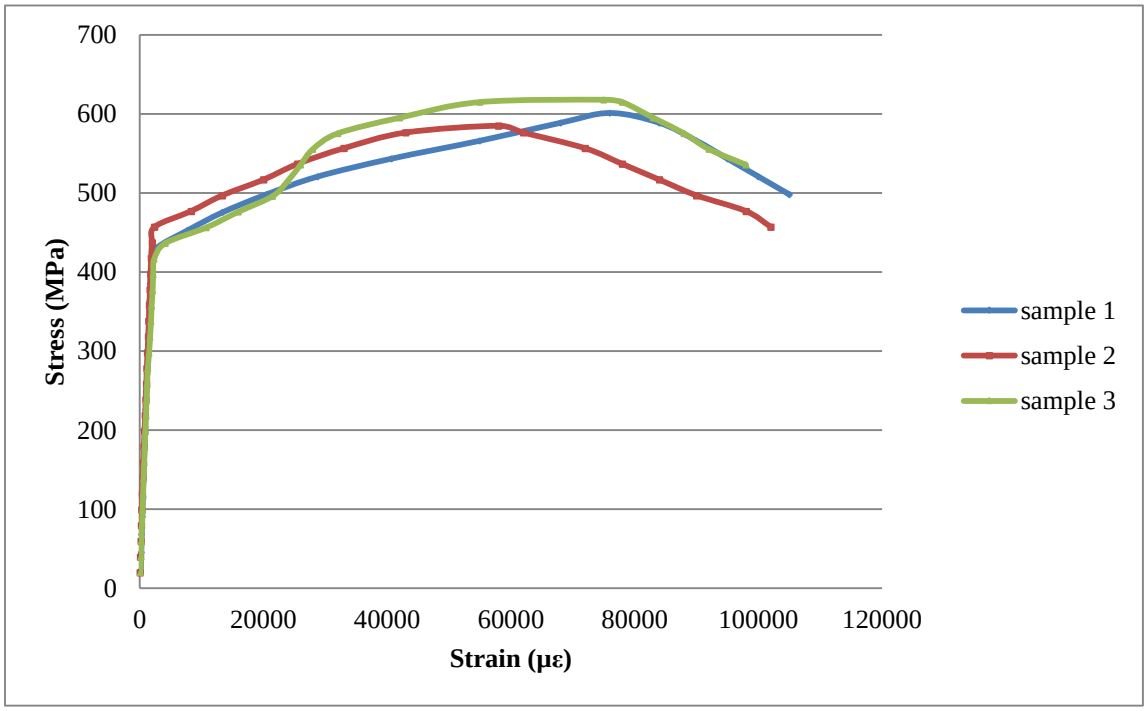

Fig. 4- 15 Stress-strain diegram of steel reinforcement bar

4.2.3 Mechanical Properties of CFRP

CFRP used was Grade 230 Nitowrap FRC whose mechanical properties are listed in Table 8. The tensile strength of CFRP was obtained from the manufactory, and checked by a tension test of CFRP coupon.

Table 8 Mechanical properties of CFRP

Thickness (mm)	Width (mm)	Design Tensile strength (MPa)	Ultimate design strain	Modulus of Elasticity (GPa)	Density (gm/cm3)
0.131	500	3483	0.015	232.2	1.8

4.2.4 Strength of Epoxy Adhesive

Nitowrap primer base and Nitowrap hardener, mixed according to the company specifications (2 base: 1 hardener), formed the used epoxy adhesive for bonding CFRP to the concrete. The shear strength measured using pull-out test as shown in Fig. 16. Strain gauges were fixed to the CFRP and epoxy as shown in the same figure. The rate of loading was 1 mm/min, and epoxy adhesive failure (de-bonding) was obtained as shown in Fig. 17.

Total of five strain gauges were fixed to the specimen, three fixed to the CFRP whereas the other two fixed to the bonded CFRP by epoxy adhesive. In pull-out test, the strain readings of the bonded area were measuring actually slip between the two materials [27, 28], whereas the other strain gauges are measuring strain in CFRP. This test provided the maximum stress in CFRP up to failure; rupture failure of CFRP or de-bonding. The results were used to plot average shear stress vs slip for epoxy adhesive (Fig. 18) and stress-strain diagram for CFRP up to de-bonding (Fig. 19).

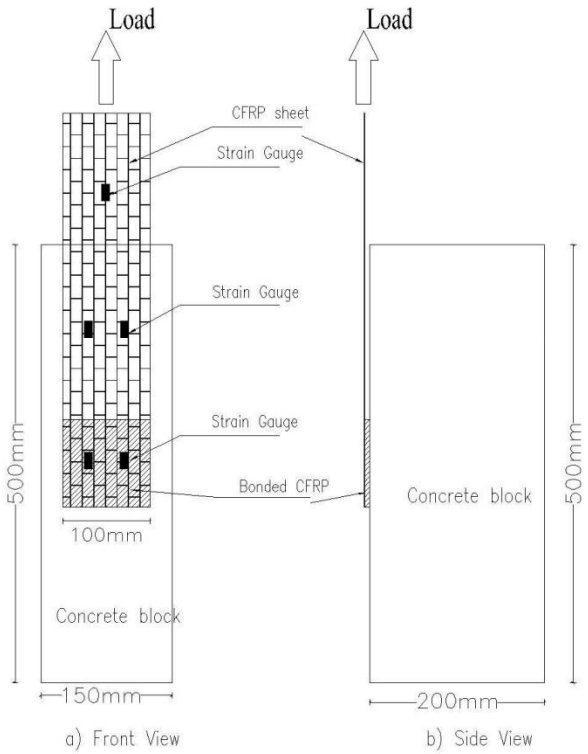

Fig. 4- 16 Schematic view of pull-out test for epoxy adhesive

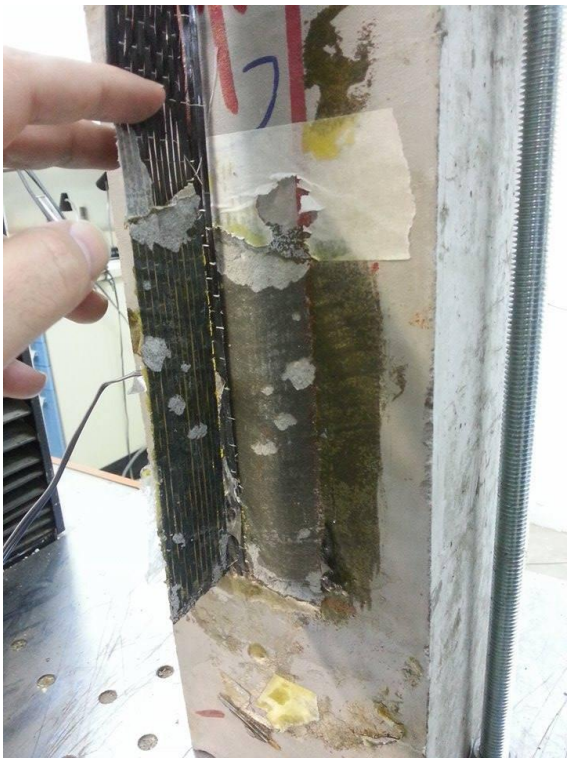

Fig. 4- 17 De-bonding of CFRP

Analysis of pull-out test showed that CFRP de-bonding is the expected failure of CFRP sheets bonded to the top of concrete slab of girders rather than rupture of CFRP. This is because de-bonding occurred first. The epoxy adhesive strength (shear strength) was 2 MPa but it behaved elastically up to 1.4 MPa. At failure of epoxy adhesive, the stress in CFRP is 1526 MPa (strain is 0.0067) which indicated that epoxy adhesive strength controls the behavior of CFRP matrix (CFRP and epoxy adhesive). The shear stress vs slip curve will be analyzed further in FE modeling

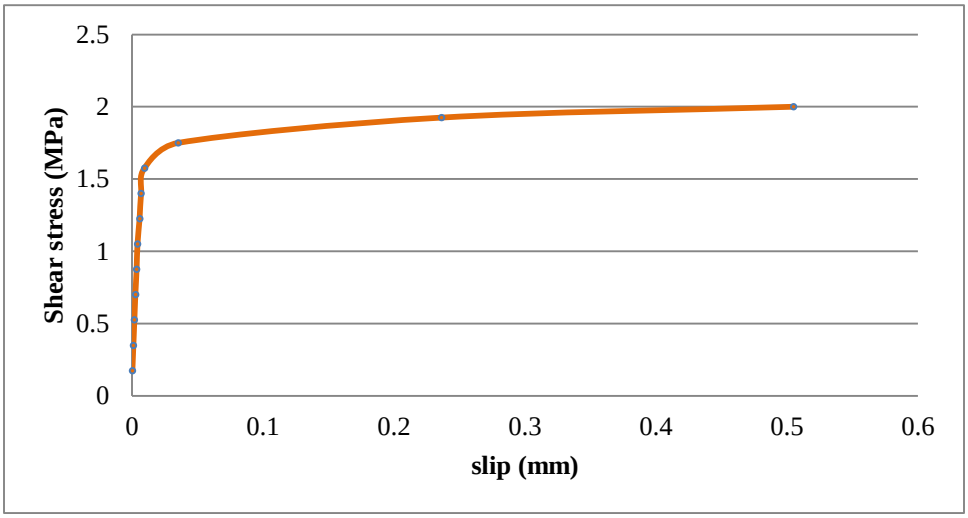

Fig. 4- 18 Shear stress vs slip of epoxy adhesive

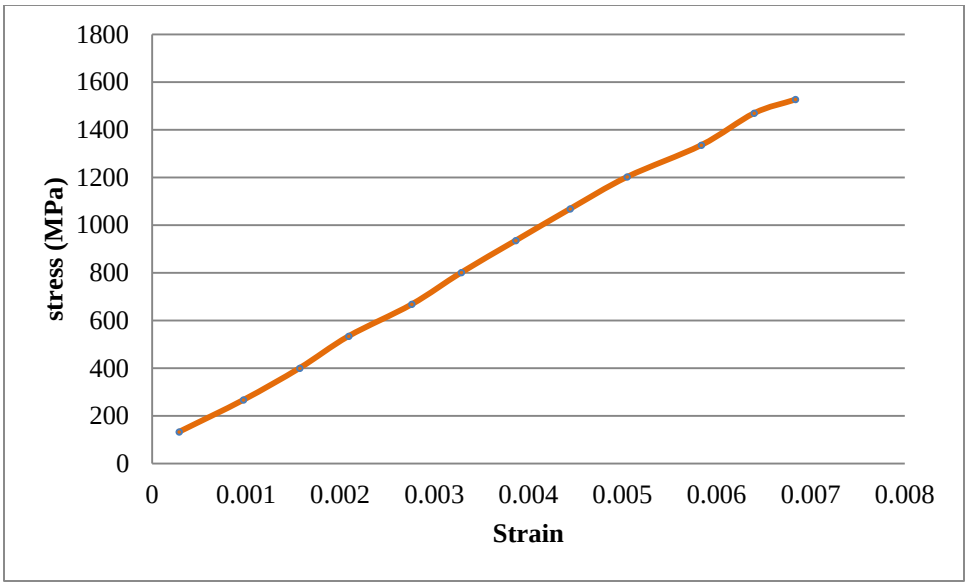

Fig. 4- 19 Stress-strain diagram of CFRP

4.2.5 Shear Strength of Shear Studs

The shear capacity of shear studs was measured by two-way push-out test. Steel section with two shear studs at each side was cast with concrete as shown in Fig. 4-20. LVDT was fixed at the bottom of steel section to measure the slip as shown in Fig. 4-21, whereas the opposite end of steel section as loaded at a rate of 1mm/ min. Shear failure in concrete that splitting the concrete was the mode of failure that observed as shown in Fig. 4-22. This shows that the ultimate shear capacity of the shear studs controlled by concrete failure.

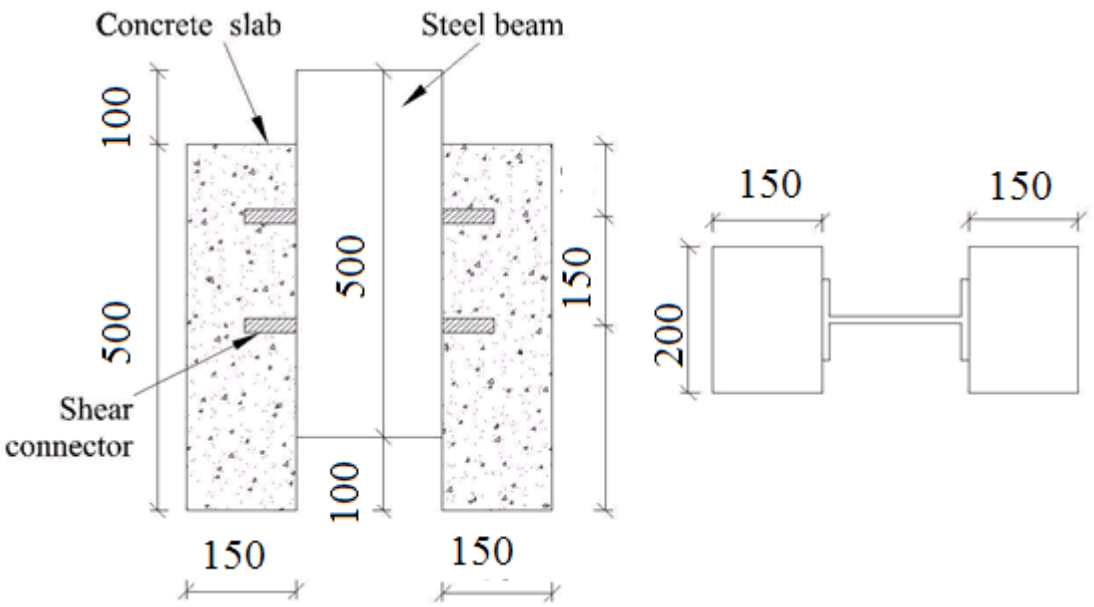

Fig. 4- 20 Schematic view of two-way push-out test (dimensions are in mm)

Fig. 4- 22 Failure of concrete in push-out test

Fig. 4- 21 Testing of shear studs

The load-slip curve for the shear studs is illustrated in Fig. 4-23 to reflect the shear capacity of shear studs. The shear strength of each shear studs is 70 KN. This curve will be used to estimate the slip of the composite girders as well as in FE modeling.

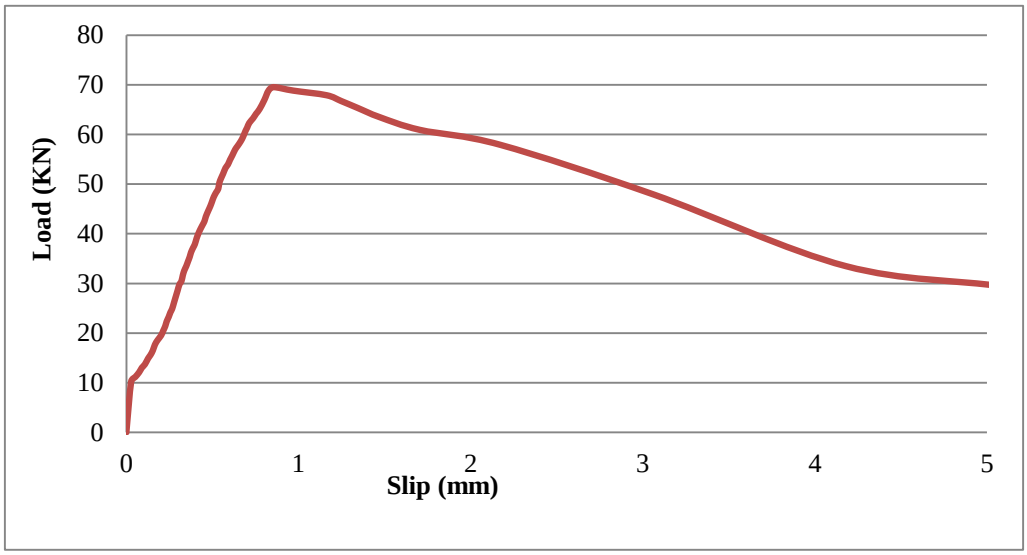

Fig. 4- 23 Load-slip curve for shear studs

4.3 FULL-SCALE CONTINUOUS COMPOSITE GIRDERS TESTING

The continuous composite steel-concrete girders composed of built-up steel section, and casted concrete slab. Preparations of the composite built-up steel concrete girders were carried out by a professional manufactory in Dammam as will discuss in section 4.3.1. After finalizing the steel-concrete girder, CFRP sheets bonded to the top of concrete for all girders except reference girders. The following sections present detail description of the preparation and instrumentation of composite girders in addition to the testing set-up.

4.3.1 Preparations and Instrumentations of Girders

This section includes preparations of steel section, casting concrete slab, and bonding CFRP to the concrete slab. At the same time, fully description of all instruments that fixed to the composite girders for measurements are included also.

4.3.1.1 Preparation of steel girders

The steel section composed of steel flanges, web, and stiffeners that welded together according to welding design specifications which conducted in chapter three. Full length welding was conducted at stages to avoid buckling of plates due to heat of welding as shown in Fig. 4-24. Steel stiffeners were welded also to the steel web and flange by partial length welding. After completion of steel beam welding, shear studs were welded to the top of the steel flange according to the weld size calculations which conducted before. Spacing and welding of shear studs are shown in Figs. 4-25a & 4-25b, and the final built-up steel section with shear studs is shown in Fig. 4-26.

Fig. 4- 24 Welding of steel plates and finalizing steel beam

a. **Over the interior support** **b. at mid-span**

Fig. 4- 25 Shear studs spacing

Fig. 4- 26 Finalized steel beam

4.3.1.2 Finalizing the composite girders

Following to the welding of the built-up steel beam, the steel beams were fixed along with the framework as shown in Fig. 4-27. Longitudinal and transverse steel reinforcement were fixed using spacers of 35 mm top to the steel flange as shown in the same figure.

The concrete was cast as shown in Fig. 4-28, and damped using shaking machine before smoothen the concrete surface to have proper surface. Standard cylindrical concrete samples were molded according to the ASTM specifications to be used for material testing. Curing of concrete slab applied for 28 days. The composite steel-concrete girders transferred to the Lab to apply the CFRP sheets and to provide the required instruments before testing. The finalized steel-concrete composite girders are shown Fig. 4-29.

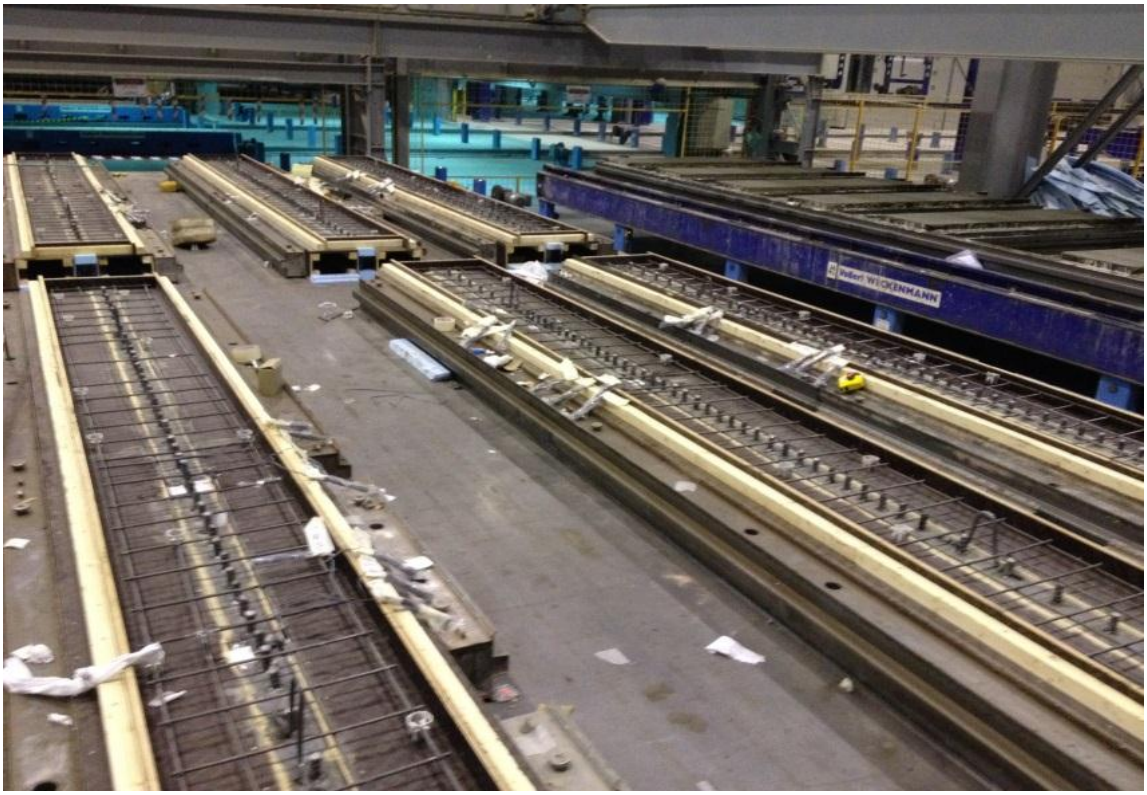

Fig. 4- 27 Preparation of steel beam for casting

Fig. 4- 28 Pouring of concrete slab

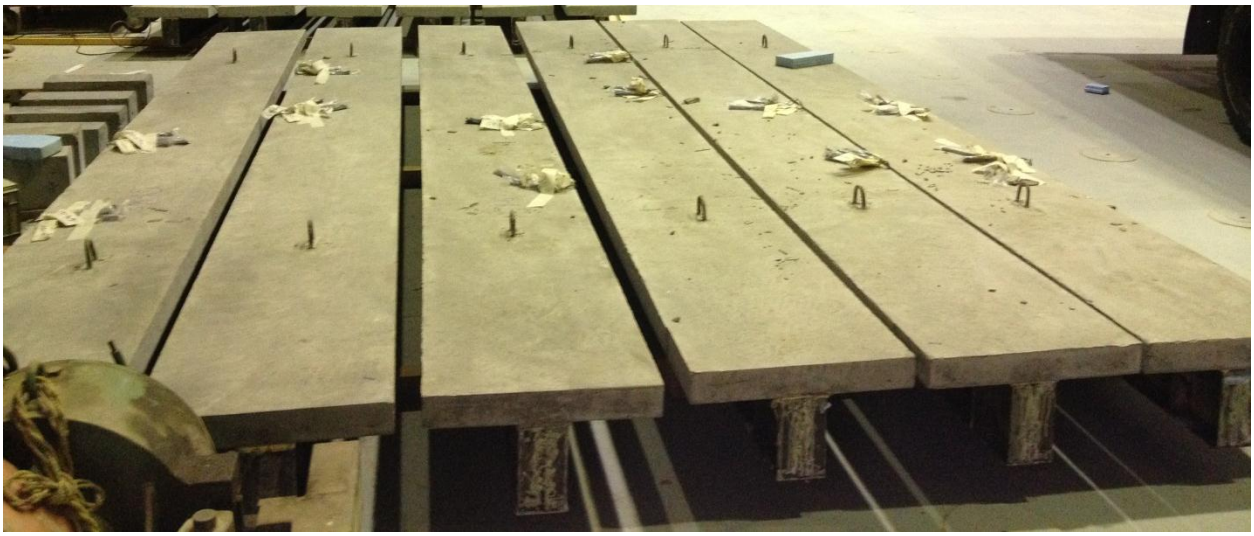

Fig. 4- 29 Composite steel-concrete girders

4.3.1.3 Bonding of CFRP to the Concrete Slab

CFRP sheets was bonded to the top of concrete slab at the negative moment region and extended for an adequate development length. The length of CFRP was taken according to ACI specifications [29] for girders with one or more number of CFRP layers as shown in Figs. 4-30a & 4-30b. Extension of CFRP by 150 mm from each side beyond the inflection point is required by ACI for use of one layer of CFRP. Additional extension of 150 mm is required for each layer increase. Concrete surfaces were roughened and cleaned by removing the surface laitance and ensuring dry flat and sound surface before CFRP fabrics were bonded to concrete slab. Epoxy adhesive was applied to fully cover the prepared concrete surfaces, then CFRP fabrics were firmly laid on the concrete slab and left to cure for one week before testing. Primer adhesive was mixed according to the specifications by the manufactor (2 base: 1 hardener).

Rounding of edges of the concrete slab was carried out for composite girders which wrapped by CFRP at mid-span region. Rounding of edges is required by ACI to provide effective confinement of concrete.

a. **One layer of CFRP** **b. Two layers of CFRP**

Fig. 4- 30 Applying CFRP to the concrete slab

4.3.1.4 Fixing strain gauges and LVDT's

Strain gauges were used to measure strains in concrete, steel and CFRP. FLA – 6 -11 – 3LT was used to measure strain in steel, PFL – 30 – 11 – 3LT for concrete and CFRP. Strain gauges were mounted to the steel flanges, steel web, top and bottom surface of concrete along both cross sections; mid-span and over the interior support. Because of stiffeners, strain gauges were fixed 200 mm to the right of mid-span and same over the interior support. Description of the location of the strain gauges for one of the girders with CFRP is illustrated in Fig. 4-31.

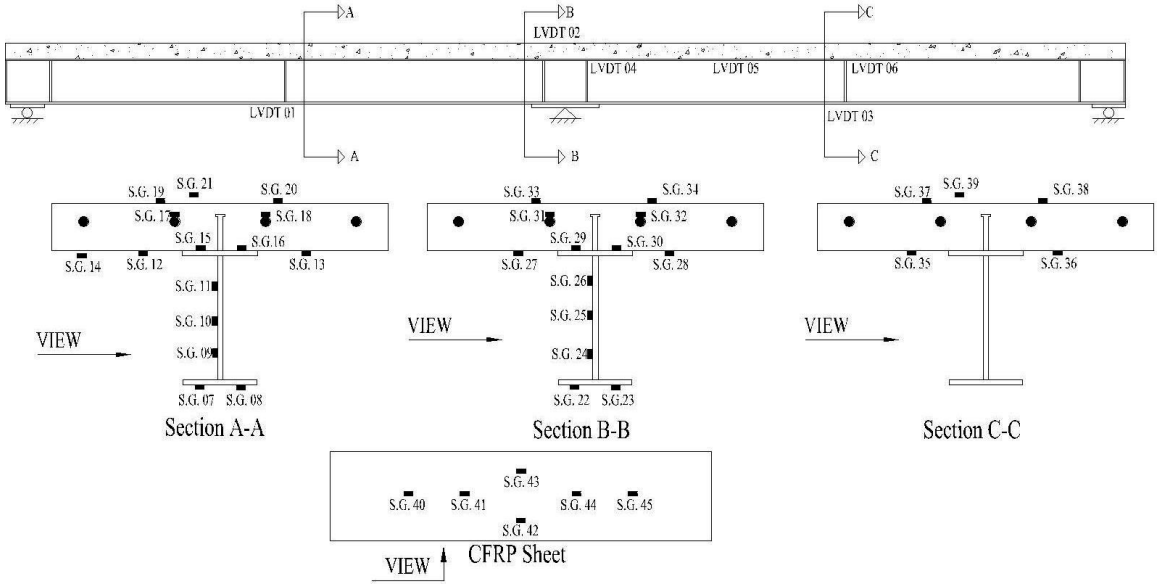

Fig. 4- 31 Location of strain gauges (S.G) and LVDT's

Prior to the casting of concrete slab, strain gauges were fixed to the steel reinforcement and top surface of the top steel flange at mid-span and over the interior support after smoothen the steel surface. Total of eight strain gauges were bonded to the steel reinforcements and top surface of the top steel flange. At mid-span, two strain gauges were bonded to the steel reinforcement as well as other two strain gauges bonded to the top of steel flange and similarly at the interior support as shown in Fig. 4-31a. All strain gauges were labeled before concrete casting to avoid any conflict later. Water proof used to protect strain gauges from damage and moisture as shown in Fig. 4-31b. The resistance of strain gauges was measured using voltmeter and compared with the specifications, before concrete casting as indicated in Fig. 4-32.

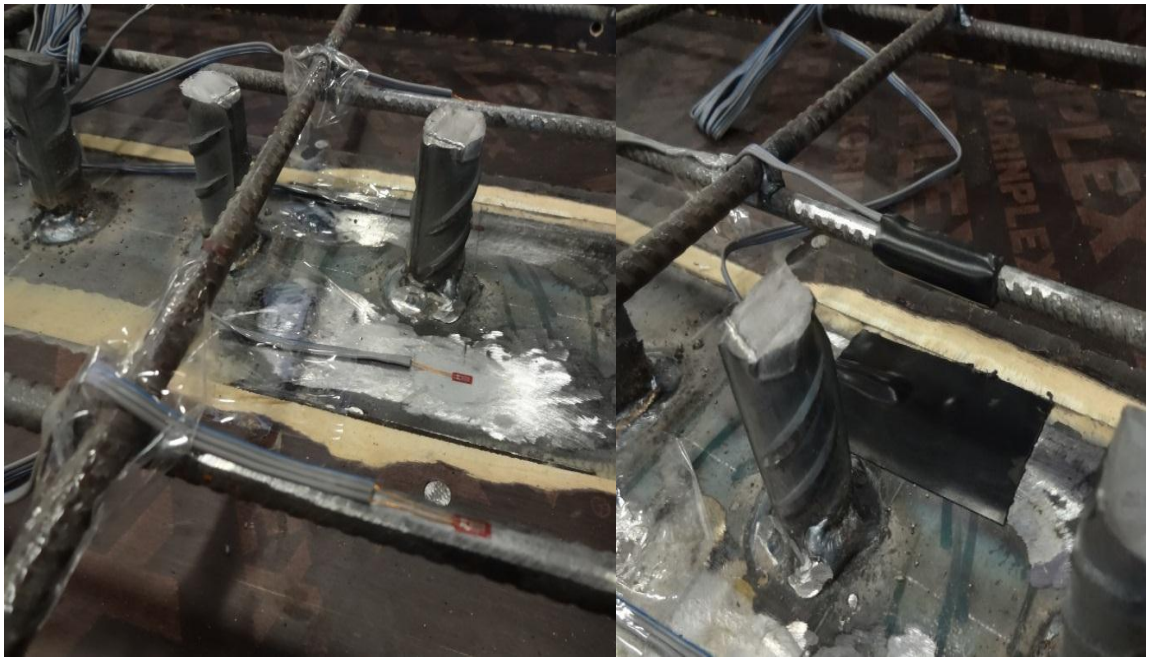

a. **Installing S.G to steel beam and reinforcement** **b. Protecting S.G using water proof**

Fig. 4- 32 Installing strain gauges prior concrete casting

Fig. 4- 33 Checking resistance of S.G using voltmeter

Linear variable differential transformers (LVDT's) were fixed to the steel-concrete girders to measure crack width and relative slip between concrete and top steel flange as illustrated in Fig.4-31. One LVDT was bolted to the top of concrete slab at the negative moment region to measure crack width as shown in Fig. 4-34. Concrete to steel slip at mid-span, inflection point, and over the interior support were measured by LVDT's as shown in Fig. 4-35. Those LVDT's were bolted into the bottom surface of concrete slab, and fixed to the top steel flange by a plate.

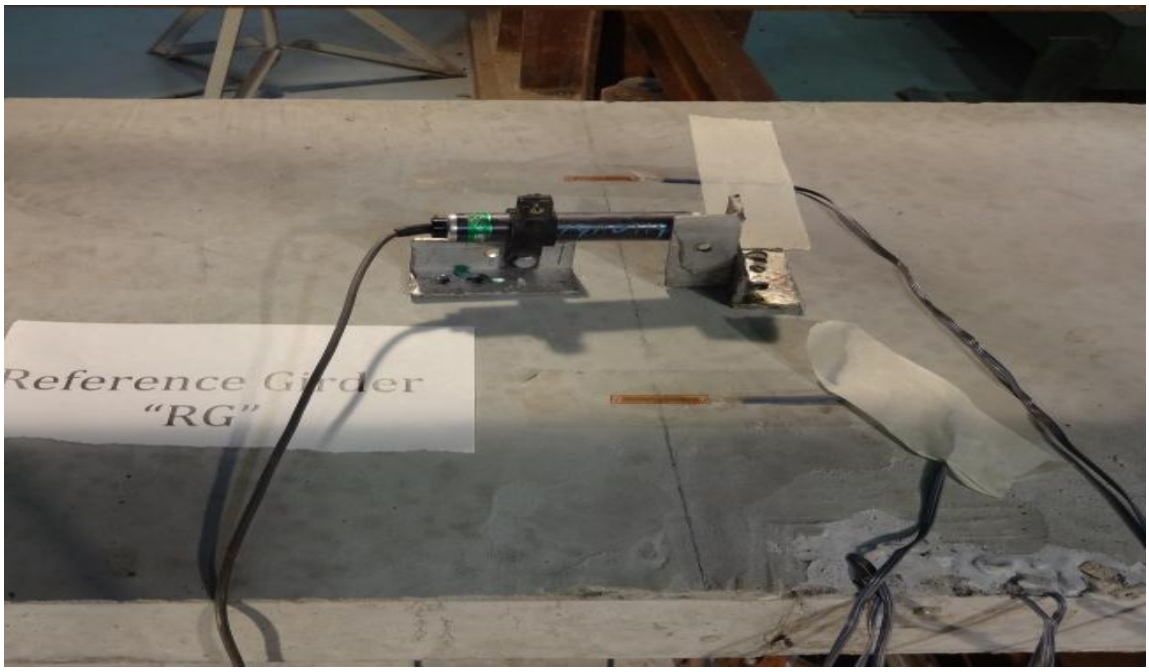

Fig. 4- 34 LVDT bolted to the top of concrete slab to measure crack width

Fig. 4- 35 LVDT's for measurement of steel-concrete slip

4.3.2 Testing Set-up

The complete set-up finalized before start testing. Loading cell, hydraulic jack, rigid beam to transfer jack load into two point loads at mid-spans were prepared. The composite girder was installed over support. Rigid beam was fixed over the composite girder to transfer the load followed by hydraulic jack and loading cell as shown in Fig. 4-36. All of these were installed under the testing frame as shown in Fig. 4-37. Lateral support (steel beam) provided at interior support to prevent lateral torsional buckling. The lateral support was fixed between loading frame and compression flange as shown in Fig. 4-38.

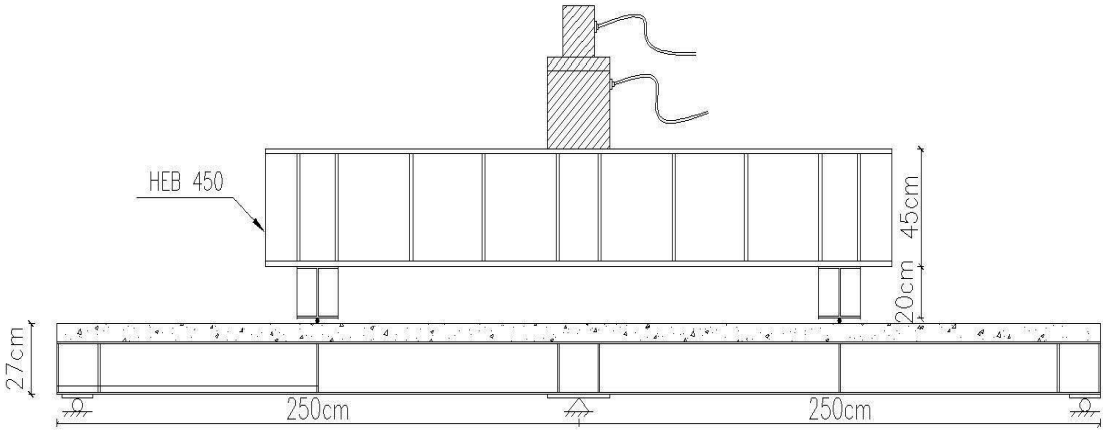

Fig. 4- 36 Schematic view of testing set-up

Fig. 4- 37 Testing of composite girder

Fig. 4- 38 Lateral support

The deflection at mid span under each step of loading was recorded using LVDT. This LVDT was connected to the bottom steel flange under each point load to measure the deflection as shown in Fig. 4-39.

Fig. 4- 39 Measuring mid-span deflection by LVDT

All strain gauges, load cell, and LVDT's were connected to the data logger. Testing of girders was conducted as a load control test and data logger programmed to record load step of TWO KN. The rate of loading varied between initial and final stage of loading. In average the loading rate was 1 KN/second. All the composite girders were tested up to the failure load or until recording reduction in the applied load.

CHAPTER FIVE

EXPERIMENTAL RESULTS AND ANALYSIS

Total of six composite girders were fabricated and casted. In the first phase, four girders, RG, G1, G2, and G3 are listed in Table 9 under group 1 were tested to evaluate the effectiveness of the use of CFRP at the negative moment region as shown in Fig. 5-1. Girder RG was fabricated without CFRP as the control girder, and the girders G1, G2 and G3 had varying thicknesses of CFRP that was bonded to the top of concrete slab as shown in Fig. 5-1.

For more enhancement of ultimate strength and utilization of CFRP at negative moment region, two additional girders, RGR and G2R (Table. 9) were tested as group II by wrapping the slab of theses girders with CFRP at the positive moment region as shown in Fig. 5-2. RGR without CFRP at the negative moment region was the control girder for group II and girder G2R had CFRP bonded to top of the concrete slab at the negative moment region. In other words, girder RGR had wrapping at the positive moment region and G2R had both the CFRP wrapping at the positive moment region and bonded CFRP sheet at the negative moment region. The thickness of CFRP used for the girders was the same as that of girder G2 of group I.

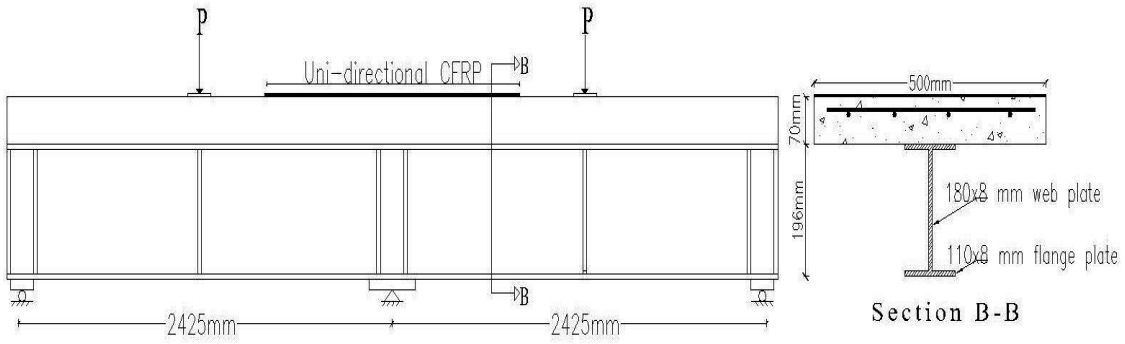

Fig. 5- 1 Composite girder bonded with CFRP at negative moment region

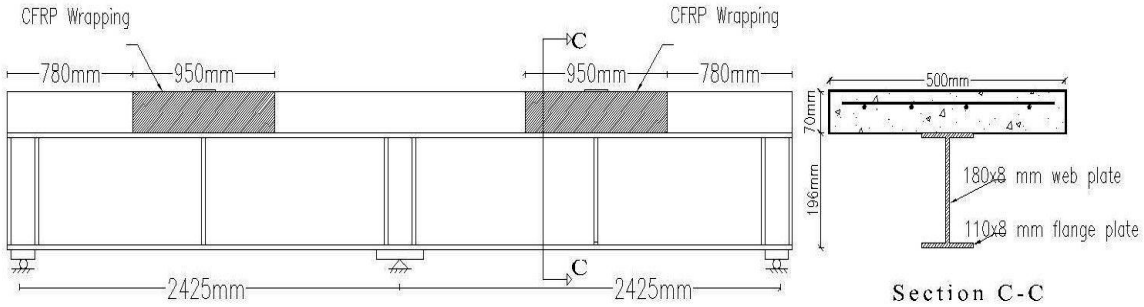

Fig. 5- 2 Composite girder wrapped with CFRP at mid-span

Table 9 Girder matrix

Group	Girder	Thickness of CFRP (mm)	Concrete slab wrapped with CFRP at positive moment region
I	RG	-	No
	G1	0.131	
	G2	0.262	
	G3	0.393	
II	RGR	-	Yes
	G2R	0.262	

5.1 COMPOSITE ACTION AT THE NEGATIVE MOMENT REGION

The loss of composite action at the negative moment regain for continuous composite girders reduces its strength and stiffness. This study aims to maintain the composite action at the negative region by use of CFRP top of concrete slab. The ability of CFRP sheets to maintain the composite action at the negative moment region is investigated experimentally in this section.

In this study, the cracking load, P_{cr} is defined as the load initiating cracks in concrete slab over the interior support. Yielding load, P_y, is defined as the upper limit of service load at which yielding of the bottom flange of the steel girder at mid span occurs. The ratio of cracking load to yielding load, λ, is taken as the indicator of the level up to which composite action should be maintained at the negative moment regain under service load to prevent premature cracking of the slab. The higher values of λ would indicate higher load level to cause cracking of the slab. The values of P_{cr} and P_y, recorded from test observations, are shown in Table 10 along with values of λ. Girders with CFRP bonded to the top of concrete slab at the negative moment region, G1, G2, G3 and G2R, recorded considerably higher value of P_{cr} and λ than those of the control girders RG and RGR. This clearly confirms that the proposed strengthening has maintained composite action at the negative moment region at load level closer to the maximum service load.

Table 10 Cracking load, yielding load and ratio of cracking to yielding loads for girders (Load presents sum of both point loads)

Group	Girder	P_{cr} (KN)	P_y (KN)	λ
I	RG	77	163	0.46
	G1	123	165	0.74
	G2	136	173	0.79
	G3	150	175	0.86
II	RGR	65	172	0.38
	G2R	150	182	0.82

The first crack in the two-span girders occurred transversely across the concrete slab over the interior support, and subsequent cracks were developed immediately adjacent to the first crack. Beyond the service load (yielding of bottom steel flange at mid-span), the CFRP sheets were able to confine the crack width in concrete at negative moment region up to the ultimate load. The crack width of control girders (RG, RGR) was higher than other girders bonded with CFRP at negative moment zone for all stage of loading as illustrated in Fig. 5-3. Prior to the ultimate load, control girders were developed excessive increase in crack width, whereas the use of CFRP sheets limited the crack width. Figs. 5-4 and 5-5 show the concrete cracking at ultimate load for girder RGR and G2 respectively.

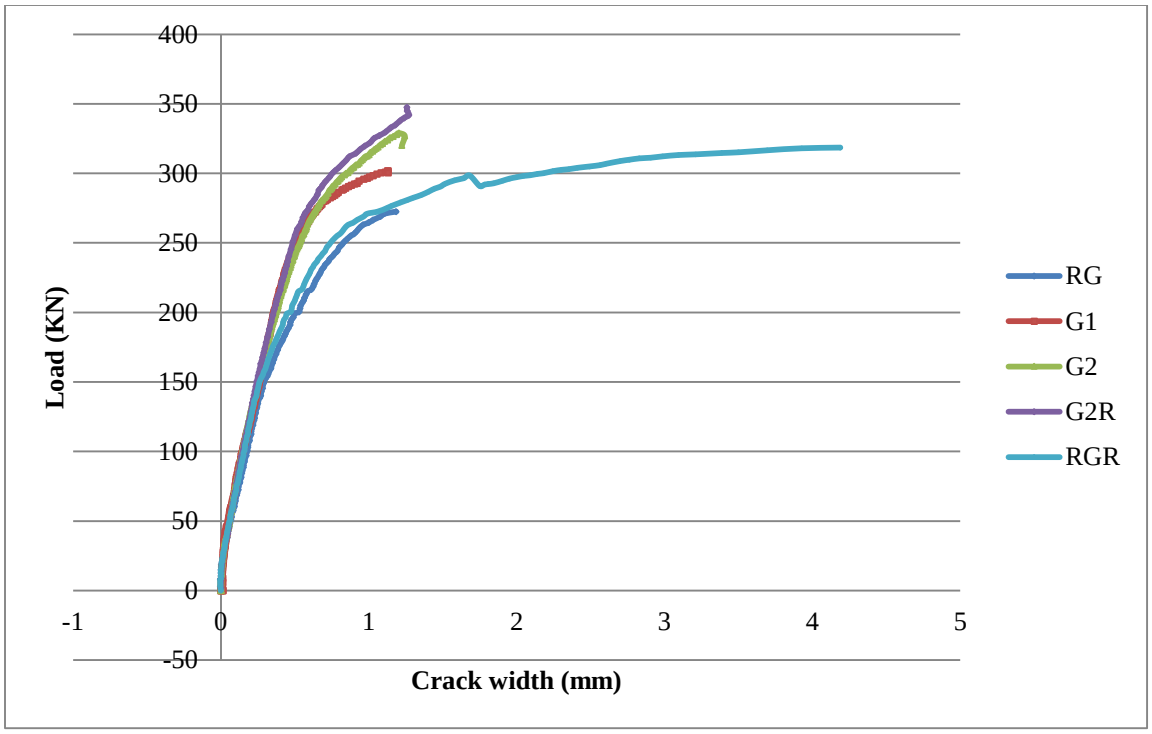

Fig. 5- 3 Concrete crack width at negative moment region

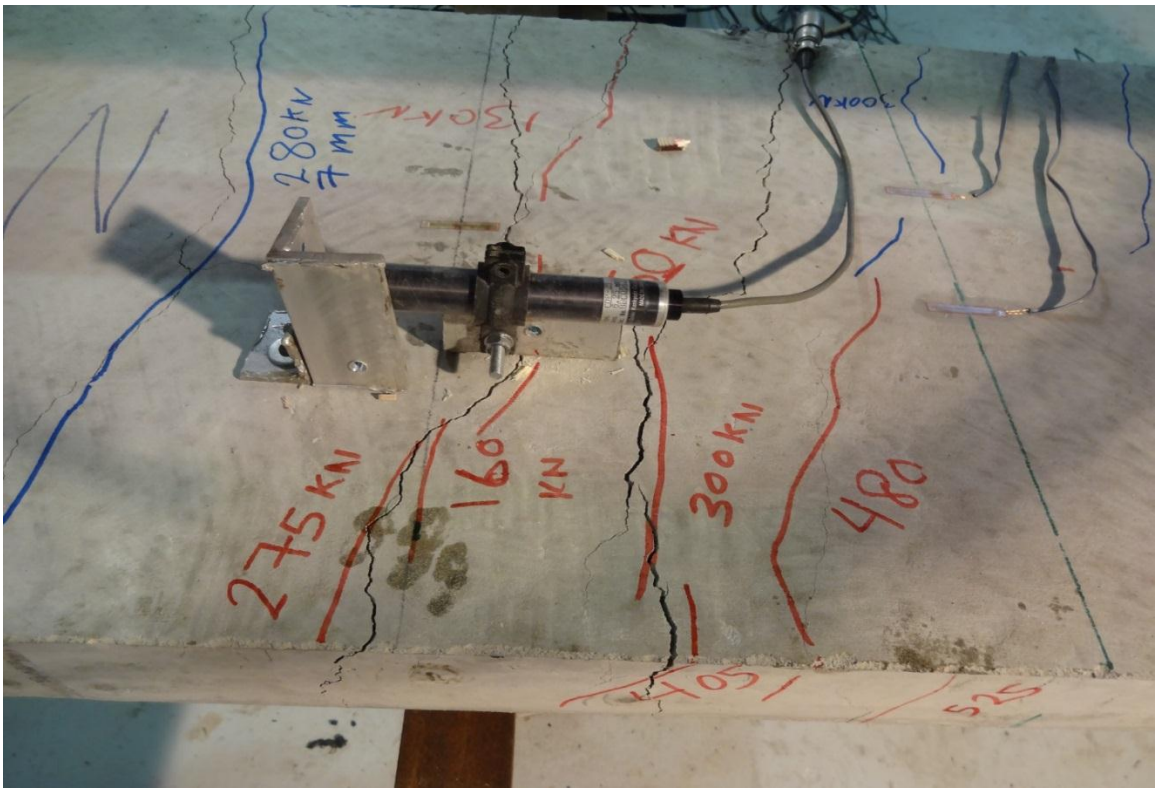

Fig. 5- 4 Concrete cracks at ultimate load for girder RGR

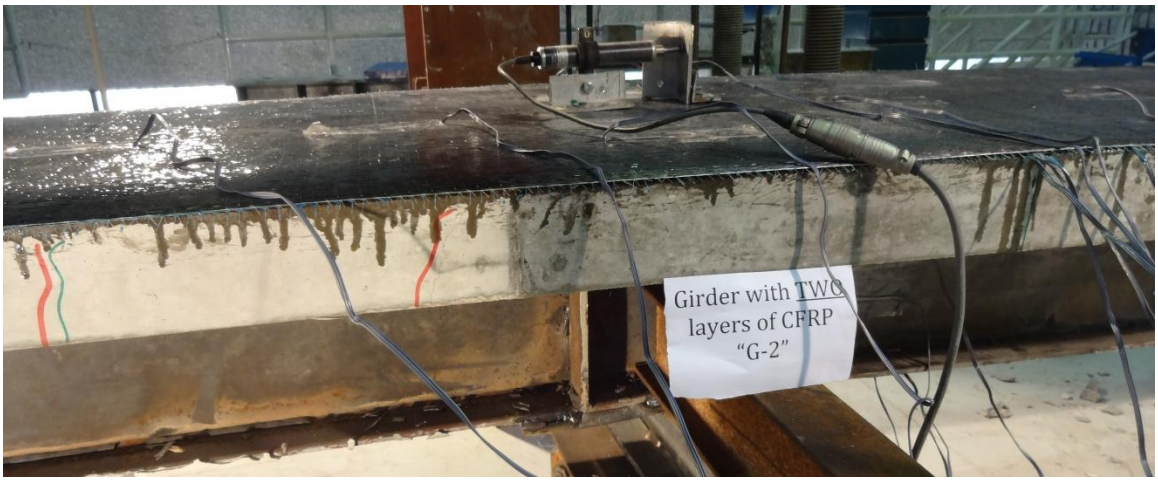

Fig. 5- 5 Concrete cracks at ultimate load for girder G2

5.2 BEHAVIOR AND ULTIMATE MOMENT CAPACITY OF COMPOSITE GIRDERS

The use of CFRP sheets to the top of the concrete slab at the negative moment region aims to maintain the composite action and increase the flexural capacity of continuous composite girders. This section is presenting the behavior of composite girders bonded with CFRP sheets, and the effect of CFRP on the ultimate capacity of girders.

All girders exhibited linear and nonlinear behavior as noted from load-deflection plots shown in Fig. 5-6, the latter is occurring soon after the load causing tension yielding of the bottom flange plate at mid-span. The improvement in strength and stiffness of the girders due to CFRP inclusion can be observed from Fig. 5-6.

The loads corresponding to the yielding of the flange plate at the mid-span and at the interior support, as observed from the measurements of strains, are listed in Table 11 for all girders RG, G1, G2, and G3. The yield load at the mid-span was lower than that load caused yielding of the bottom flange plate at the support because of the upward shift of

the neutral axis at mid-span due to full composite action. At a load P higher than the yield load (e.g. 228 KN for RG), the yielded part of the beam section underwent strain hardening (Fig. 4-12) causing the section to rotate inelastically at the interior support. The resulting bending moment distribution for the girders as such was influenced by a major increase in the positive moment and only a marginal increment in the negative moment. The use of CFRP produced only a small change in the yield loads (Table. 11), though it increased P_u considerably (Fig. 5-6).

The inelastic rotation of the girders at support due to post-yield load was caused by yielding of the significant part of the steel section as evidence from the measured strains at the ultimate load as shown in Figs. 5-7 and 5-8.

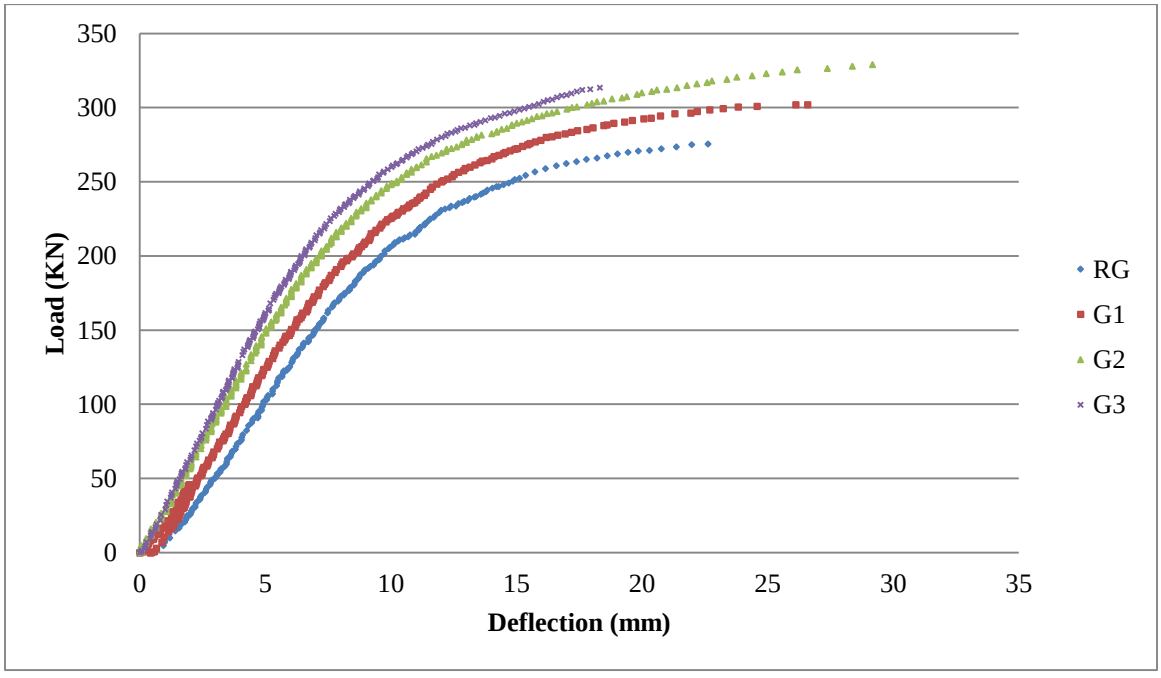

Fig. 5- 6 Load-deflection curve of girders in group I

Table 11 Load corresponds to yielding of steel section (KN)

Girder	RG	G1	G2	G3
Cracking Load	75	122	136	150
Yielding of bottom flange (mid-span)	163	165	173	175
Yielding of bottom flange (interior support)	228	225	222	249
Yielding of top flange (interior support)	240	255	260	263
Ultimate Load	273	303	330	314

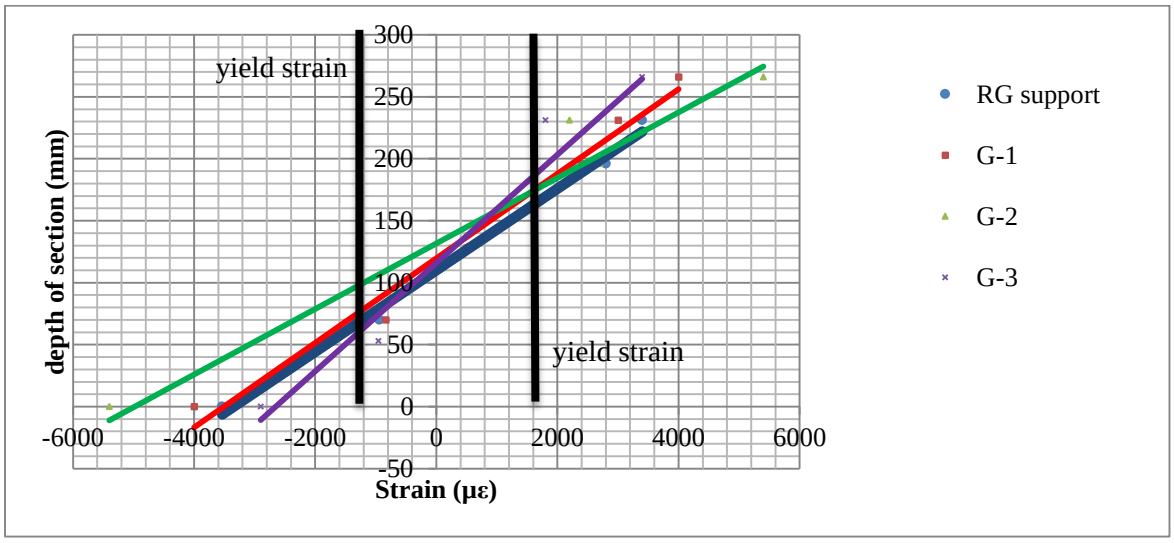

Fig. 5- 7 Strain distribution at interior support for group I at ultimate load

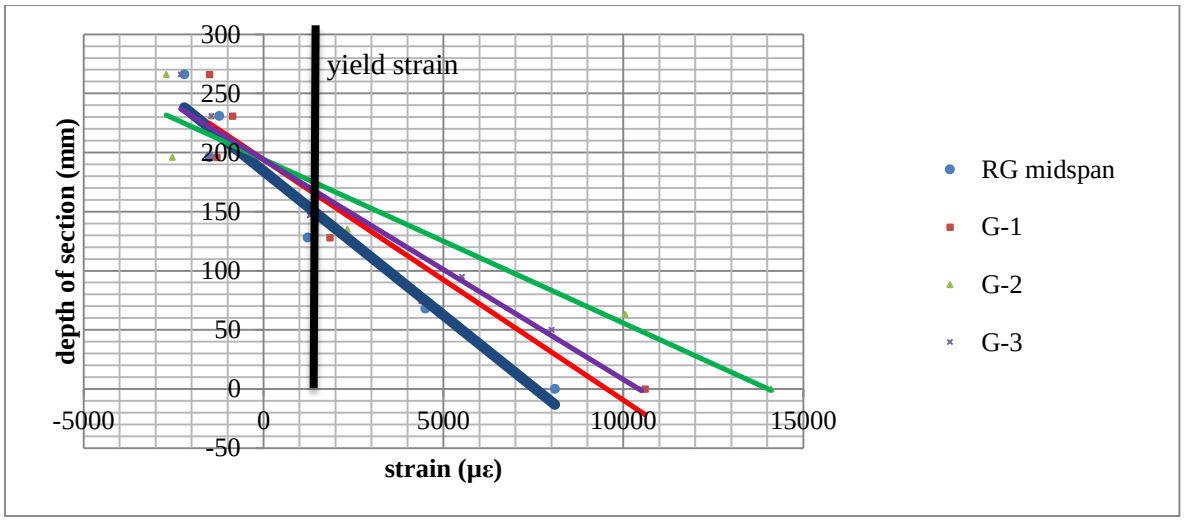

Fig. 5- 8 Strain distribution at mid-span for group I at ultimate load

The strain distribution along the cross section at mid-span an at interior support indicated linear behavior of girders prior to yielding of bottom steel flange as illustrated in Figs. 5-9 and 5-10. The strain distribution showed negligible effect of CFRP on composite section prior to yielding of bottom steel plate at mid-span

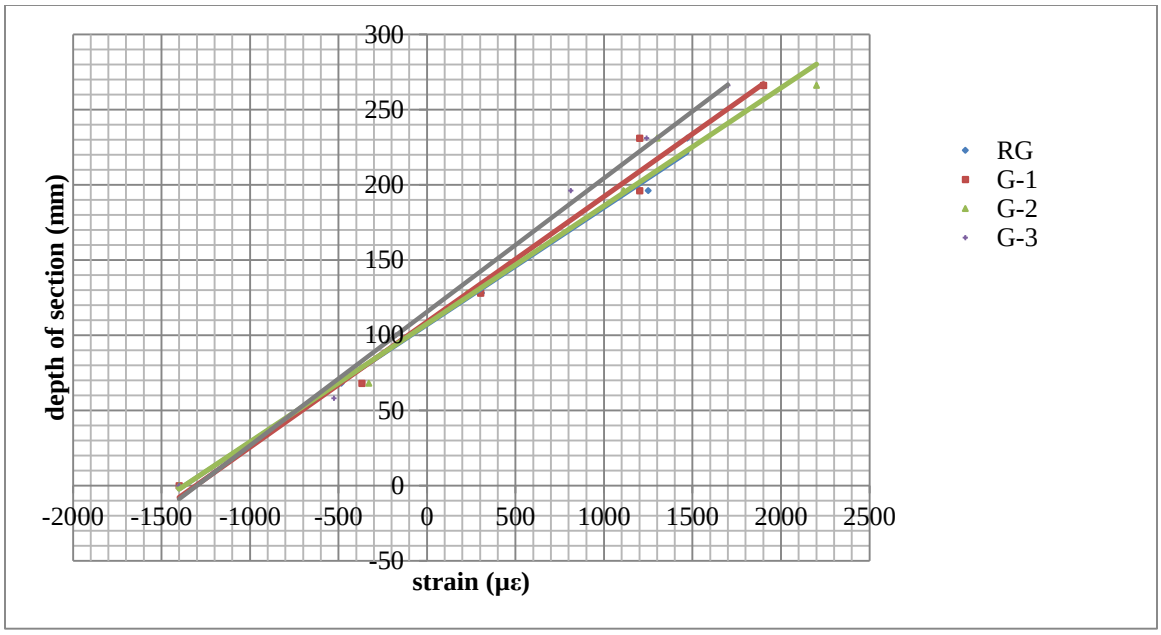

Fig. 5- 9 Strain distribution over the interior support for group I at yielding load

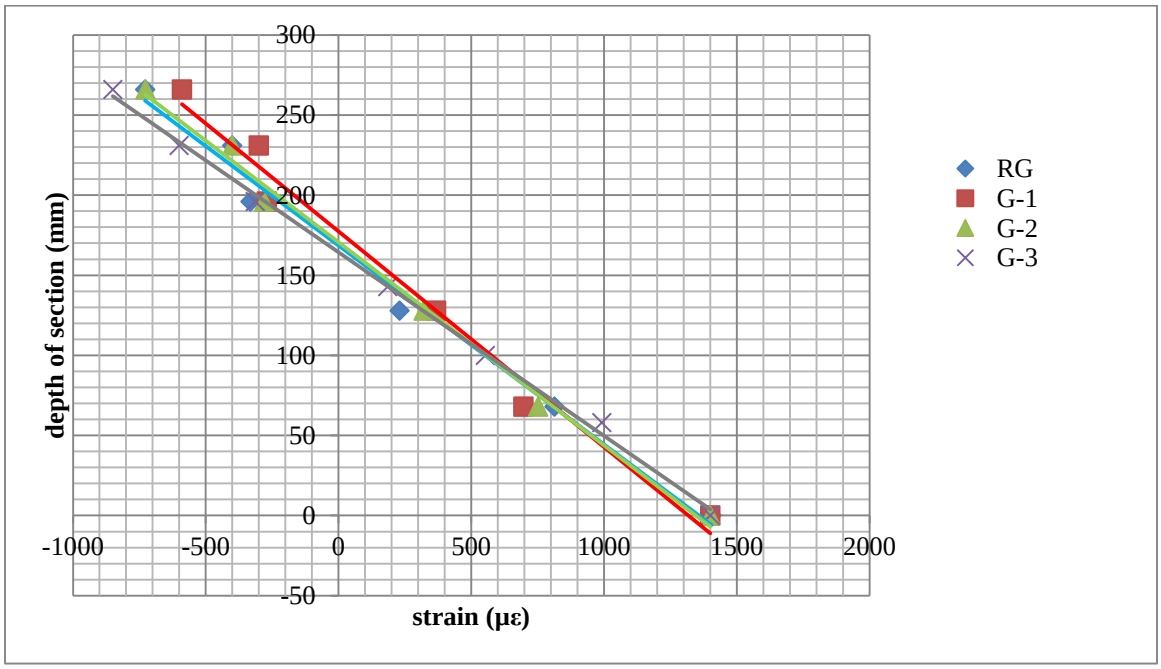

Fig. 5- 10 Strain distribution at mid-span for group I at yielding load

Based on the measured strains, the moment capacities of the girders at the positive *(M_{+ve})* and negative *(M_{-ve}* for RG, M^*_{-ve} for G1, G2, and G3) moment locations were calculated. The values of these experimentally determined moment capacities are shown in Table 12.

The theoretical values of the ultimate capacities of the girders at the positive and negative moment were calculated as follows assuming the stress distributions as shown in chapter three (Figs. 3-3 to 3-5), which corresponds to elastic-plastic behavior of steel without strain hardening. The theoretical moment capacities at mid-span and at inter support is calculated using the following equations:

$$\breve{M}_{+ve} = T_s\,(d_1) + C_c\,(d_2) + C_{S.R}\,(d_3) \quad (5\text{-}1)$$

$$\breve{M}_{-ve} = C_s\,(d_1) + T_{S.R}\,(d_4) + T_s\,(d_2) \quad (5\text{-}2)$$

$$\breve{M}^*_{-ve} = C_s\,(d_1) + T_{S.R}\,(d_4) + T_s\,(d_2) + T_{CFRP}\,(d_3) \quad (5\text{-}3)$$

Equ. (5-2) includes the contribution of the slabs' longitudinal reinforcing bars in composite action and Equ. (5-3) applies to the girders having CFRP glued to the top of concrete slab at the negative moment region. In Equ's (5-1 to 5-3), T_s and C_s are the tension and compression forces in steel section respectively, C_c is the compression force in concrete, $T_{S.R}$ and $C_{S.R}$ are the tension and compression forces in steel reinforcement respectively, and T_{CFRP} is the tension force in CFRP sheets corresponding to an assumed maximum tensile stress 0.3 times the ultimate tensile strength of CFRP. This level of stress was selected to ensure yielding of both steel flanges, and to limit the stress in CFRP because of the rupture failure of this material.

The theoretical values of moment capacities $\breve{M}_{+ve}$ and $\breve{M}_{-ve}$ for all girders calculated using Equ's (5-1 to 5-3) are shown in Table 13. Because of the composite action at the positive moment region, $\breve{M}_{+ve}$ values are higher than $\breve{M}_{-ve}$ values. The addition of CFRP increases the negative moment capacity, reducing the ratio $\breve{M}_{+ve}/\breve{M}_{-ve}$ from 1.49 for the control girder RG to 1.05 for G3. For girder G3, the used thickness of CFRP yielded almost the same strength $\breve{M}_{+ve}$ and $\breve{M}^{*}_{-ve}$. It appears this is the theoretical upper limit of CFRP in this case which will be investigated further. The values of the failure load P_u for the girders recorded from tests as shown in Table 12. An attempt has been made to compare P_u with those determined from plastic analysis and from strains along the depth of the girder at negative and positive moment locations. Using plastic analysis, the theoretical maximum value of load P to cause failure, P is given as:

$$P = \left(\frac{2(2\alpha+1)Mp}{L} \right) \qquad (5\text{-}4)$$

Where M_p is the negative moment capacity ($\breve{M}_{-ve}$ for RG or $\breve{M}^{*}_{-ve}$ for G1, G2, and G3) as shown in Table 13, and $\breve{\alpha} = \breve{M}_{+ve}/\breve{M}_{-ve}$ or $\breve{M}_{+ve}/\breve{M}^{*}_{-ve}$. The theoretical calculated values of load named as $\breve{P}_{tf}$ are shown in Table 13 and compared with the experimental values (Table 12) of failure load P_{tf} computed from Equ. (5-4) using the values of experimental moment capacities M_{+ve}, M_{-ve}. It should be noted that the strain in the girders at the negative moment zone were measured at a location 200 mm away from the centerline of the interior support. Thus, the strain values were slightly lower than those at the interior support due to lower negative moment. Consequently, the calculated load P_{tf} values are therefore slightly smaller than the actual ultimate load P_u. Table 12 and 13 show that the analytical values calculated assuming full yielding of sections are lower than

experimental P_u values for all girders. This implies that the failure load $\breve{P}_{tf}$ as calculated is a safe estimate of the actual failure load, which would be higher as the steel girders possess excess capacity due to strain hardening.

Table 12 Experimental moment capacities and ultimate load

Girder	M_{+ve} (KN.m)	M_{-ve} *or* M^*_{-ve} (KN.m)	α	P_{tf} (KN)	P_u (KN)
RG	112	76	1.48	248	273
G1	112	86	1.30	256	303
G2	120	95	1.26	276	330
G3	111	93	1.19	260	314

Table 13 Theoretical moment capacities and ultimate expected load

Girder	$\breve{M}_{+ve}$ (KN.m)	$\breve{M}_{-ve}$ *or* $\breve{M}^*_{-ve}$ (KN.m)	ᾰ	$\breve{P}_{tf}$ (KN)
RG	110	74	1.49	243
G1	110	84	1.31	250
G2	110	90	1.22	256
G3	110	104	1.05	267

5.3 VARIATION OF CFRP THICKNESS

The use of CFRP increases the ultimate strength as indicated last section. Strength and stiffness improvements for girders are directly proportional to the increase in CFRP thickness as illustrated in load-deflection curve (Fig. 5-6). The increase of ultimate capacity is listed in Table. 14. It was observed that girder G3 had minimal strength improvement relative to girder G2. The increase of CFRP thickness for girder G3 increased the ultimate capacity at negative moment region to be close to the positive moment region. This restricted rotation of steel section at negative moment, so that girder failed at mid-span before reaching the moment capacity at negative moment zone resulting in reduction of ultimate strength compare to girder G2

Table 14 Ultimate capacity and deflection of girders in group I

Girder	RG	G1	G2	G3
Ultimate capacity (KN)	273	303	330	314
Increase of capacity (%)	-	11%	21%	15%
Deflection at ultimate load (mm)	21.3	24.7	29.5	18

The strain distribution shown in Fig. 5-7 illustrated the effect of CFRP thickness to increase the yielded part of steel section over the interior support. The increase of CFRP thickness caused an increase in the capacity of composite section over the interior support as well as allows the steel section to have more rotation. Therefore, moment-redistribution was allowed and more part of steel section at mid-span was yielded. The strain readings at the top of concrete slab showed that concrete reached higher level of strain by bonding CFRP sheets at negative moment region. Most of girders in group I reached strain of 0.0025. For girder G2, it reached higher level, 0.0029, since this girder had reached the highest capacity of girders in group I.

The increase of CFRP thickness such that section capacity at negative moment region is close to the capacity at positive moment region limited the ability of steel section to rotate. This caused failure in concrete slab before full yielding of steel section at negative moment region and consequently full capacity cannot reach.

5.4 EFFECT OF WRAPPING CONCRETE SLAB AT MID-SPAN

As all girders failed at mid-span location due to failure of the slab leaving the negative moment region structurally intact, it was of interest to examine if the load carrying capacity can be further enhanced by preventing the failure of slab at mid-span. As stated earlier, in two girders in group II, RGR and G2R, the slab was wrapped with CFRP. Tests confirmed that further increase in load capacity was achieved. Load-deflection plot in Fig. 5-11 show the enhancement in load capacity and stiffness. The enhancement in capacity compare to girder RG is presented in Table 15.

Confining concrete slab at mid-span allowed the steel section over the interior support to undergo more rotation compared to the girders in Group I. Measured strain plot shown in Fig. 5-12 and Fig. 5-13 respectively for the mid-span and the interior support locations, clearly demonstrates that a substantial part of steel section has yielded at both locations. The strain distribution along the cross section at mid-span showed that both RGR and G2R developed almost the full capacity of section. At negative moment region, the steel section of girder RGR almost fully yielded compared to partially yielding of that section for G2R because of the different type of failure as discussed later. However, the yielded part of steel section of girder G2R at negative moment zone is higher than those in group I girders. For concrete at mid-span, both girders in group II had reached the crushing strain (0.0035) and ultimate strength of concrete.

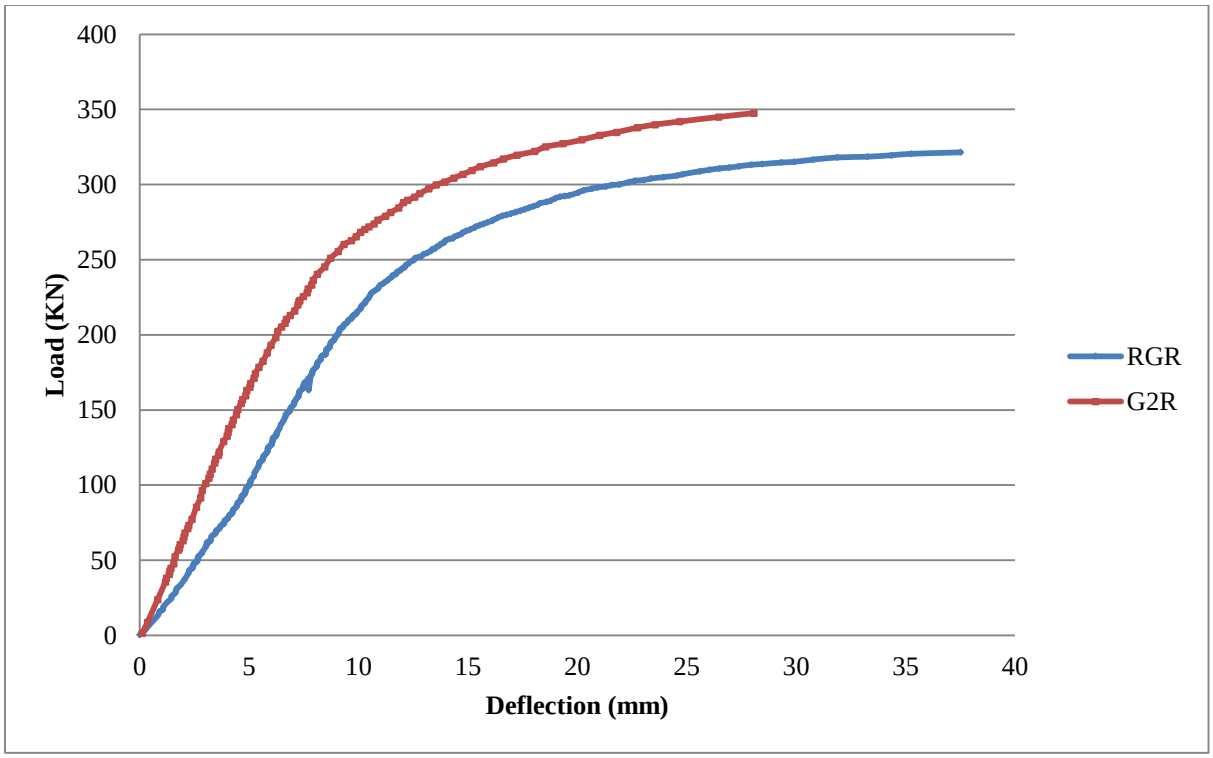

Fig. 5- 11 Load-deflection curves of girders in group II

Table 15 Ultimate capacity and deflection of girders in group II compared to girder RG

Girder	RG	RGR	G2R
Ultimate capacity (KN)	273	323	352
Increase of capacity (%)	-	18.4 %	29.5%
Deflection at ultimate load (mm)	21.3	38.5	39

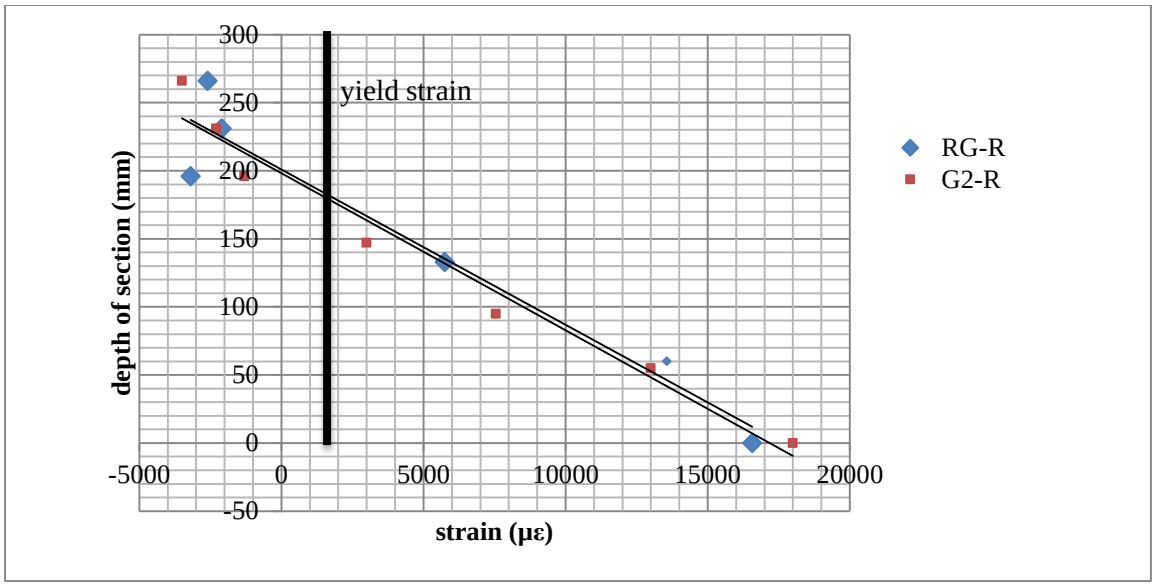

Fig. 5- 12 Strain distribution at mid-span for group II at ultimate load

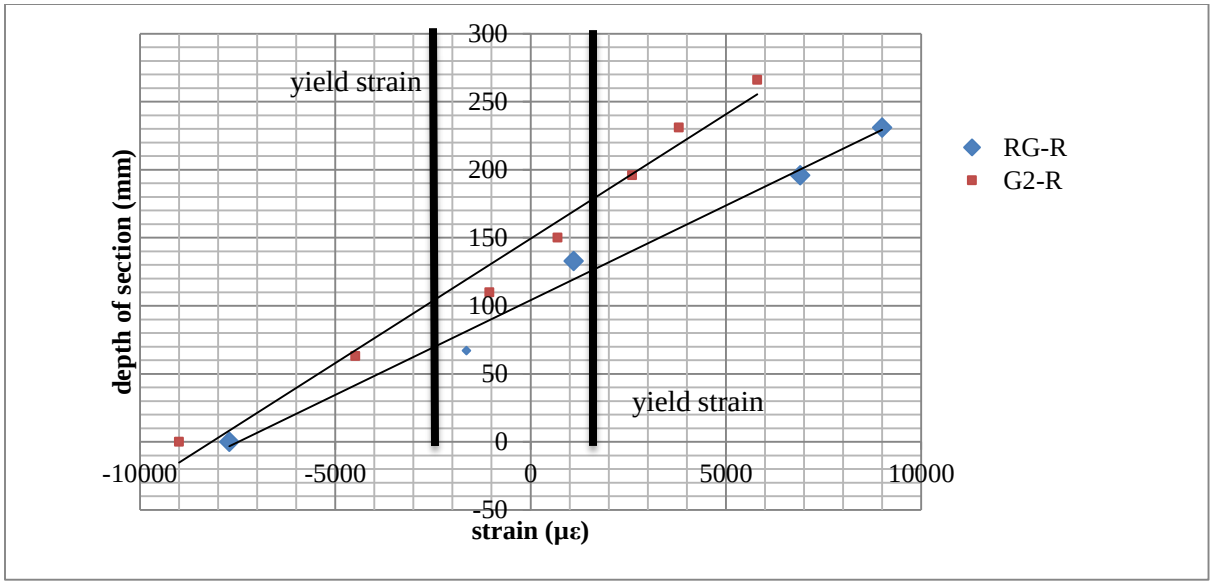

Fig. 5- 13 Strain distribution at interior support for group II at ultimate load

Failure mechanism of girders in group II is quite similar to girders in group I through loading of girders as shown in Table. 16. However, steel section at negative moment developed more rotation and different mode of failure was occurred at ultimate load as will discuss in the next section.

Table 16 Load corresponds to yielding of steel section in group II (KN)

stages	RG R	G2R
Cracking Load	65	150
Yielding of bottom flange (mid-span)	172	182
Yielding of top flange (interior support)	234	270
Yielding of bottom flange (interior support)	240	238
Ultimate Load	322	352

5.5 FAILURE MODE

Three different modes of failure were occurred in the study. All girders of group I were failed by shear-compression failure of concrete slab at the positive moment region as shown in Fig. 5-14. The control girder RGR of group II reached its full capacity by crushing of concrete slab at the positive moment region as captured in Fig. 5-15 after the removal of CFRP sheet at mid-span. Girder G2R failed prematurely by de-bonding of CFRP fabrics over interior support as shown in Fig. 5-16.

Typical design of composite steel-concrete girders assumes that shear force is resisted by the steel web as conducted in chapter three. This failure occurred because of exceeding shear stresses in concrete slab under the point load since the maximum shear force was under the applied load as shown in in Fig. 5-17. The maximum applied load that cause shear failure was estimated using elastic formula (Equ. 5-5). According to the calculation below and assuming plain concrete, the shear capacity of concrete was exceeded after 110 KN. However, the composite action with the steel beam was resisting the shear force according to the AISC specifications. This prevented and delayed the sudden shear failure.

$$V = \frac{11\,(p)}{16} \qquad \text{Equ. (5-5)}$$

$$\tau = \frac{VQ}{It} \qquad \text{Equ. (5-6)}$$

Where:

τ: Shear stress.

V: Shear force.

Q: 1st moment of area.

I: Moment of inertia.

t: Width of section.

τ = 5 Mpa

I (transformed section) = $54x10^6$ mm^4

Q = 225000 mm3

t (transformed section) = 60.5 mm

P = 110 KN

Fig. 5- 14 Shear compression failure of girder G-1

For girder RGR, Confinement of concrete slab at mid-span by use of CFRP wrapping allowed the concrete to reach the crushing strain. This prevented the shear-compression failure and allowed the concrete to develop the typical failure (crushing of concrete) at ultimate load. The strain gauges measurements of concrete showed that the ultimate strain was exceeded.

The de-bonding failure of girder G2R occurred because the shear capacity of the epoxy adhesive at the interface between CFRP and concrete slab was exceeded. De-bonding of CFRP occurred when the strain in CFRP exceeded 0.0062. The transferred shear force due to CFRP over the interior support at failure is 188KN which caused shear stress at the interface between concrete and CFRP that exceeded the epoxy adhesives' ultimate strength of 2 MPa.

Fig. 5- 15 Crushing of concrete at mid-span in girder RGR

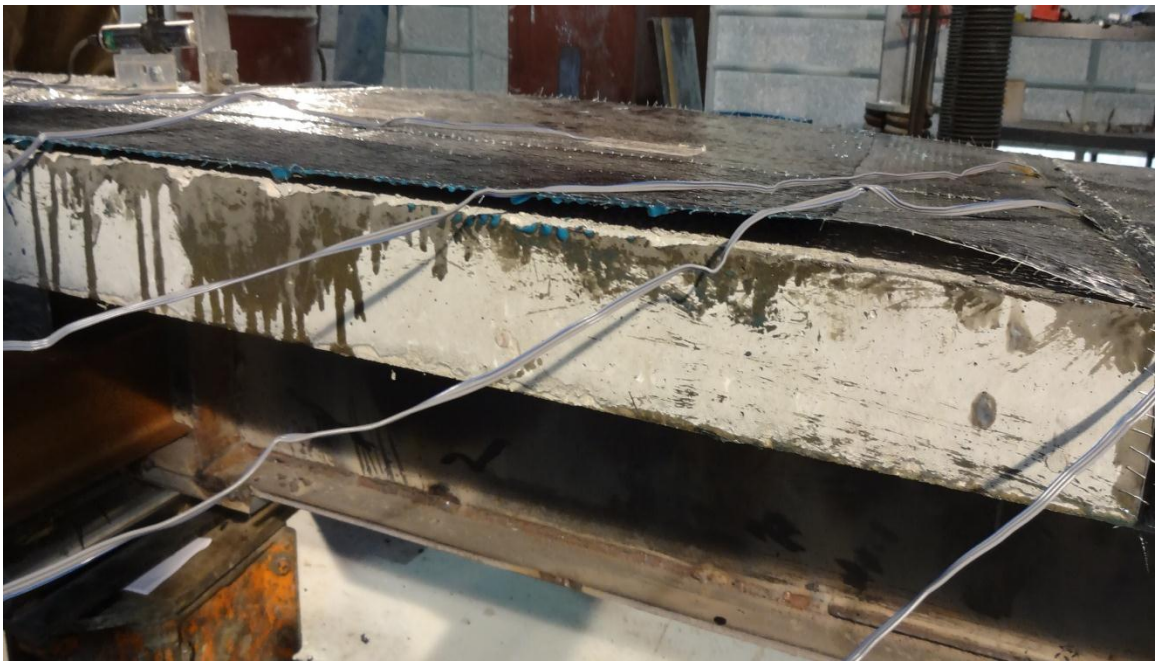

Fig. 5- 16 De-bonding of CFRP in girder G2R

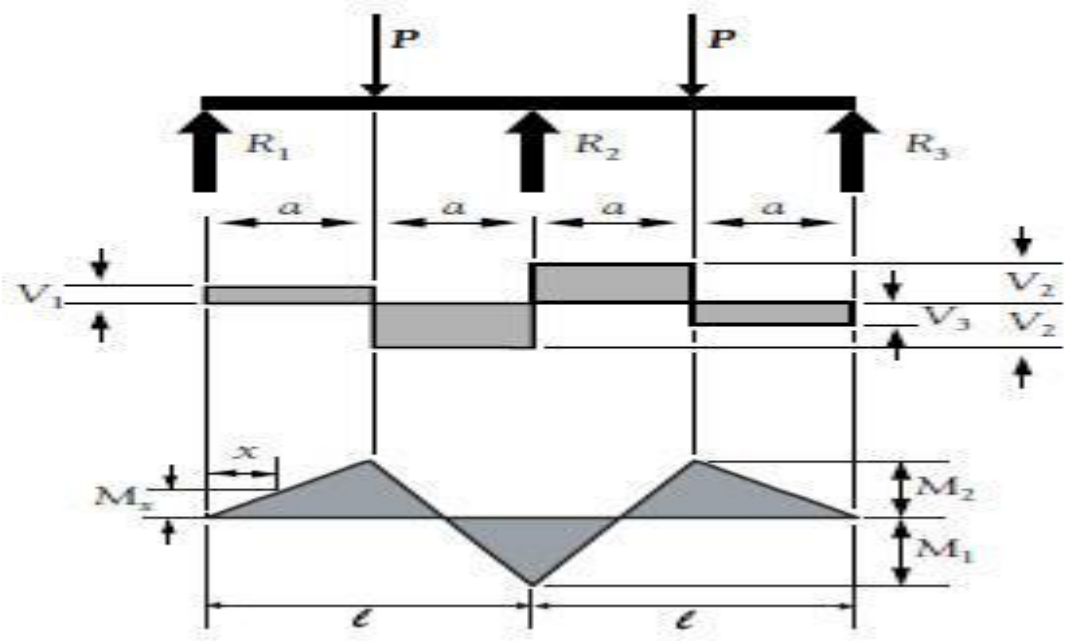

Fig. 5- 17 Moment and shear diagrams

5.6 CFRP STRAIN MEASUREMENTS

Strain measured along CFRP fabrics at negative moment region is used to assess CFRPs' contribution to load resistance at different load levels. The strain in CFRP was the same for all girders up to cracking of concrete slab. After cracking, strain measurements showed that the strain in CFRP decreased a little as thickness of CFRP increased as shown in Fig. 5-18. This was because of the upward shift of the neutral axis due to increase of CFRP thickness. However, the strain in CFRP is increased sharply after yielding of both steel flanges at the interior support, and the final strain in CFRP controls with the level of rotation at that section. Measured strains in CFRP fabrics occurred at the interior support as expected. Sudden increase in measured strain was noticed at locations where cracking of the concrete slab took place.

The maximum strain in CFRP at ultimate load was controlled with the level of rotation in the steel section at interior support. Strain compatibility along the cross section indicated that the strain in CFRP was increased as the strain in steel section increased. Fig. 5-19 shows the strain distribution along CFRP at the negative moment region at ultimate and the CFRP strain in girder G2R was the highest followed by G2 whereas G3 developed the minimal strain of all girders. This is an expected point since G2R developed higher rotation compare to other girders. However, strain in CFRP for girder G2R could develop higher load in case that de-bonding failure is eliminated.

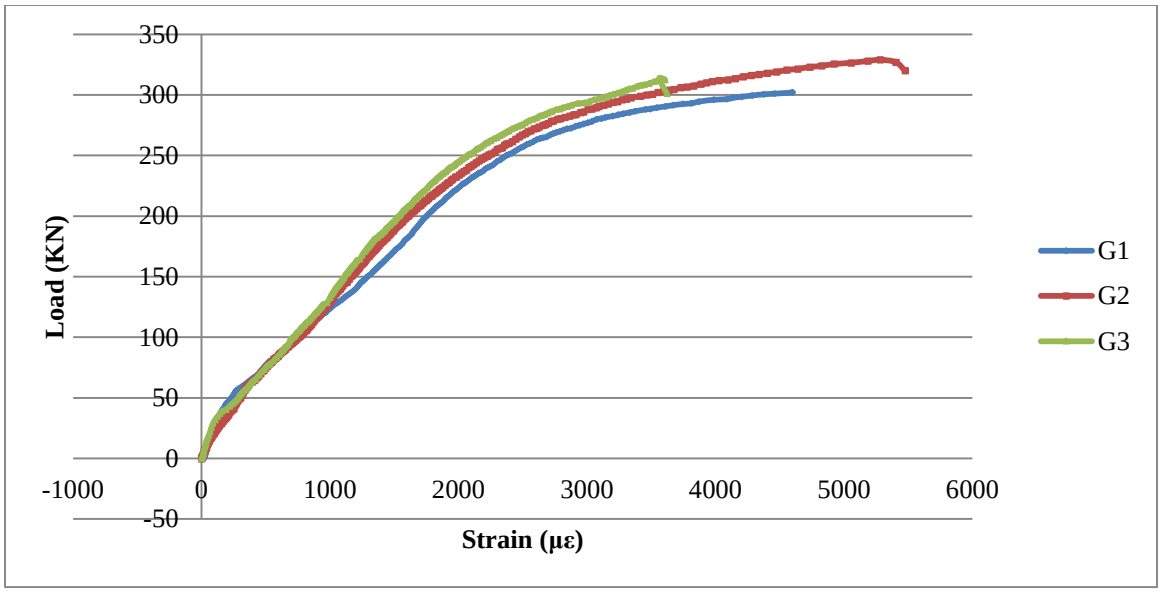

Fig. 5- 18 Load vs strain in CFRP

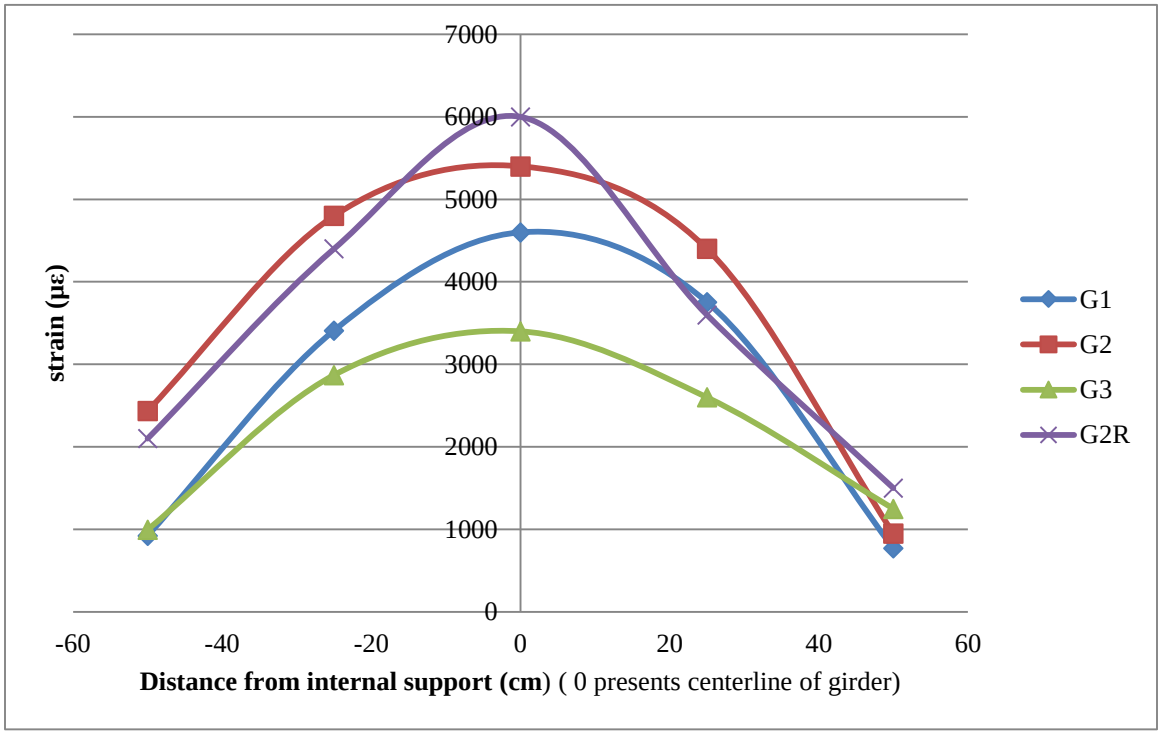

Fig. 5- 19 Distribution of strain along CFRP fabric at ultimate load

Prior to the yielding of steel section at mid-span, the level of strain in CFRP was close for all girders as shown in Fig. 5-20. Significant increase of CFRP strain after yielding of steel section at the interior support was recorded. This increase because steel section started to rotate to allow stress re-distribution and therefore strain in CFRP was increased. Strain measurements for girder G2R shown in Fig. 5-21 at yielding and ultimate loads indicated a sudden increase of measured strain at locations where cracks were initiated in the concrete slab. Maximum strain recorded along CFRP fabrics was over interior support as expected.

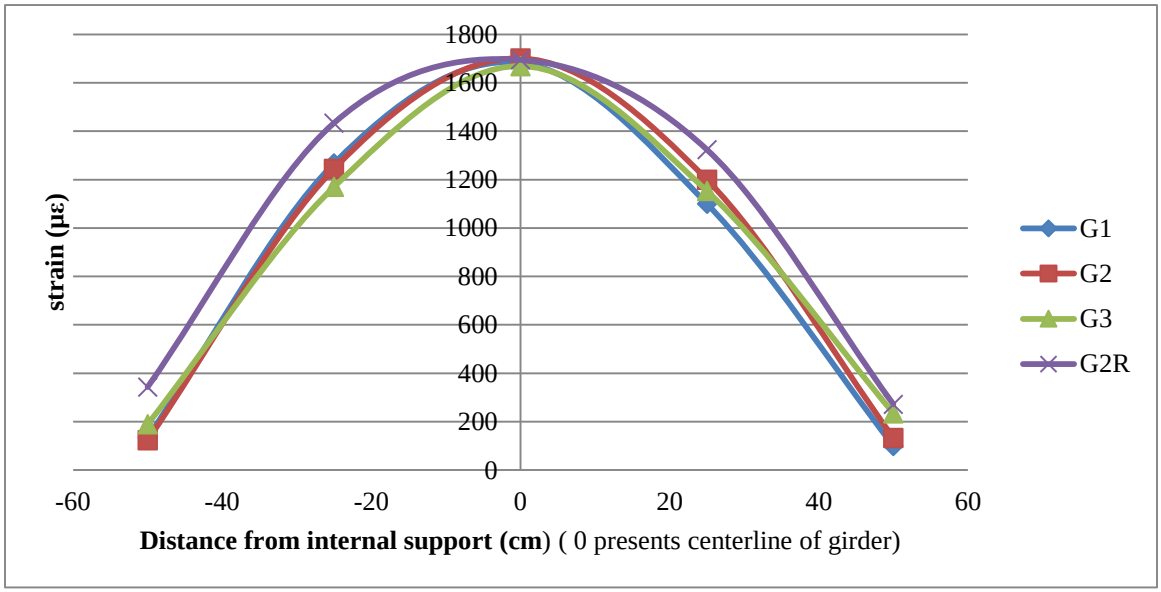

Fig. 5- 20 Distribution of strain along CFRP fabric at yielding load

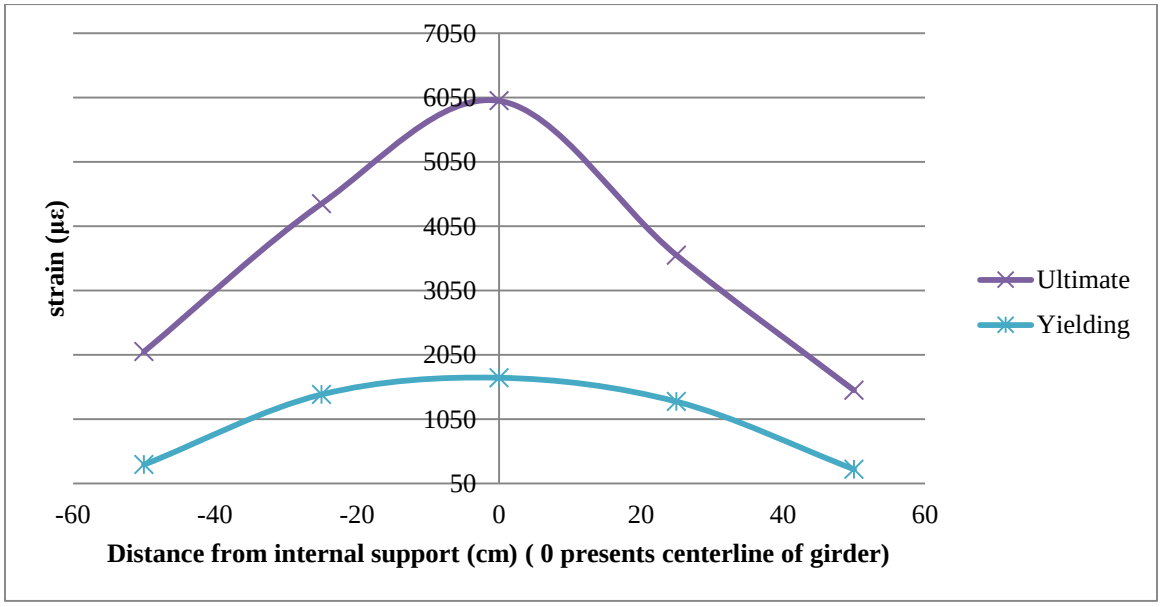

Fig. 5- 21 Longitudinal strain in CFRP at negative moment region for girder G2R

5.7 STEEL-CONCRETE INTERFACE SLIP

The relative slip between concrete slab and steel beam is important to be limited to maintain the composite action. Three LVDT's were fixed to measure relative slip between bottom of concrete slab and top of steel beam as mentioned in chapter four. The load-slip curves are illustrated for both sections; at mid-span and at interior support as shown in Fig. 5-22. This curve is plotted for girder G2R since this girder achieved the full capacity at positive and negative moment zones and reached the highest capacity. The steel-concrete slip could be seen using strain distribution along the cross section. It can be noted that strain in concrete was less than the expected strain if steel strains are extended linearly as illustrated in Figs. 5-23 and 5-24 for interior support and mid-span respectively. The strain distribution indicated negligible effect of slip up to yielding of bottom flange at mid-span whereas slip was considerably effect stresses in concrete, steel reinforcement and CFRP at ultimate load. However, slip was more considerable at mid-span. At inflection point, the LVDT readings were close to zero

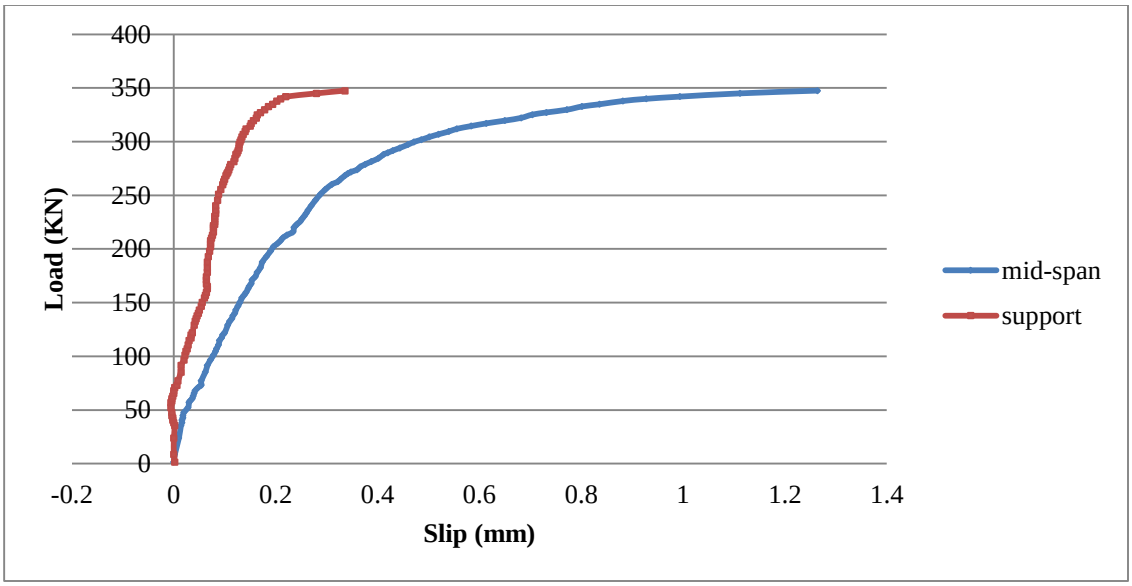

Fig. 5- 22 Relative slip at mid-span and over the interior support for girder G2R

Load-slip curve indicated a relatively small value of slip occurred over the interior support, whereas considerable slip was recorded at the positive moment region. However, the slip at positive moment region was at the threshold maximum limit. This is mainly because of two factors; shear studs at positive moment region were resisting higher lateral shear load compare to shear studs at the negative moment region. This is because all the steel section acting in tension and concrete in compression at the positive moment region. At negative moment region, shear studs were resisting the shear force of CFRP and steel reinforcement which is smaller than tension force of the whole steel section. The 2nd reason, testing of shear studs conducted using push-out test indicated that capacity of each stud is 70 KN whereas it had been designed to carry 105 KN as per AISC specifications.

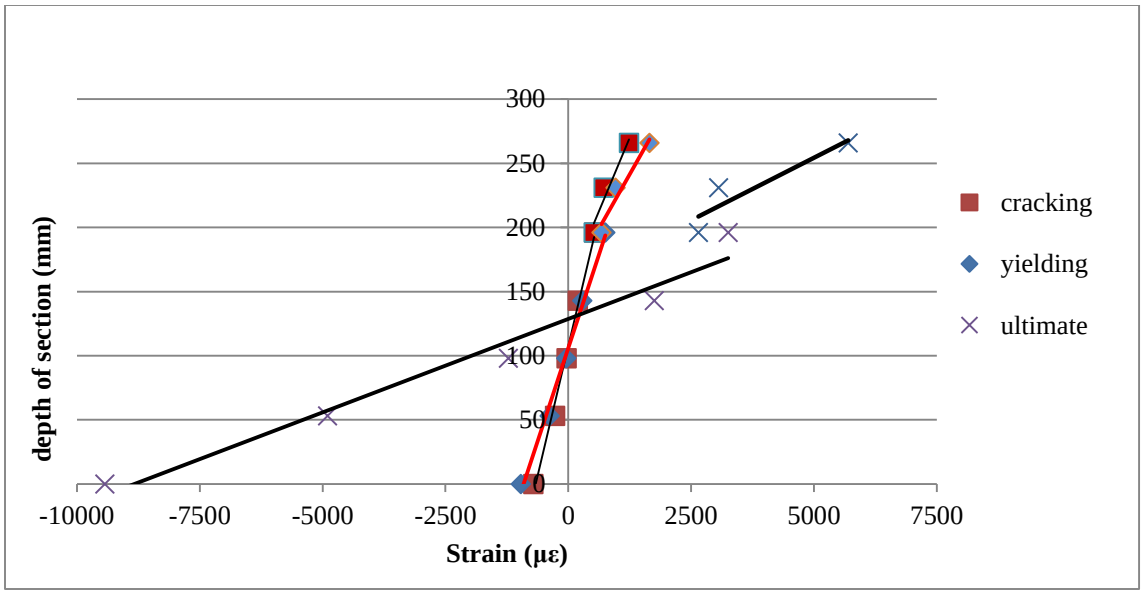

Fig. 5- 23 Slip at interior support for girder G2R

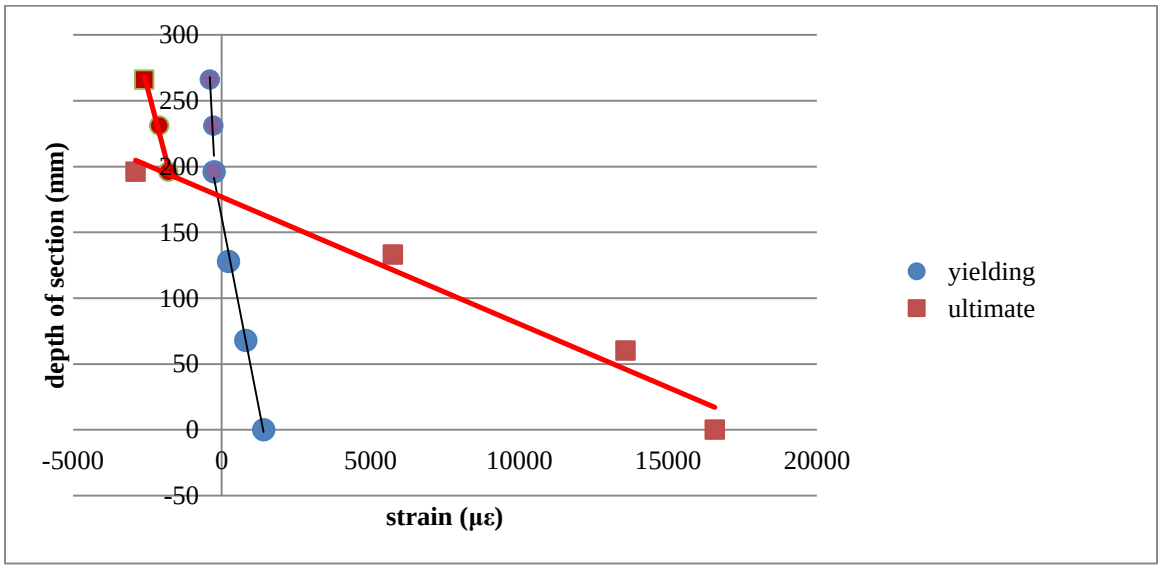

Fig. 5- 24 Slip at mid-span for girder G2R

The slip at positive moment region caused a longitudinal crack in concrete slab along the line of shear studs as shown in Fig. 5-25 and 5-26. This crack started to be visualized after exceeding 250 KN and extended as the load increased.

The capacity of section at mid-span was calculated considering the relative slip. The capacity is 110 KN.m which is approximately close to the actual capacity. However,

experimental results showed that the steel-concrete section developed higher capacity than the calculated one, which indicates that the available slip had minimal effect on the ultimate capacity of girders.

Fig. 5- 25 Concrete crack along the line of CFRP

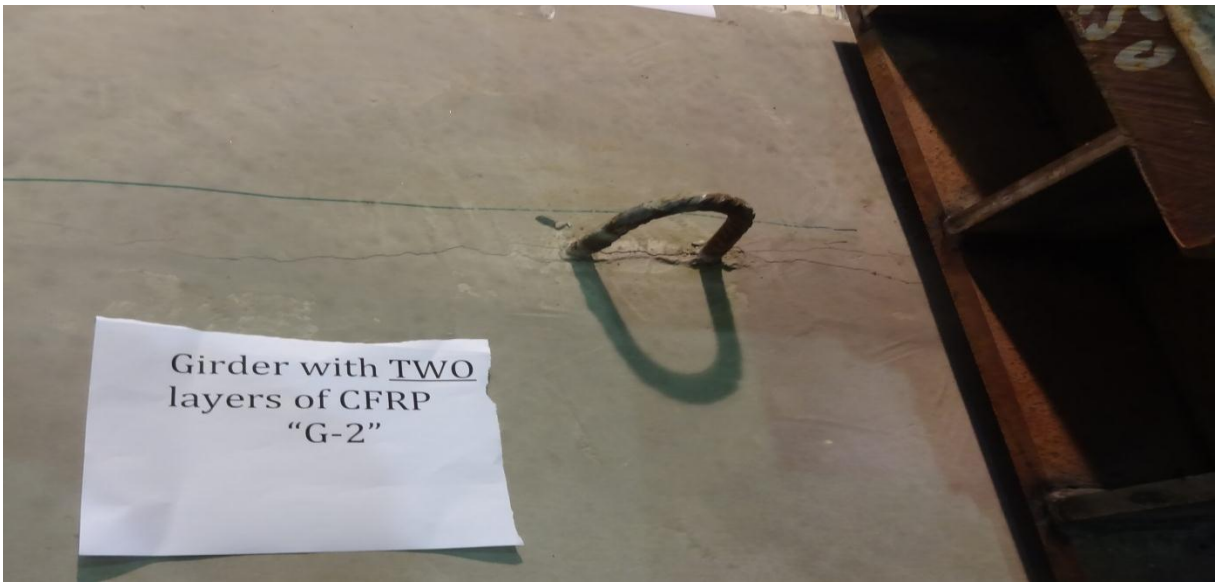

Fig. 5- 26 Mid-span crack along the line of shear studs for girder G2

CHAPTER SIX

NUMERICAL ANALYSIS OF COMPOSITE GIRDER

6.1 INTRODUCTION

The use of finite element modeling and numerical analysis becomes an important investigation technique in conducting researches and developing new structural techniques. Use of FE modeling offers a relatively free cost method of investigation structures compare to the experimental testing. However, the accuracy of FE model depends on the accuracy of assumptions, number of elements, and size of elements. The FE software could be used to analyze and investigate the behavior of composite structures including geometrical and material nonlinearities.

Three-dimensional FE model of continuous composite girder bonded with CFRP top of concrete slab was developed in this study using commercial software ABAQUS 6.13 [30]. The model was validated with the conducted experimental results. Suitable interface models were used to define the contact regions of the composite girder components.

The developed model was used to investigate the ability of CFRP sheets to maintain the composite action at the negative moment region. The verified model was used to investigate the effect of CFRP thickness, and length of CFRP sheets in addition to the shear studs spacing at the negative moment region.

6.2 MODELING OF CONTINUOUS COMPOSITE GIRDER BONDED WITH CFRP

Finite element modeling of continuous composite girders is presented in this section. The six composite girders which introduced in chapter five were used to create and validate the model. This model is used to investigate other girders to obtain the proper thickness and length that needed to strengthened any continuous composite girder.

6.2.1 Geometry and Elements Type of the Modeled Girder

A two-span composite steel-concrete girder monotonically loaded under a point load at the mid of each span was modeled in this study as illustrated in Figs 5-1 and 5-2 (chapter five). All components of the composite girder including steel beam, concrete slab, stiffeners, bearing plates, and shear studs were modeled as 3-D element with their actual size. However, CFRP sheets was modeled as shell element as will discuss later. Two steel plates of 50 mm width were mounted top of concrete slab under the point load to avoid stress concentration in that region. Fig. 6-1 shows the modeled girder.

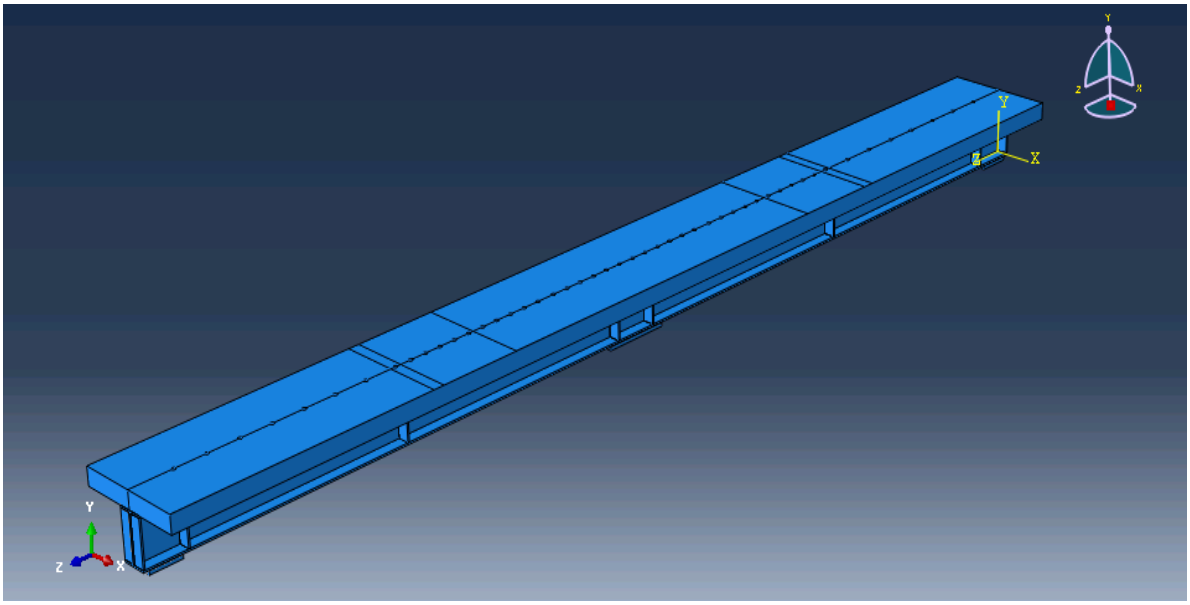

Fig. 6- 1 Typical girder bonded with CFRP at negative moment region

Eight-node linear brick element (C3D8R) was used to model the solid elements; concrete, steel, and shear studs. The steel reinforcement was modeled as 2-node linear 3-D truss (T3D2) whereas 4-noded shell element (S4R) was used to model CFRP.

6.2.2 Modeling of Composite Girder Materials

The composite girders compose of different materials including concrete, steel plate, steel reinforcement, and CFRP sheets. This section is presenting the used material model for each ingredient.

6.2.2.1 Modeling of concrete

The behavior of concrete in compression was modeled as elastic–plastic including strain softening using stress-strain diagram (chapter four). In tension, the stress-strain behavior was assumed increasing linearly up to cracking stress and tension behavior was assumed to decrease linearly after reaching the crack stress.

Concrete is modeled using a damage plasticity model as proposed by Lubliner et al. (1989) [31] and modified by Lee & Fenves (1998) for cyclic loading [32] and followed a non-associated flow rule. This model requires as input the stress-inelastic strain of concrete for both compression (Fig. 6-2) and tension which obtained from uniaxial compression and tension tests. The parameters for the concrete damage plasticity model are tabulated in Table 17 [30].

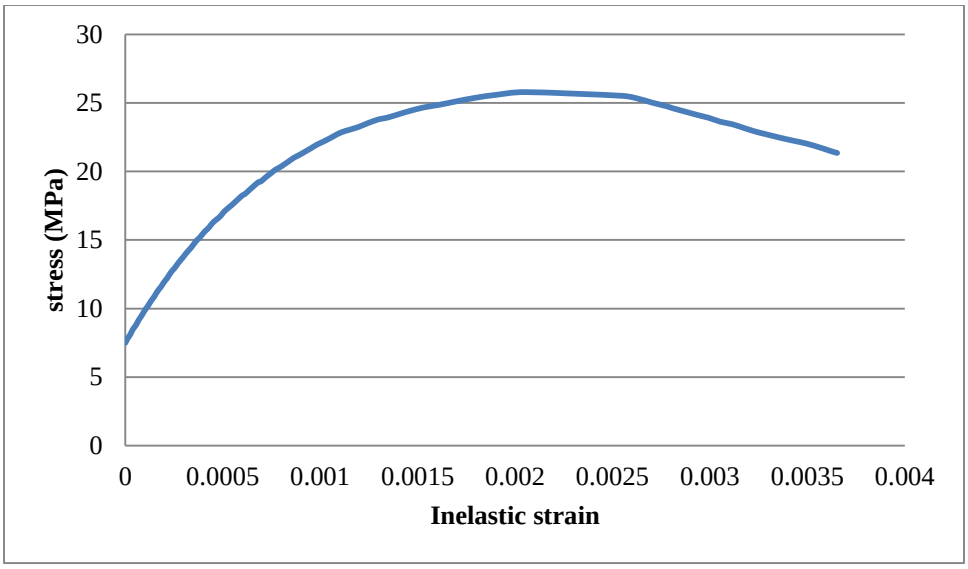

Fig. 6- 2 Stress vs Inelastic strain of concrete

Table 17 plastic damage model input parameters

Mass Density (Kg/mm^3)	Modulus of Elasticity (MPa)	Poissons' ratio	Dilatation Angle ψ	Eccentricity	f_{bo}/f_{co}	K	Viscosity parameter
2.45E-6	**23800**	**0.2**	**36**	**0.1**	**1.16**	**0.67**	**0**

Elastic-plastic response of the concrete is described in terms of the effective stress $\bar{\sigma}$ and the hardening variables, $\dot{\varepsilon}^{pl}$ and $\tilde{\varepsilon}^{pl}$

$$\bar{\sigma} = D_o^{el} : (\varepsilon - \varepsilon^{pl}) \in \{\bar{\sigma} | F(\bar{\sigma}, \tilde{\varepsilon}^{pl}) \leq 0\} \quad \text{Equ. (6-1)}$$

Where

$$\tilde{\varepsilon}^{pl} = h(\bar{\sigma}, \tilde{\varepsilon}^{pl}).\dot{\varepsilon}^{pl} \quad \text{Equ. (6-2)}$$

$$\dot{\varepsilon}^{pl} = \dot{\lambda} \frac{\partial G(\bar{\sigma})}{\partial \bar{\sigma}} \quad \text{Equ. (6-3)}$$

$\dot{\lambda}$ is defined as non-negative plastic multiplier whereas F is yield function. The yield function and the plastic multiplier adopted the conditions: $\dot{\lambda} F = 0; \dot{\lambda} \geq 0; F \leq 0$ **(**Kuhn-Tucker). The flow potential G is governs the plastic flow. The Cauchy σ is calculated in term of the stiffness degradation variable d($\bar{\sigma}, \tilde{\varepsilon}^{pl}$) and the effective stress as:

$\sigma = (1\text{-}d)\,\bar{\sigma}$ Equ. (6-4)

The elastic modulus of the damaged concrete is reduced by stiffness degradation variable. The constitutive relations are described by Equ. 6-3. To simplify the damage plasticity model for numerical implementation, Constitutive relations for the elastic-plastic responses are decoupled from the stiffness degradation responses using Equ. (6-4).

The hardening variables in compression $(\tilde{\varepsilon}^{pl})_c$ and tension $(\tilde{\varepsilon}^{pl})_t$ are formulated by considering uniaxial loading conditions first and then extended for multi-axial conditions. When the concrete specimen is unloaded from any point on the strain softening branch of the uniaxial nonlinear stress-strain curve, the unloading response weakened, due to which the elastic stiffness of the material appears to be damaged as shown in Fig's. 6-3 and 6-4. Degradation of the stiffness is significantly different between compression (Fig. 6-3) and tension (Fig. 6-4) [33]. For both cases, the effect was more considerable as the plastic strain increases. Two independent uniaxial damage variables (d_t and d_c) were used to characterize the response of degraded concrete (both have the value between 0 and 1). These variables were assumed to be functions of the plastic strains, and field variables. The loading-unloading compression test was conducted to find the compression damage parameter. The stress-strain diagram was shown in Fig. 4-8. The slope of each loading step was measured and used to find concrete damage parameter in compression

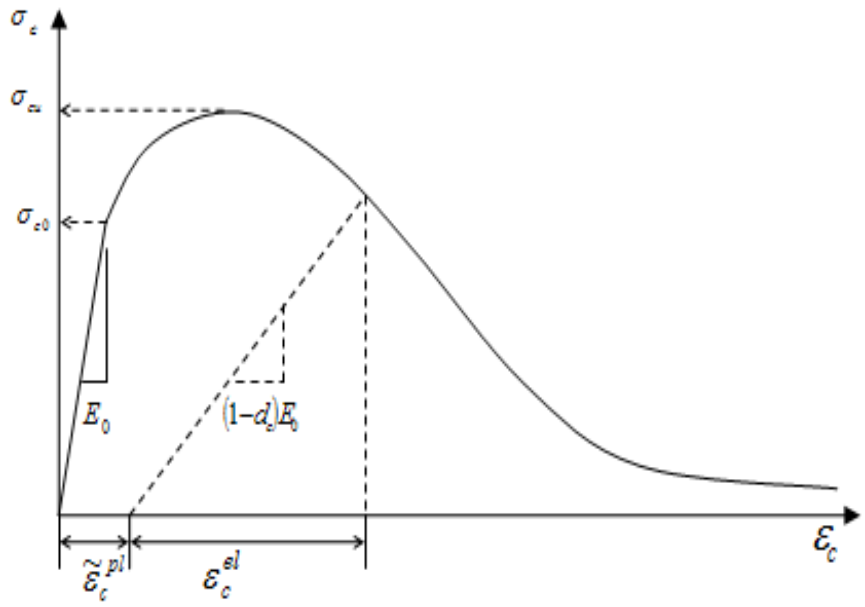

Fig. 6- 3 Damage variable for uniaxial compression [33]

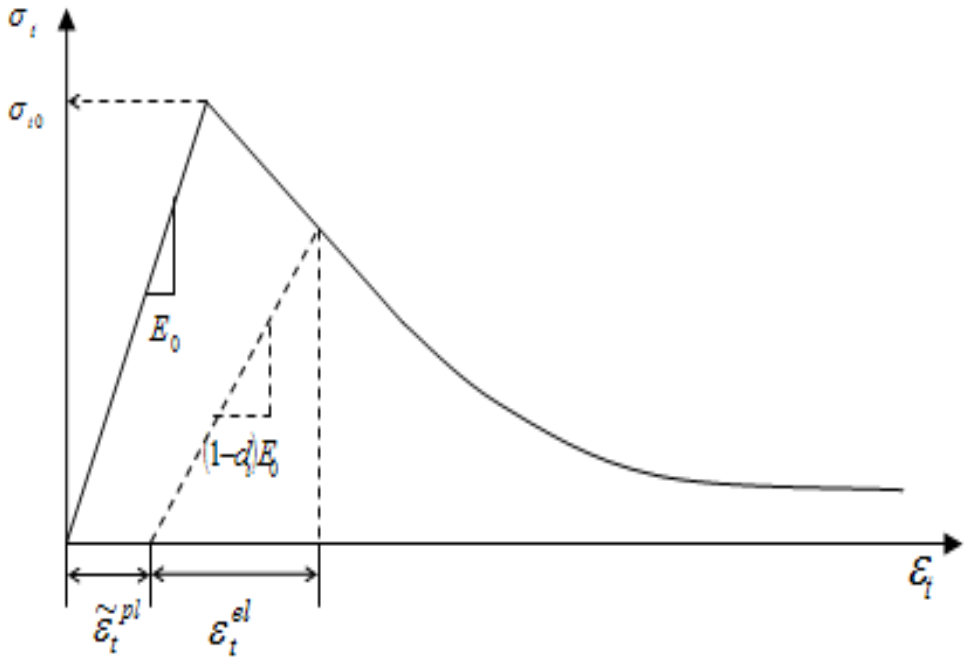

Fig. 6- 4 Damage variable for uniaxial tension [33]

The uniaxial degradation variables were modelled as monotonically increasing functions of the equivalent plastic strain. The degradation variables can take values ranging from 0, (undamaged material), to 1, (fully damaged material). If E_0 is the undamaged elastic

stiffness of the concrete, the stress-strain relation under uniaxial tension and compression loading is expressed as in Equ. 6-5

$\sigma_t = (1-d_t)\, E_0\, (\varepsilon_t - (\tilde{\varepsilon}^{pl})_t)$ Equ. (6-5a)

$\sigma_c = (1-d_c)\, E_0\, (\varepsilon_c - (\tilde{\varepsilon}^{pl})_c)$ Equ. (6-5b)

Under uniaxial loading, cracks propagate in a direction transverse to the stress direction. Nucleation and propagation of cracks caused reduction of the available load-carrying area, which in turn leads to increase in the effective stress. The effect is less pronounced under compressive loading since cracks run parallel to the loading direction; however, after a significant amount of crushing, the effective load-carrying area is also significantly reduced. The effective uniaxial cohesion stresses with respect to tension $\bar{\boldsymbol{\sigma}}_{\mathbf{t}}$ and compression $\bar{\boldsymbol{\sigma}}_{\mathbf{c}}$ are determine using Equ (6-6)

$\bar{\sigma}_t = \frac{\sigma t}{(1-dt)} = E_0\, (\varepsilon_t - (\tilde{\varepsilon}^{pl})_t)$ Equ. (6-6a)

$\bar{\sigma}_c = \frac{\sigma c}{(1-dc)} = E_0\, (\varepsilon_c - (\tilde{\varepsilon}^{pl})_c)$ Equ. (6-6b)

6.2.2.2 Modeling of structural steel and steel reinforcement

Structural steel, steel reinforcement and shear studs were modeled using isotropic plasticity model. Stress- plastic strains of steel and steel reinforcement were obtained from the mechanical properties of materials. Stress vs Inelastic strain for structural steel and steel reinforcement were shown in Figs 6-5 and Fig. 6-6 respectively. Other material properties like modulus of elasticity, poissons' ratio and other parameters were used as an input data for the model.

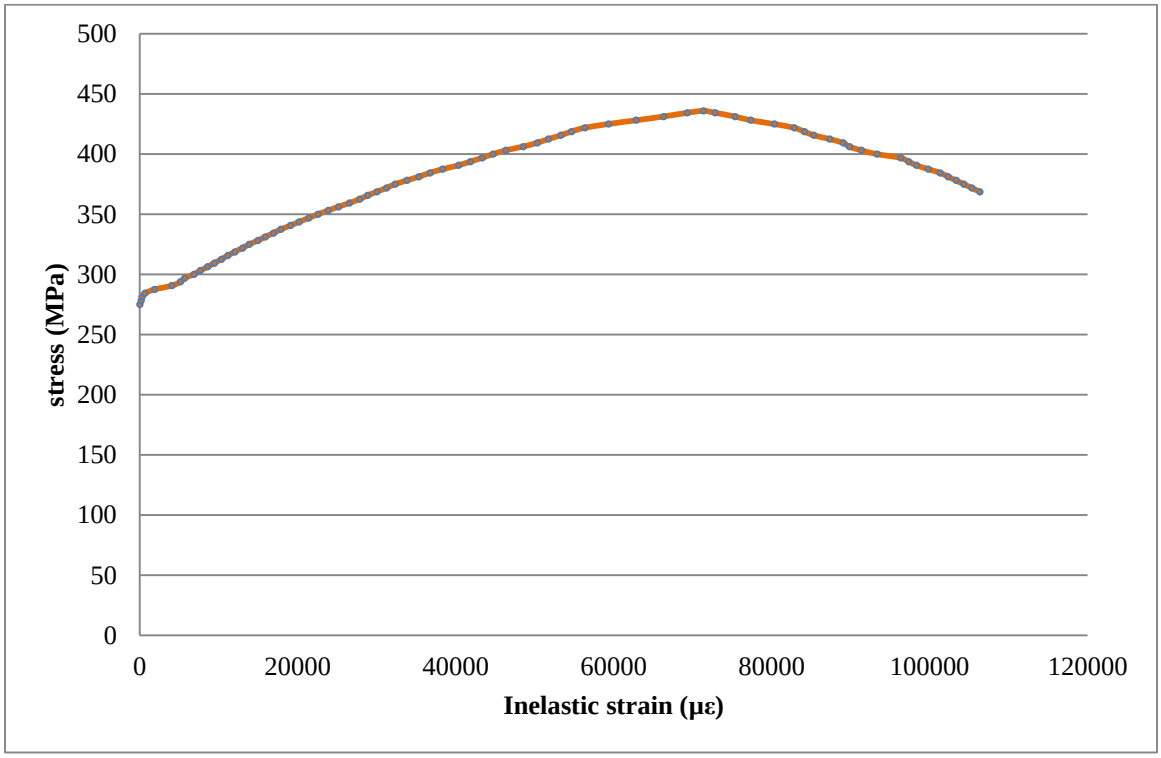

Fig. 6- 5 Stress vs Inelastic strain of structural steel

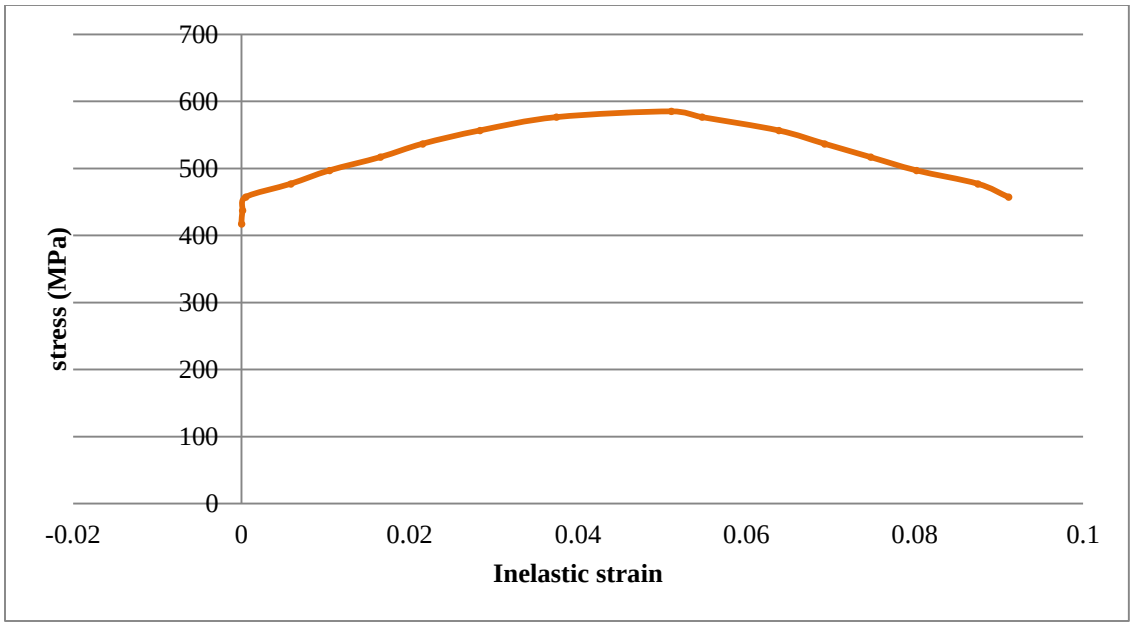

Fig. 6- 6 Stress vs Inelastic strain for steel reinforcement

6.2.2.3 Modeling of CFRP

CFRP modeled as linear elastic composite laminate. Thickness of 0.131 mm for each layer was used, and modulus of elasticity was used for material definition. Properties of CFRP lamina are tabulated in Table. 18. The mechanical properties were used according to the manufacture specification and the results of epoxy adhesive. For girders with more number of CFRP layers, the composite laminate defined with the required number of CFRP layers, and assigned with the same mechanical properties.

Table 18 Properties of CFRP lamina

E_1 (MPa)	E_2 (MPa)	υ	G_{12} (MPa)	G_{13} (MPa)	G_{23} (MPa)	σ_{ult} (MPa)
232000	9000	0.25	5000	50	50	1520

6.2.3 Modeling of Contact Region

Many interfacial regions were included in this model to define the interaction between all components. Surface-surface contact was used to model those regions. Different models of surface contact were used to simulate the interaction of Steel-concrete, concrete-CFRP, and stiffeners-steel beam. Mechanical interaction between the stud and concrete surfaces was modeled using friction formulation in tangential direction and hard contact in normal direction to avoid penetration of shear studs. The penalty method was used for tangential behavior along with the coefficient of friction as 0.2, and the maximum shear stress was specified according to the load-slip curve shown in chapter four. Studs defined as a master whereas the surrounded concrete was considered as slave.

The interaction between steel stiffeners, support steel plate with the steel beam was modeled as a tie constrain. In addition, shear studs connection with the steel beam was modeled as tie contact. The steel reinforcement in both directions were defined as embedded element inside the concrete slab

Cohesive contact was used to simulate the behavior of adhesive material between concrete and CFRP. This model allows de-bonding of CFRP if the epoxy adhesive capacity is exceeded. The value of tangential stiffness was calculated using the shear stress vs slip curve for epoxy adhesive. The normal stiffness, K_{nn}, in direction of CFRP peeling off was considered equal to 20.

According to Ziraba et al (1994), the tangential stiffness of adhesive could be calculated as the slope between shear stress per unit length and the corresponding slip [27]. This curve is shown in Fig. 6-7. According to the figure below, the value of tangential stiffness in both directions (K_{xx}, K_{tt}) is 4000 N/mm^2.

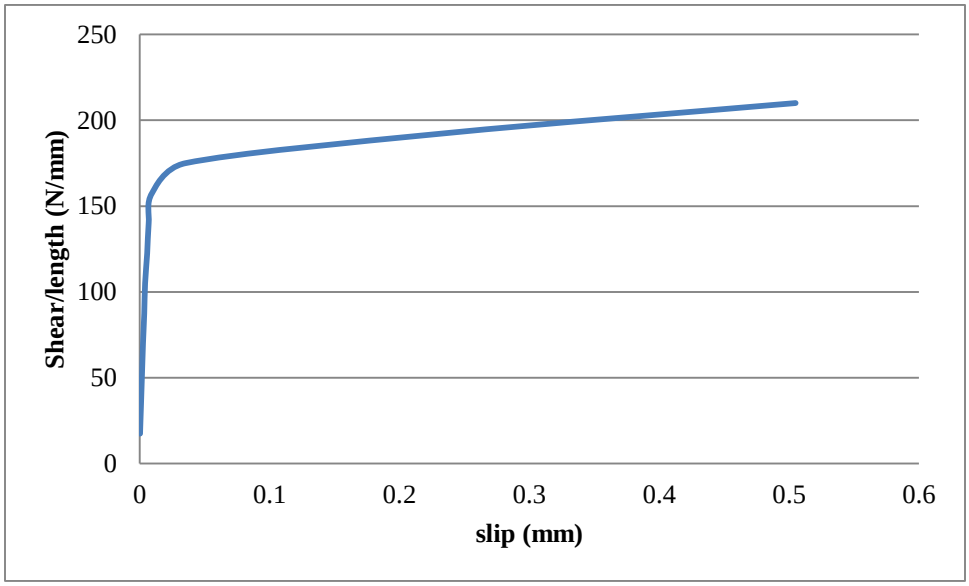

Fig. 6- 7 Shear stress per unit length vs slip

The use of contact models between shear studs, concrete and CFRP, concrete gave the model ability to figure out relative slip between surfaces as well as prediction of CFRP de-lamination

6.2.4 Model Meshing

Adequate attention has been paid in the development of hex-dominated mesh and assigning interaction between various surfaces. Cell and surface partitions of concrete slab, steel beam, and around shear studs (Fig. 6-8) were used to be able to use hex-dominated mesh by use of sweep features. The mesh size was selected after number of trials to confirm accuracy and efficiency of the model as shown in Figs. 6-9 and 6-10. Thus a regular structured hex-dominated mesh generated.

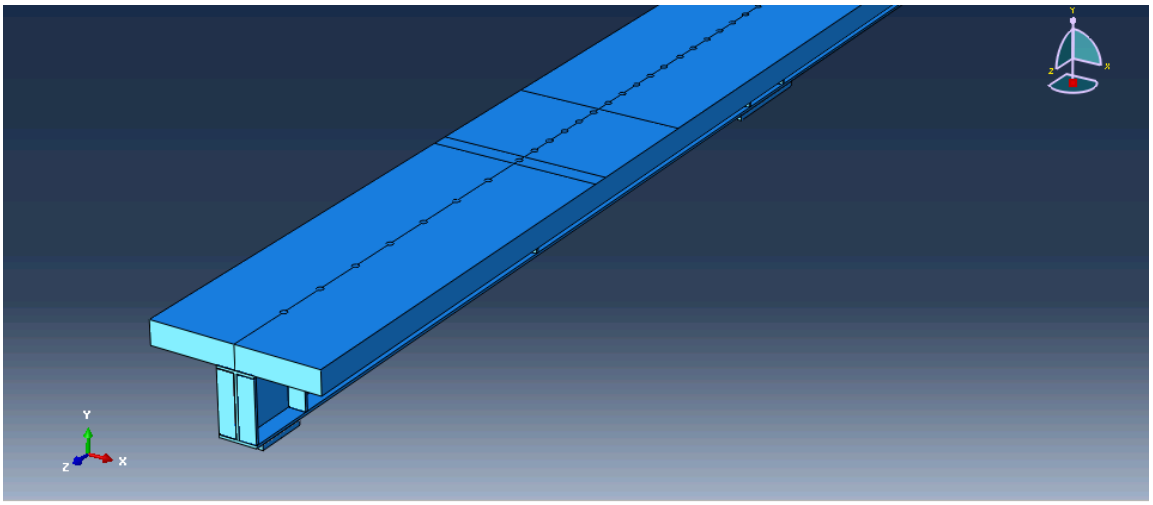

Fig. 6- 8 Cell and surface partitions of the model before meshing

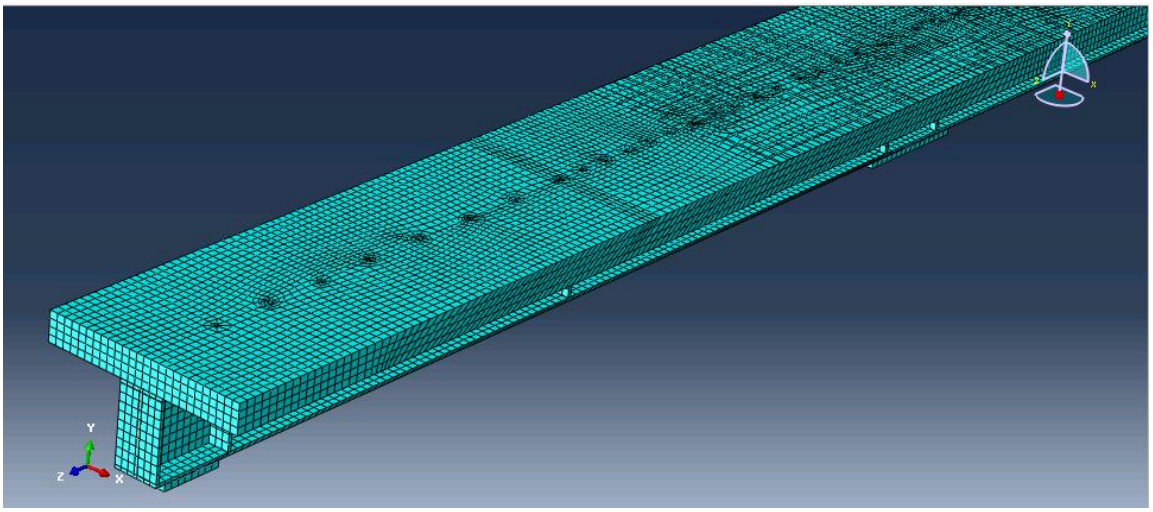

Fig. 6- 9 Meshing for the modeled girder

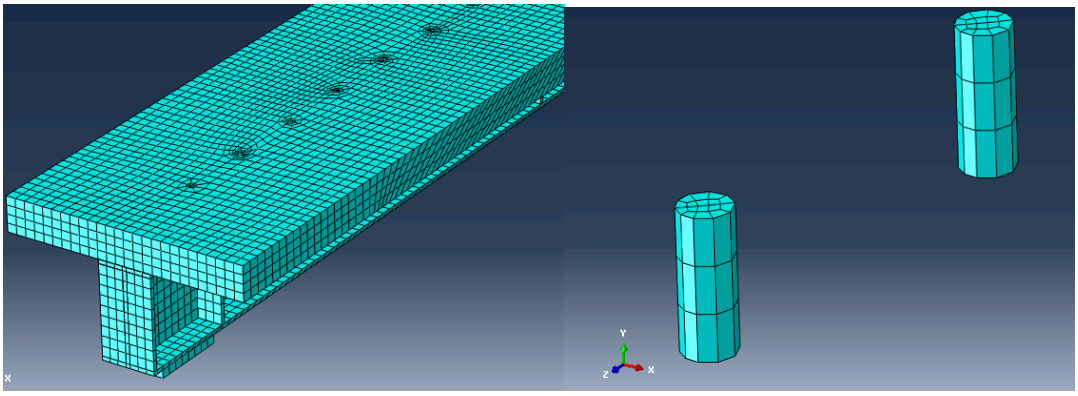

Fig. 6- 10 Meshing of different components of the modeled girder

6.2.5 Boundary Condition and Loading

The 5 m continuous composite girders were modeled using ABAQUS/Explicit solver. The point load was applied as an equivalent pressure load on 50 mm bearing steel plates that were mounted to the top of concrete slab and covered the full width of concrete slab. Load control was used to apply the load. Two roller and one pin support were assigned as line restrains to the mid of the 16 mm bearing steel plates at the bottom surface of bottom flange. Number of increments and load step were selected to ensure convergence and smooth transfer between steps.

6.3 VALIDATION OF THE MODEL

The FE model was validated with experimental results of testing continuous composite girder bonded with CFRP which presented in chapter five. The experimental load-deflection curve, stresses, concrete cracking, mode of failure, and steel-concrete interface slip were used for validation.

6.3.1 Load-Deflection Behavior

The numerical load-deflection curves were showed good agreement with the experimental ones as shown in Figs. 6-11a – 6-11f. The load-deflection curve obtain from the modeled girders was able to predict the ultimate capacity of composite girders bonded with CFRP at the negative moment region in addition to the stiffness and deflection at failure. However, the failure deflection of the FE results was relatively higher than experimental one. Comparison between experimental and numerical ultimate capacity is summarized in Table 19.

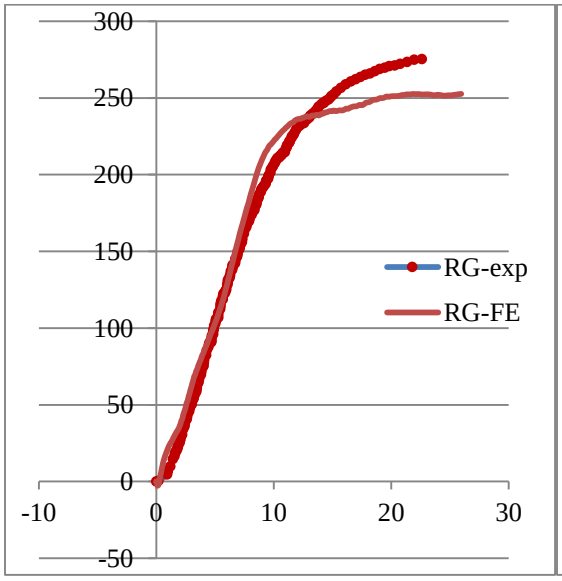

a. Girder RG

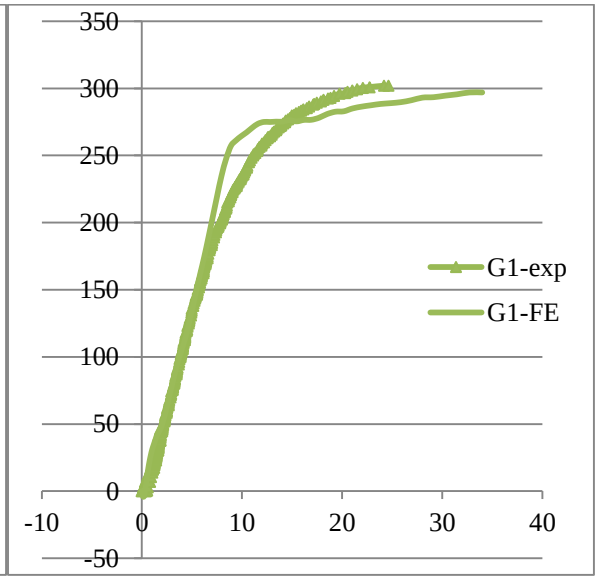

b. Girder G1

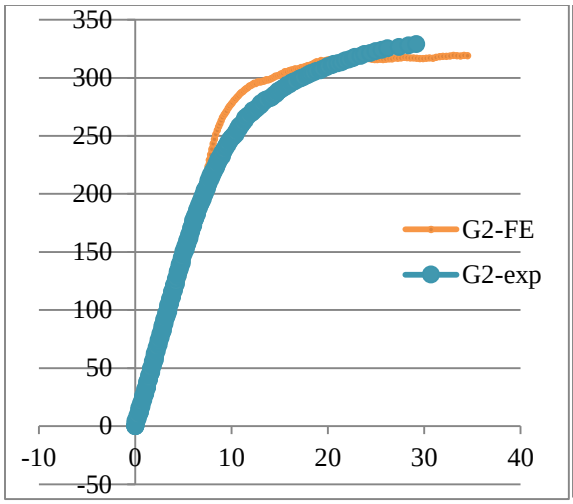

c. Girder G2

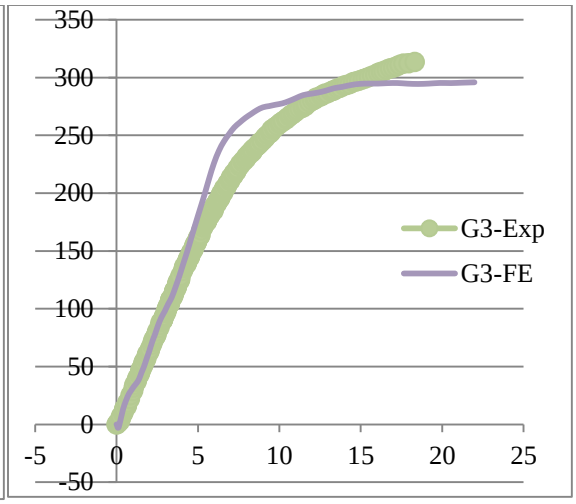

d. Girder G3

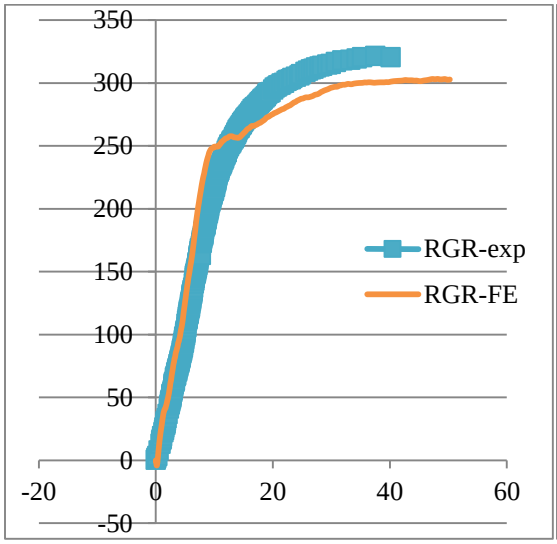

e. Girder RGR

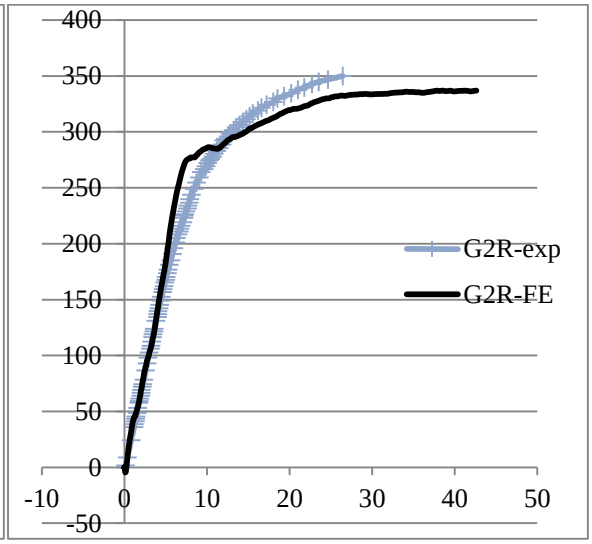

f. Girder G2R

Fig. 6- 11 Comparison between numerical and experimental Load-deflection curve

Table 19 Comparison between numerical and experimental ultimate capacity (KN)

Girder	RG	G1	G2	G3	RGR	G2R
Experimental	273	303	330	314	323	352
Numerical	253	297	319	285	304	337

6.3.2 Stress and Strain Distributions

At ultimate load, the model stresses of steel-concrete section at mid-span were compared for all girders with the experimental results as summarized in Table 20. The strain distribution (plastic strain) at mid-span for girder G2 is shown in Figs. 6-12 and 6-13. This distribution shows good agreement with the experimental strain of girder G2 (Chapter five). The experimental strain at bottom flange was 0.015 whereas the numerical one was 0.0164 (0.015 plastic strain + 0.0014 elastic strain). Similar comparison was conducted at interior support as shown in Table 21. The stress in CFRP was compared with the experimental maximum stress for all girders as summarized in Table 21. The distribution of stress along CFRP sheet for girder G2R is shown in Fig. 6-14 which indicated that the maximum stress is over the interior support and reduced to close to zero at the inflection points.

Table 20 Comparison between experimental and numerical stresses at mid-span at ultimate load

Girder	Stresses at the top of concrete slab (MPa)		Stresses at bottom flange of steel section (MPa)	
	Exp.	Numerical	Exp.	Numerical
RG	22	19.1	293	308
G-1	21	18.8	308	310
G-2	24.5	23.1	320	328
G-3	22	16.8	308	305
RG-R	26.5	26.5	321	333
G2-R	26.5	28	320	338

Table 21 Comparison between experimental and numerical stresses at interior support at ultimate load

Girder	Stresses in CFRP over the interior support (MPa)		Stresses at the bottom flange of steel section (MPa)	
	Exp.	Numerical	Exp.	Numerical
RG	-	-	282	285
G-1	1067	1069	283	287
G-2	1250	1100	287	290
G-3	789	850	281	284
RGR	-	-	286	294
G2R	1420	1511	285	292

Comparison between the numerical and experimental model was conducted also through loading of girders. The load corresponds to cracking load and yielding of steel section were compared in Table 22 and showed good agreement.

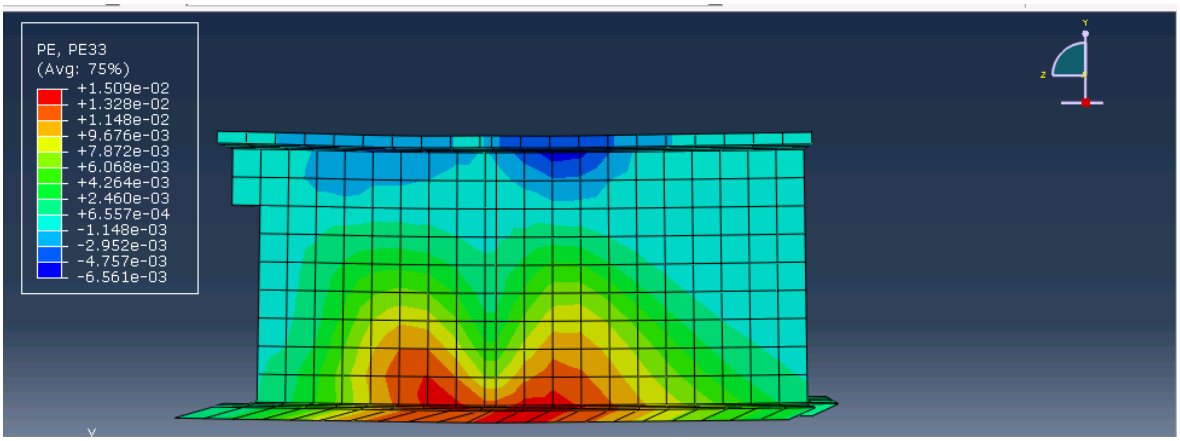

Fig. 6- 12 Plastic strain at mid-span for girder G2

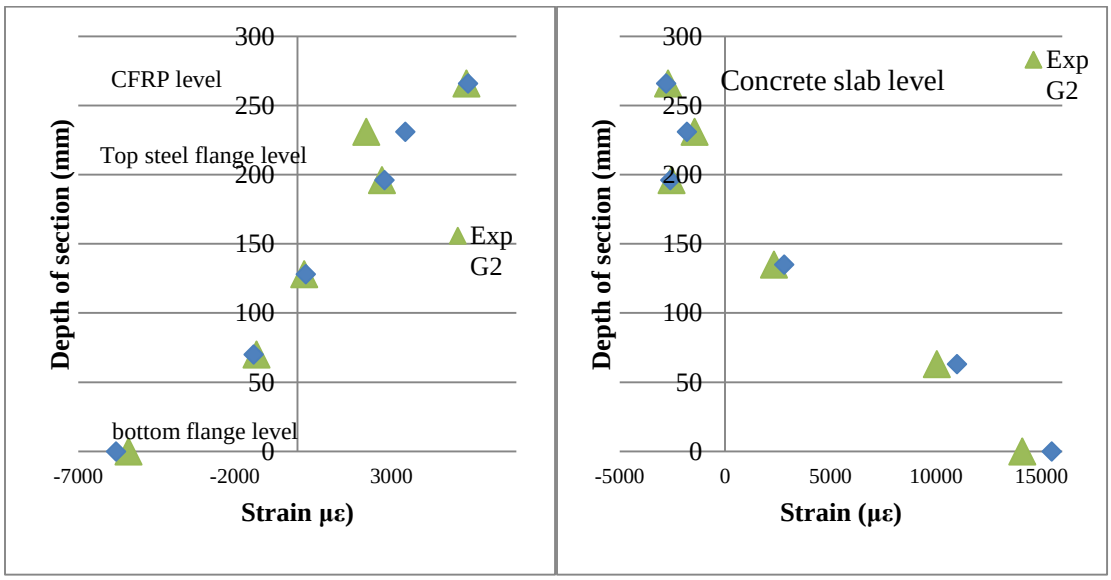

a. Interior support b. Mid-span

Fig. 6- 13 Strain distribution along the cross sections of girder G2at ultimate load

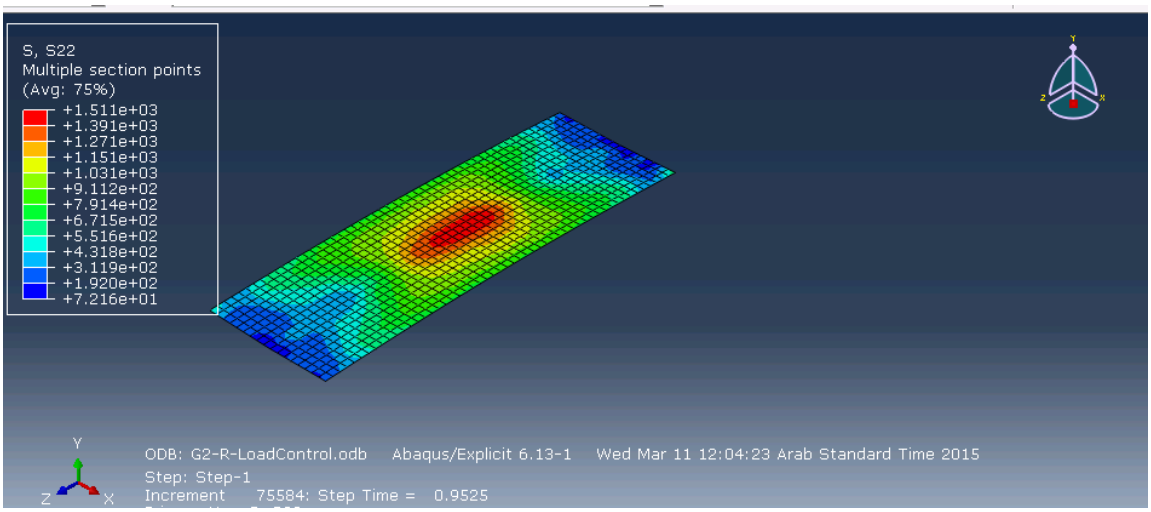

Fig. 6- 14 Stress in CFRP for girder G2R

Table 22 Numerical and experimental comparison between yield load of steel section (KN)

Stage of loading	Girder	RG	G1	G2	G3
Cracking Load	Experimental	75	122	136	150
	Numerical	73	120	131	143
Yielding of bottom flange (mid-span)	Experimental	163	165	173	175
Yielding of bottom flange (mid-span)	Numerical	157	163	170	171
Yielding of bottom flange (interior support)	Experimental	228	225	222	249
Yielding of bottom flange (interior support)	Numerical	225	220	216	263

6.3.3 Mode of Failure Validation

The experimental results showed different types of modes of failure. Girders in group I were failed in a shear-compression failure whereas girders in group II failed by crushing of concrete slab at mid-span or de-bonding of CFRP for girders RGR and G2R respectively. The FE model was able to predict failure of continuous composite girders. The tension and compression concrete damage for girder G2 are shown in Figs. 6-15a & 6-15b respectively. It could be noticed the diagonal tension damage at the bottom of concrete slab and the compression damage at the top of concrete slab at mid-span. The ultimate strain in concrete was not reached and shear-compression failure was occurred in concrete slab at mid-span which eliminated developing of full capacity of concrete. Concrete damage in compression for girder RGR is shown in Fig. 6-16 which reflects crushing of concrete slab at ultimate load.

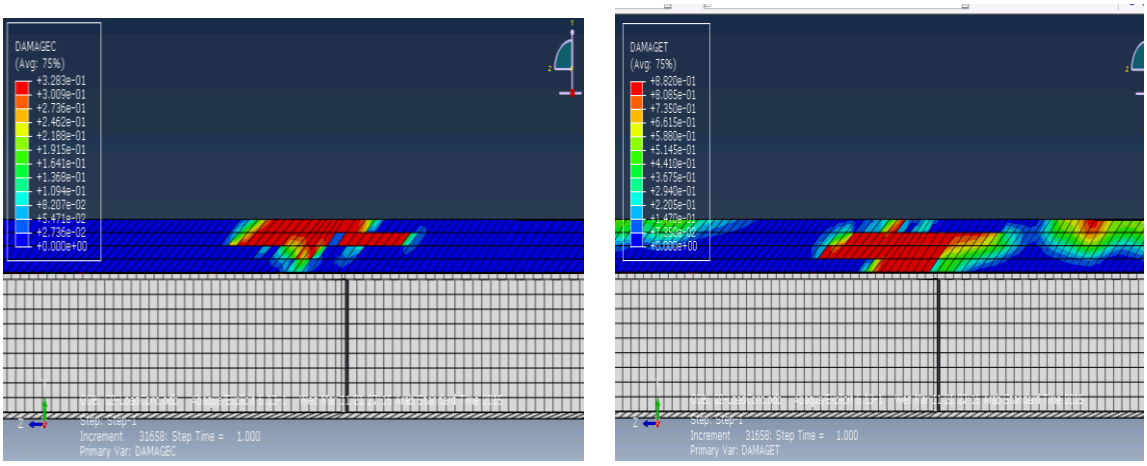

a. **Compression damage** **b. Tension damage**

Fig. 6- 15 Concrete damage

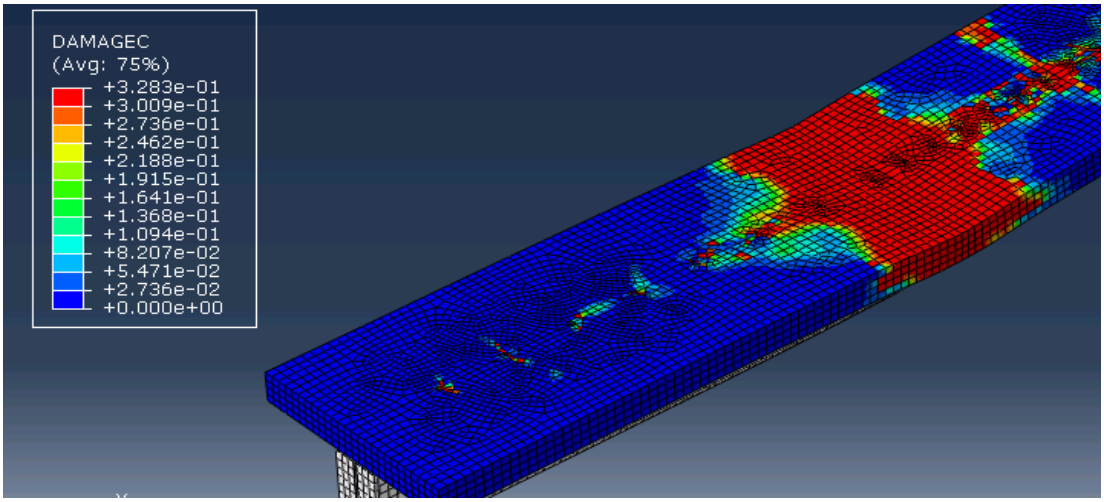

Fig. 6- 16 Concrete damage in compression for girder RGR

6.3.4 Concrete Cracking Validation

The concrete damage model was able to predict most of the experimental crack. Concrete cracks at the negative moment region of concrete slab (Fig. 6-17), along the line of shear studs (Figs. 6-18 and 6-19), in addition to the shear-compression failure cracks were visualized by the use of this model. FE results of modeling the composite girder bonded with CFRP to the top of concrete slab at negative moment region showed ability of this model to predict all notified experimental cracks. Further, cracks under CFRP sheets could be visualized by use of concrete damage model in compression and tension.

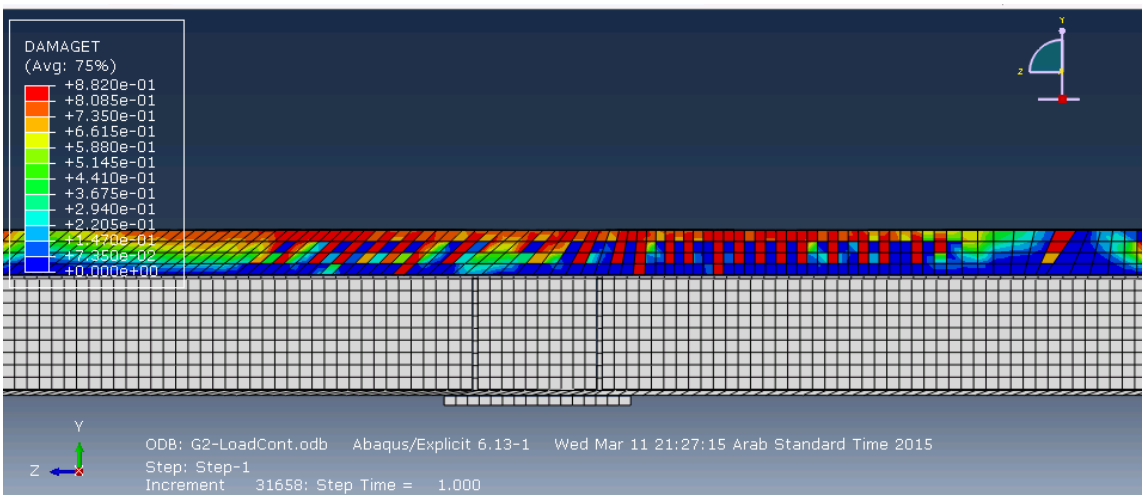

Fig. 6- 17 Concrete damage at negative moment region

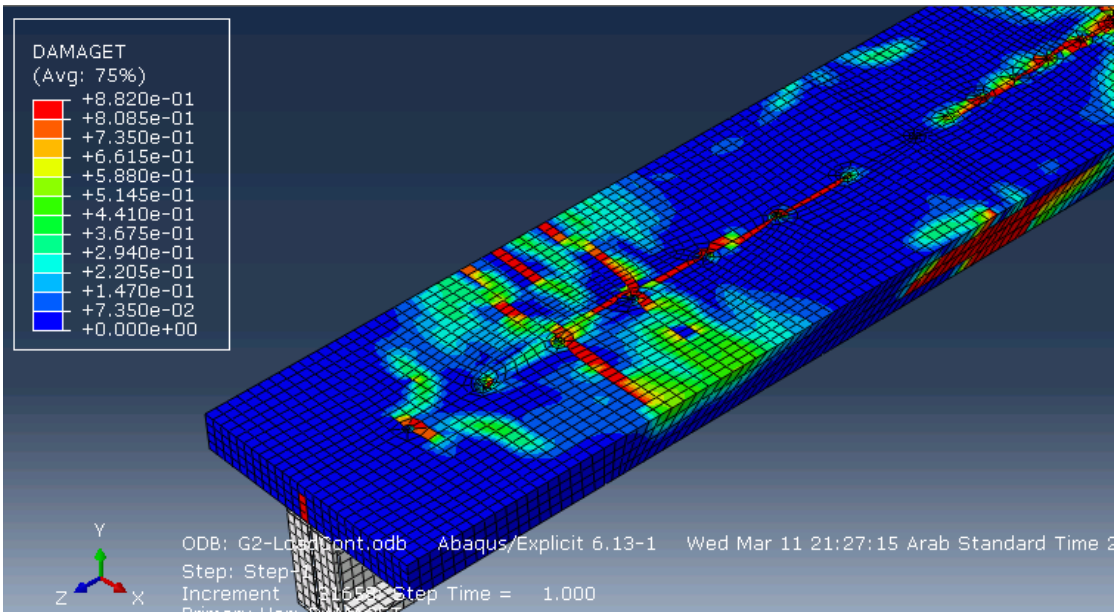

Fig. 6- 18 Concrete damage along the line of shear studs

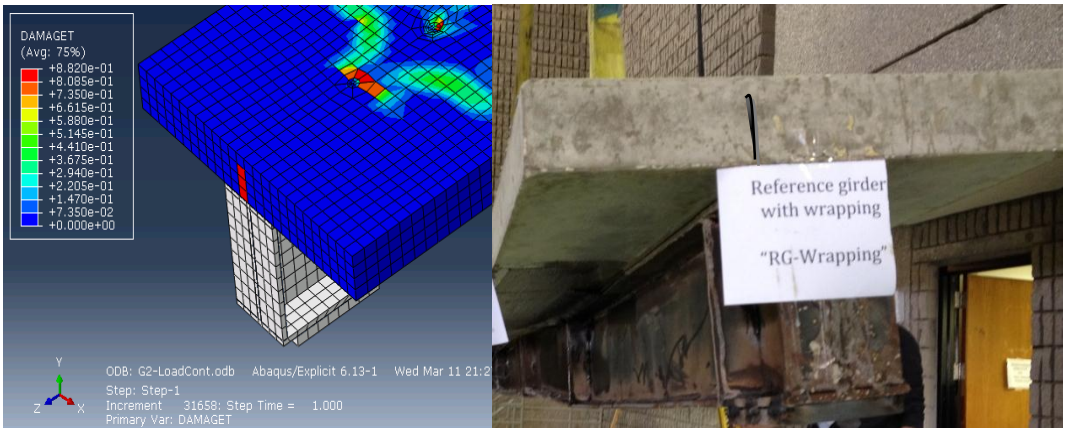

Fig. 6- 19 comparison between experimental and numerical crack at the end of concrete slab

6.3.5 Steel-concrete Interface Slip

Surface-surface contact model was used to model the interface between shear studs and the surrounded concrete. Introducing the interface gave the model an ability to figure out the relative slip between concrete and steel. The numerical interface slip was compared with experimental LVDT's readings at the same locations and showed good agreement. Comparison between experimental and numerical load-slip curves of girders G2R is illustrated in Fig. 6-20. This girder (girder G2R) is used for comparison because it developed the highest ultimate capacity, therefor the highest tangential shear force on shear studs.

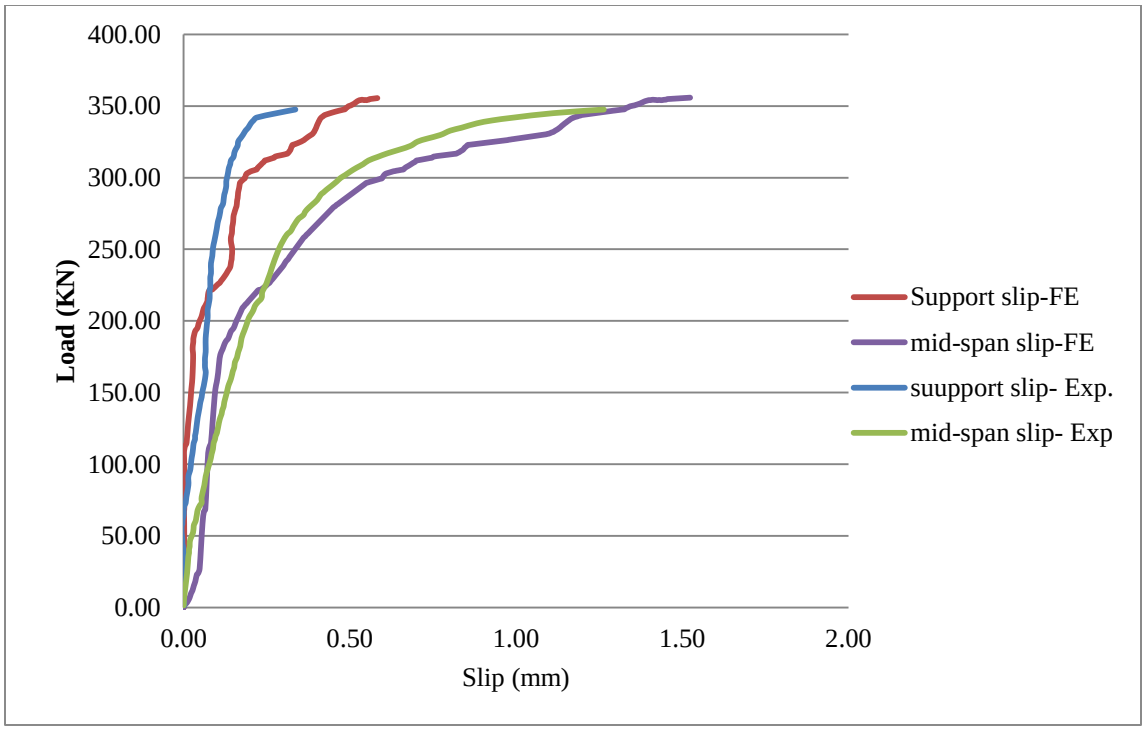

Fig. 6- 20 Comparison between numerical and experimental slip for girder G2R

6.4 NUMERICAL INVESTIGATION OF THE REQUIRED THICKNESS AND LENGTH OF CFRP

FE model of continuous composite girder bonded with CFRP top of concrete slab at the negative moment region was developed in the previous sections. In this section, the verified model is used to investigate numerically the appropriate thickness, length of CFRP, as well as number of shear connectors to strengthen continuous composite girders. Modeling of composite girder with 90 mm slab thickness is conducted in this section. The geometry and material properties of steel section was the same as girders in group I. The 90 mm slab thickness was selected to insure yielding of steel section and crushing of concrete slab at ultimate load.

6.4.1 Evaluation Effect of CFRP Thickness

The appropriate thickness of CFRP is defined as the maximum thickness of CFRP that could be bonded to the top of concrete slab and allows reaching the moment capacity at positive and negative moment zone with no de-bonding or rupture failure of CFRP. The moment capacity at negative moment region is described as reaching full yielding of steel section and considerable level of stress in CFRP. Three main expected modes of failure for girders with different thicknesses of CFRP; de-bonding of CFRP sheets prior reaching the ultimate load because exceeding the shear capacity of epoxy, or reaching the moment capacity at mid-span prior full yielding of steel section at negative moment zone due to thick layer of CFRP. The third type of failure is the desired failure; this failure occurs

when the steel section reaches full yielding at negative moment region followed by reaching the moment capacity and crushing of concrete slab at mid-span.

Four girders with 90 mm slab thickness were modeled to investigate the proper thickness of CFRP that needed to increase the flexural strength of the composite girder. One girder considered as control girder with no CFRP at negative moment region ($\check{C}_0$) and the other three girders were strengthened with one, two, and three layers of CFRP ($\check{C}_1$, $\check{C}_2$, $\check{C}_3$ respectively). Epoxy adhesive strength was taken according to the pull-out test (2 MPa). CFRP length extended for the full negative moment region in addition a development length of 150 mm from each side according to the ACI specifications. The FE results showed an increase in the ultimate load capacity as thickness of CFRP increased up to certain thickness as shown in Table 23. The increase of ultimate capacity was limited to the be-bonding of CFRP sheets as for girders $\check{C}_2$ and $\check{C}_3$. For both girders, the shear stresses exceeded the epoxy adhesive strength, and therefore de-bonding occurred close to the cut points of CFRP sheets. The tensile force in CFRP is approximately the same for girders $\check{C}_2$ and $\check{C}_3$ which indicate that total tensile force of CFRP was limited to the strength of adhesive. Therefore, the increase of CFRP thickness for girder $\check{C}_3$ less utilized the tensile strength of CFRP compare to girder $\check{C}_2$. This showed that the proper number of layers to strengthen this girder is one layer (girder $\check{C}_1$) since this is the maximum thickness that allowed reaching the moment capacity at negative and positive moment zones without de-bonding of CFRP.

Table 23 Effect of thickness of CFRP on the ultimate capacity of composite girder

Girder	Thickness (mm)	Ultimate capacity (KN)	Increase of capacity	CFRP stress (MPa)	CFRP force (KN)	Type of failure
$\check{C}_0$	-	312	-	-	-	Crushing of concrete
$\check{C}_1$	0.131	341	9.3%	1480 (0.43 σ_u)	97	Crushing of concrete
$\check{C}_2$	0.262	354	13.5%	1438 (0.41 σ_u)	189	De-bonding of CFRP
$\check{C}_3$	0.393	355	13.5%	1003 (0.29 σ_u)	197	De-bonding of CFRP

As both girders $\check{C}_2$ and $\check{C}_3$ failed prematurely by de-bonding of CFRP, it was of interest to examine if the load carrying capacity can be further enhanced by preventing the failure of epoxy adhesive in order to investigate effect of other modes failure. Therefore, different type of epoxy adhesive was used (Sikadur -30). The shear strength of this adhesive is 4 MPa. However, this value cannot be reached because the concrete tensile strength is 3.1 MPa.

The FE model of composite girder with 90 mm slab thickness was used to model six girders of adhesive strength of 4 MPa and strengthened with different number of CFRP layers as listed in Table 24. The ultimate load flexural capacity was increased as thickness of CFRP increased and considerably influenced by the ratio of positive to negative moment capacities(α). The ultimate capacity of composite girders bonded with

CFRP was directly proportional to the thickness of CFRP up to specific thickness as illustrated in Fig. 6-21 and Table 24. The stiffness of girders was directly proportional to the thickness of CFRP for all girders as illustrated in Fig. 6-21.

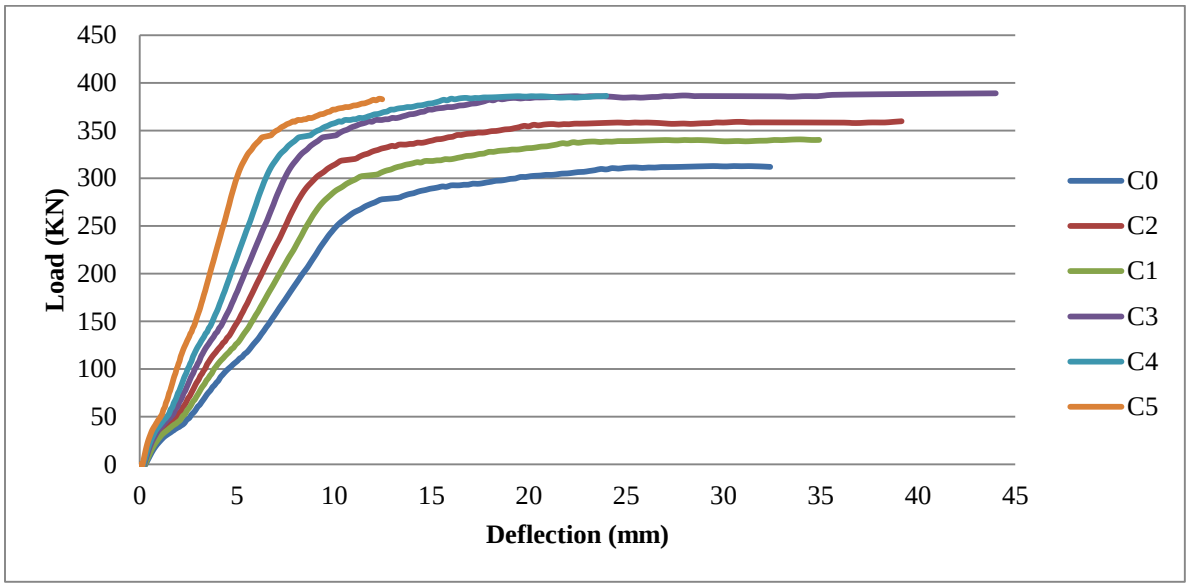

Fig. 6- 21 Load deflection curve of girders with different thickness of CFRP and adhesive strength of 4 MPa

Table 24 Increase of ultimate capacity of girders with 4 MPa adhesive strength

Girder	CFRP thickness (mm)	Ultimate load (KN)	Increase of capacity (%)
C0	-	312	-
C1	0.131	341	9.1 %
C2	0.262	361	15.7 %
C3	0.393	388	24.5%
C4	0.524	385	23.4 %
C5	0.655	375	20.3%

The increase of ultimate capacity is function of both; increasing the moment capacity at negative moment region due to the composite action with CFRP and the ratio of positive to negative moment capacity (α). The increase of CFRP thickness increased the moment capacity at interior support and decreased the ratio α. As CFRP thickness increased, the required load to yield the steel section at interior support increased. At a certain thickness, the composite steel-concrete section at mid-span was reached before developing the full yielding of steel section at interior support as for girders C4 and C5 as shown in Figs. 6-22 and 6-23. Therefore the ultimate capacity was reached while steel section at interior support structurally intact and the CFRP could not be utilized as shown

in Table 25. The compatibility of composite section at interior support restricted CFRP to develop higher strain and reduced utilizing the CFRP tensile strength. This showed that reduction of ultimate strength is due to partial yielding of steel section at interior support instead of full yielding in addition to the reduction in the tensile force of CFRP as listed in Table 25. The numerical results for this list of girders confirmed the experimental results. It showed that as the ratio α became less than 1.2, this caused to reach the failure load at mid-span while considerable part of the steel section at interior support was not yielded and the tension force in CFRP is relatively small. All girders failed by crushing of concrete slab at mid-span as listed in Table 25. Table 25 indicates that all girders with ratio α higher than 1.2 could develop stresses in CFRP higher than 0.35 σ_u. This gives an indication that CFRP stress could be assumed safely equal to 0.35 σ_u.

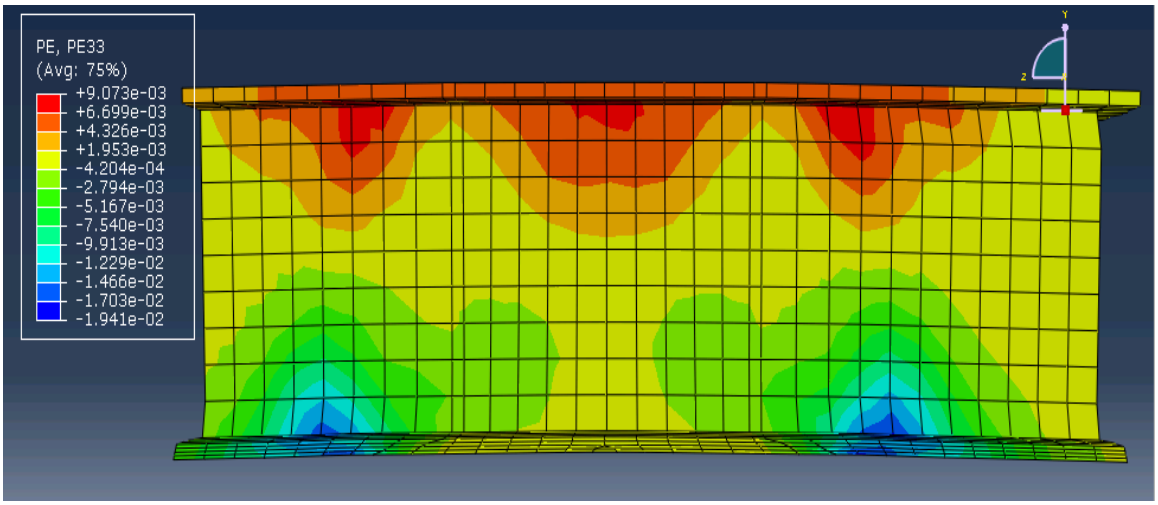

Fig. 6- 22 Plastic strain over the interior support, Girder C3

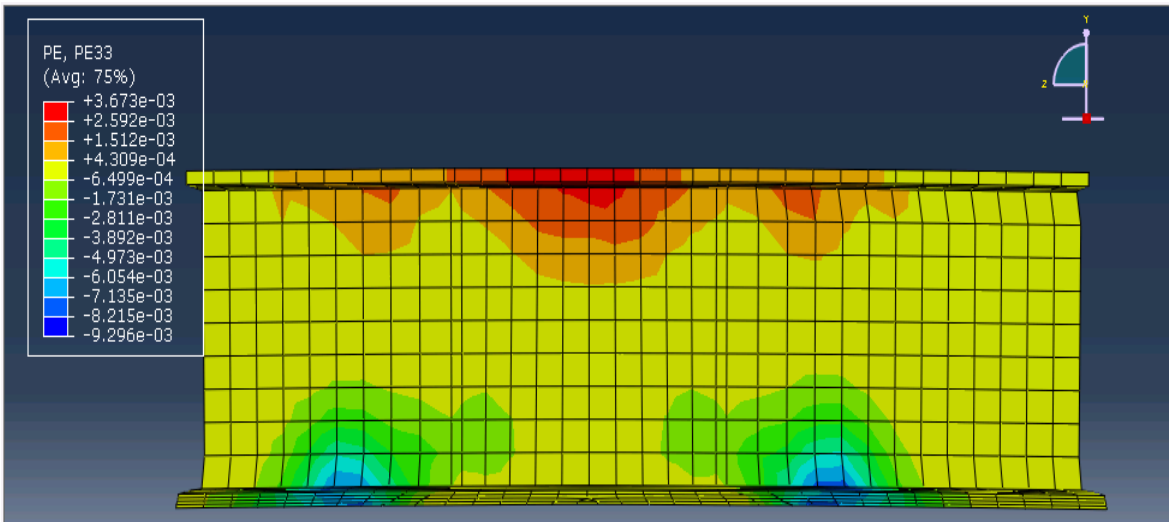

Fig. 6- 23 Plastic strain over the interior support, Girder C5

Table 25 CFRP Stress and mode of failure for girders with 4 MPa adhesive strength

Girder	CFRP stress (MPa)	CFRP force (KN)	α	Type of failure
C0	-	-	1.71	Crushing of concrete
C1	1480 (0.43 σ_u)	97	1.48	Crushing of concrete
C2	1450 (0.42 σ_u)	190	1.38	Crushing of concrete
C3	1510 (0.44 σ_u)	297	1.20	Crushing of concrete
C4	1053 (0.31 σ_u)	276	1.10	Crushing of concrete
C5	727 (0.21 σ_u)	238	1.01	Crushing of concrete

The analytical ultimate capacity of each girder along with the corresponding M_{+ve}/ M^{*}_{-ve} ratio was calculated according to chapter three and listed in Table 26. Again, the analytical calculations offered a safe estimate for the numerical results.

Table 26 Analytical ultimate capacity of girders with different CFRP thicknesses

Girder	$\breve{M}_{+ve}$ *(KN.m)*	$\breve{M}^{*}_{-ve}$ *(KN.m)*	$\breve{P}_{tf}$ (KN))	$\breve{\alpha}$	P_u (Numerical) (KN)
C0	130	76	277	1.71	312
C1	130	88	287	1.48	341
C2	130	94	292	1.38	361
C3	130	108	304	1.20	388
C4	130	118	312	1.10	385
C5	130	128	320	1.01	375

The cracking load P_{cr} and the required load to cause yielding of bottom flange at mid-span P_y were investigated as shown in Table 27. The ratio of cracking load to the yielding load, λ, was calculated and showed that use of CFRP maintained the composite action close to service load for this group of girders which confirmed the experimental results.

Table 27 Cracking load to yielding load for girders with different thicknesses of CFRP

Girder	P_{cr} (KN)	P_y (KN)	λ
C0	77	172	0.45
C1	135	174	0.77
C2	140	179	0.78
C3	149	180	0.83
C4	155	181	0.85
C5	166	182	0.91

6.4.2 Evaluation Effect of CFRP Length

According to the ACI specifications, the CFRP length should extend at least 150 mm from each side, and extra 150 mm for any additional layer of CFRP. In the section, Total of four girders were modeled to investigate the minimum required development length of CFRP sheet to reach the ultimate plastic capacity of composite girder. The CFRP development length was varied starting by no development length (L1) and up to 300 mm (L3) from each side with 100 mm increment for each girder as listed in Table 28. Girders with two layers of CFRP sheets bonded to the top of 90 mm slab thickness using an adhesive strength of 4 MPa were modeled in this section.

Table 28 List of girders with different CFRP length

Model	Development length (mm)
L1	zero
L2	100
L3	200
L4	300

The ultimate capacity of girder extended by 200 mm or more beyond the inflection point had no effect on the ultimate strength as illustrated in Fig. 6-24. Reduction of CFRP development length to 100 caused a slight reduction of ultimate strength from 360 KN to 355 KN whereas capacity was considerably decreased when CFRP cut at inflection point (338 KN). This reduction in capacity was due to de-bonding of CFRP prior reach the ultimate moment capacity of composite girders. The steel section at both sections locations; positive and negative moment zone did not fully yielded. Therefore, this agrees the ACI requirements and it's recommended to extend CFRP sheets at least 150 mm from each side.

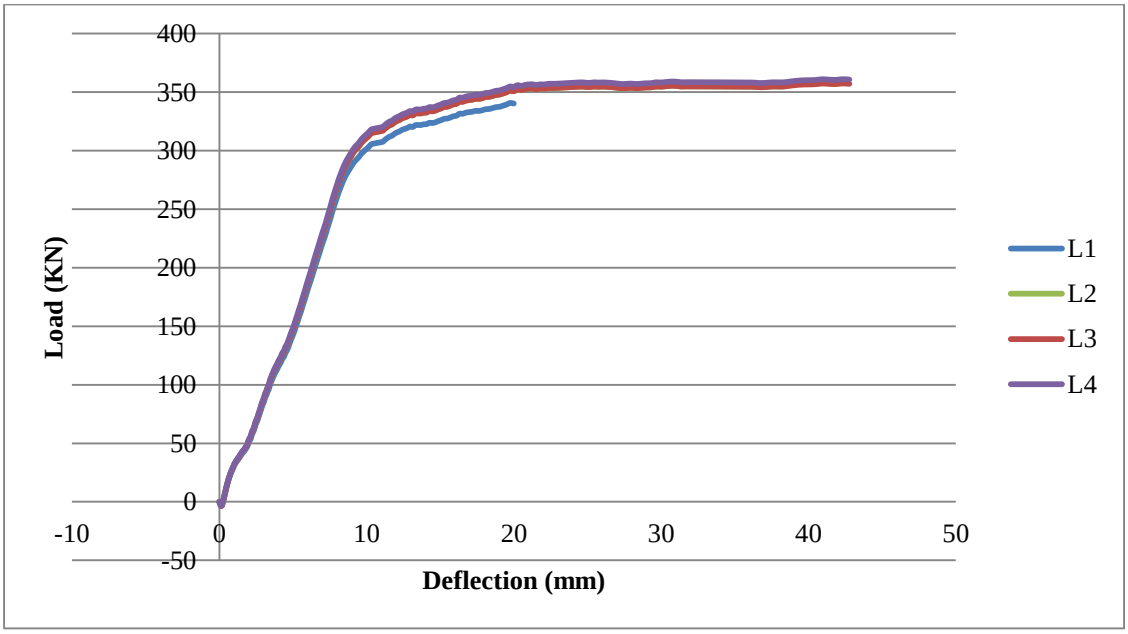

Fig. 6- 24 Load-deflection curve for girders with different CFRP length

6.4.3 Effect of Shear Studs Spacing at Negative Moment Zone

The FE model is used to simulate the effect of shear studs spacing, and investigate the required number of shear studs to form the composite action at negative moment region. Total of three girders with different shear studs spacing at the negative moment region were modeled. The three spacing are; 75, 120 and 150 mm. Spacing of 75, and 120 mm considered proper spacing to achieve full composite action whereas 150 mm presented partially composite action between steel section and the CFRP sheets that bonded to the concrete slab. The three spacing were calculated according to the push-out test for shear studs and the tensile force in CFRP was taken as girder C2 in the last section. The composite girder was considered with 90 mm slab thickness and bonded with two layers of CFRP at the negative moment region using 4 MPa adhesive strength.

The shear stud spacing had an effect on the ultimate capacity of composite girders as illustrated in Fig. 6-25. A small reduction in ultimate capacity was recorded as the shear stud spacing increased from 75 mm to 120 mm. This reduction is relatively not considerable. The increase of shear stud spacing to 150 mm which classified as partial composite had a reduction of 3.5 % in the ultimate load compare to 75 mm spacing.

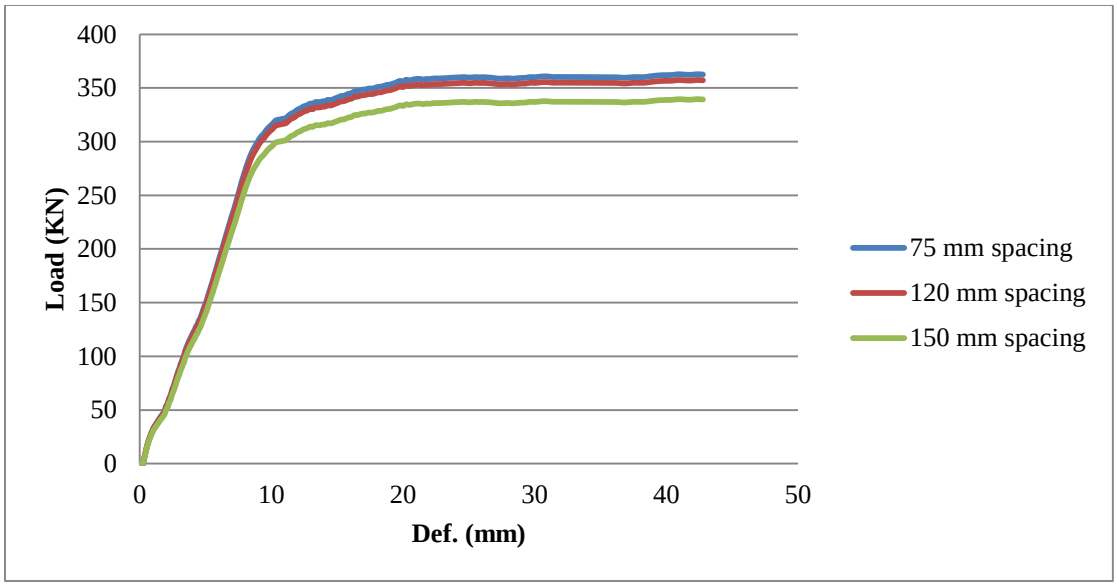

Fig. 6- 25 Load-deflection curve for girders with variable shear stud spacing at negative moment

Considerable increase of concrete-steel slip by increasing shear stud spacing as illustrated in Fig. 6-26. Girder with 150 mm shear stud spacing was exceeding the limit value of slip (1.33 mm). For girder with 120 mm spacing, this spacing was selected to have 100% full composite action compare to 130% for 75 mm. It could be seen that the relative slip between steel section and the concrete soffit is the maximum allowed slip to form full composite action as shown in Fig. 6-26. Comparison between deformation of shear studs for girder with 75 and 150 mm spacing is shown in Figs. 6-27 and 6-28. This indicated that number of shear studs could be estimated based on the assumed stress in CFRP as will discuss next chapter. No change in the failure mechanism was occurred as shear stud spacing at negative moment region varied. Varying shear studs spacing at negative moment region had minimal effect on cracking of concrete slab.

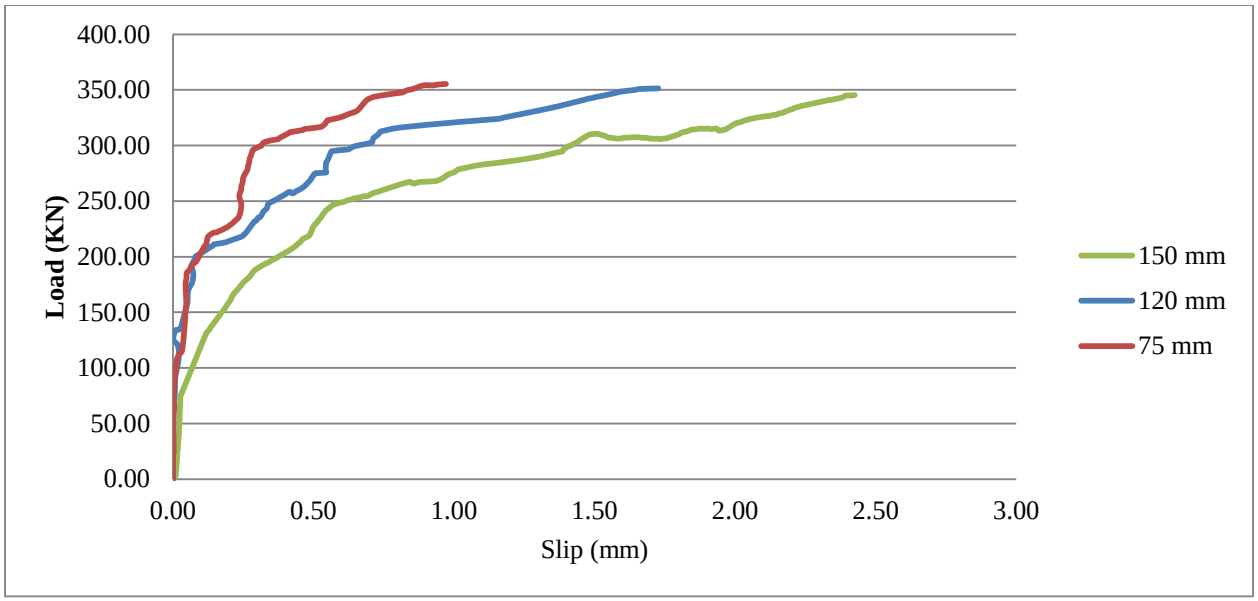

Fig. 6- 26 Load-slip curve for girders

Reduction in CFRP stress was recorded as shear spacing increased as summarized in Table 29. Steel reinforcement stress was reduced too. The reduction in CFRP and steel reinforcement stresses was the main cause to reduce the ultimate capacity for girder with higher spacing of shear studs (150 mm).

Table 29 Effect of shear stud spacing on CFRP and steel reinforcement stresses

Shear stud spacing (mm)	CFRP stress (MPa)	Steel reinforcement stress (MPa)
75	1450 (0.42 σ_u)	427
120	1413 (0.41 σ_u)	425
150	1270 (0.36 σ_u)	420

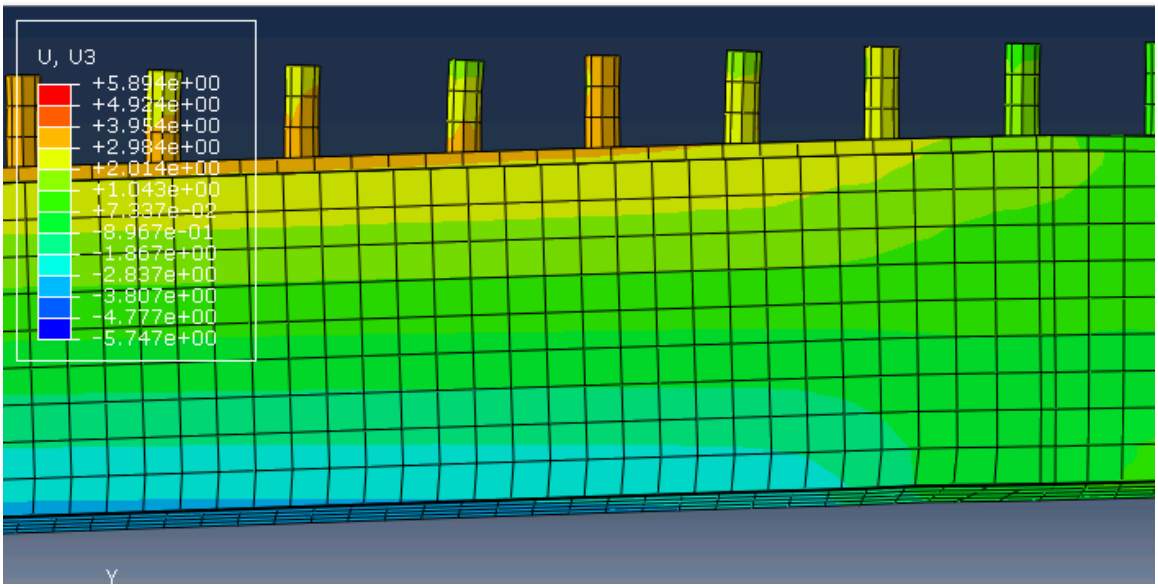

Fig. 6- 27 Deformation of shear studs-75 mm spacing

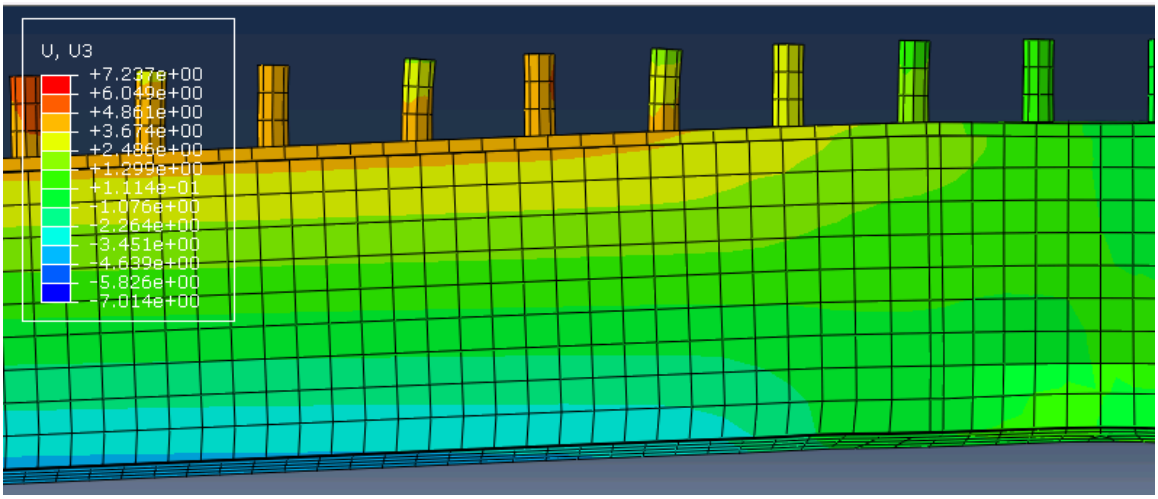

Fig. 6- 28 Deformation of shear studs- 150 mm spacing

CHAPTER SEVEN

SIMPLIFIED DESIGN OF CONTINUOUS COMPOSITE GIRDER REINFORCED WITH CFRP

Experimental and numerical works were conducted in the last chapters to investigate the behavior of continuous composite steel-concrete girders bonded with CFRP at negative moment region. The experimental and numerical results assure the ability of this technique to maintain composite action at negative moment region in addition to the increase of ultimate strength and stiffness. Many factors are controlling the increase of ultimate strength. This chapter will deal with these factors to come up with a simplified design equation that could be used by engineer. Equations to calculate ultimate capacity of section bonded by CFRP and thickness of CFRP are provided in this part. Simplified design will be adapted based on reasonable assumptions. Assumptions include material, geometry, and behavior assumptions according to the experimental and numerical results.

7.1 DESIGN PHILOSOPHY

Normal design of composite steel-concrete girders ignored the concrete slab at negative moment region because of tensile stress. The steel girder is assumed to either act alone or compositely with the longitudinal slab reinforcement. Both steel section and steel reinforcement are ductile material and have the ability to rotate to allow formation of the 2^{nd} plastic hinge at mid-span. However, use of CFRP to the top of concrete slab at negative moment region is mainly adding a high strength-to-weight ratio and rigidity material. This will restrict ability of steel section to rotate, so proper design should allow yielding of steel section at interior support prior reaching the moment capacity at mid-span without any premature or secondary failures. The simplified design solution was conducted based on several assumptions as will discuss in this section.

7.1.1 Material Assumptions

Several material assumptions are considered which basically typical assumptions for design. The assumptions are:

1) The tensile strength of concrete is ignored.
2) The structural steel and steel reinforcement are considered as elastic-perfectly plastic.
3) The strength of concrete in compression is taken as $0.85\ f'_c$.
4) The tensile and compressive capacity of steel is yielding f_y.
5) The concrete slab is fully composite with the steel section.

7.1.2 Geometrical Assumptions

1) Preventing local buckling

The local buckling should be prevented for all components of steel beam; flanges and web. Local buckling occurs if the compression force exceeds the capacity of steel plate, so that proper length/thickness ratio should be selected according to AISC requirements and limits. Buckling of steel plates limits the steel section to reach the full plastic capacity. Section classification according to the ability of each plate to develop the plastic capacity is shown in Fig. 7-1

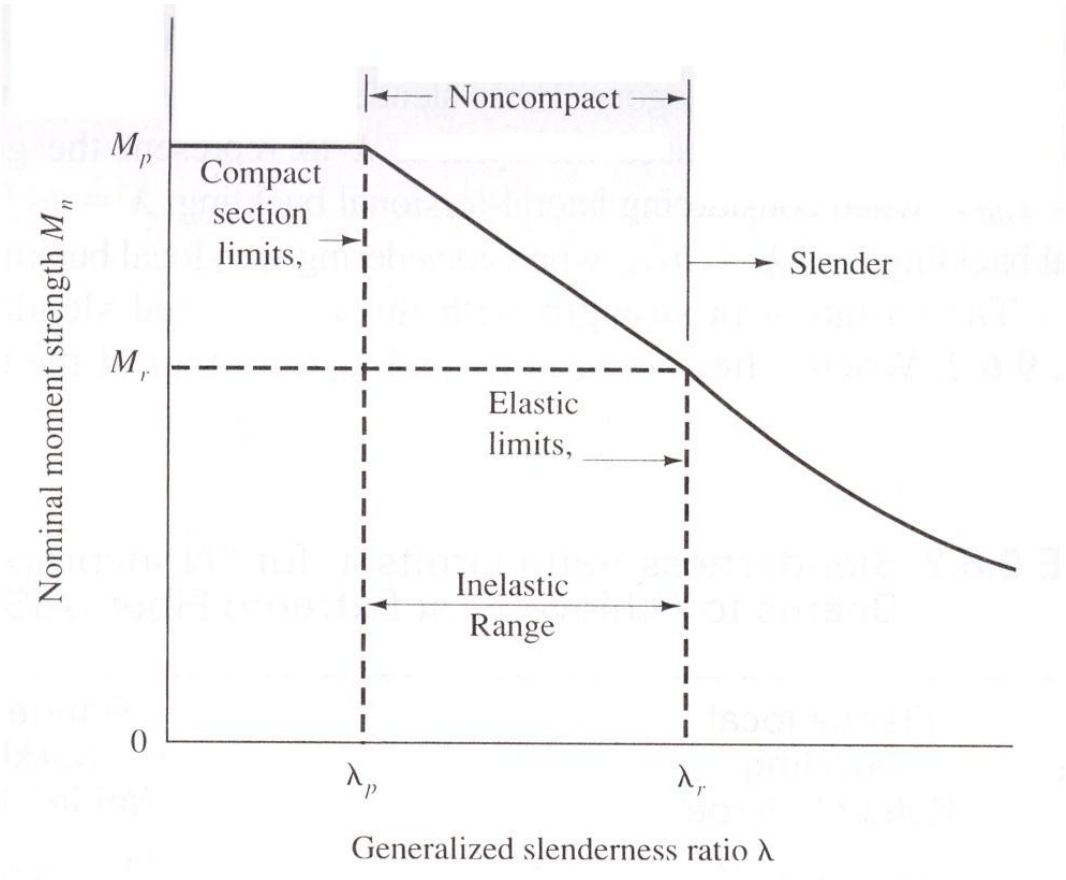

Fig. 7- 1 Classification of steel section according to the slenderness ratio

2) Preventing lateral torsional buckling (LTB)

If the flexural moment is coupled with buckling deformation in the torsional and lateral directions, then LTB is occurred. This local failure could be eliminated by use of lateral supports at adequate spacing as per AISC requirements. Fig. 7-2 shows ability of developing the plastic capacity as the unbraced length is varying.

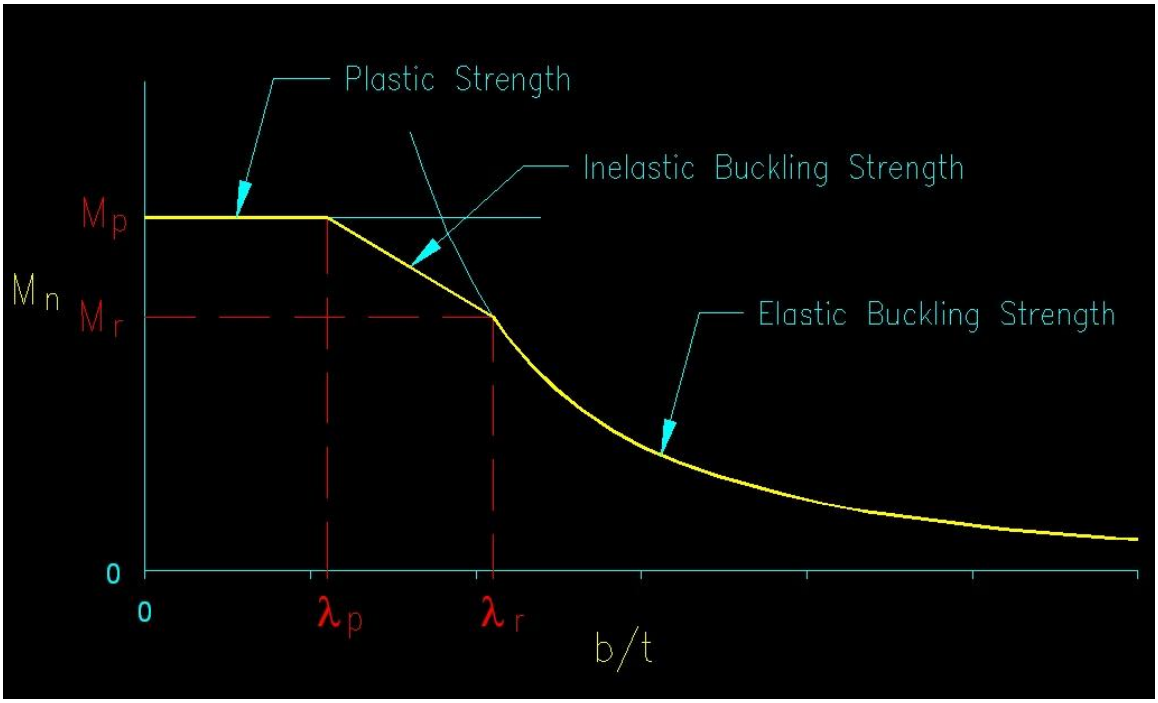

Fig. 7- 2 Effect of unbraced length on the moment capacity of steel section

3) Preventing web yielding and web crippling

Web yielding or web crippling are occurred due to the effect of point load like support reactions on steel section. So that, proper steel plates with proper thickness and length should be provided to eliminate this local failure

4) Preventing shear failure.

The shear failure should be eliminated. Shear capacity of composite steel-concrete girder is calculated according to the capacity of steel web, so proper size of steel web should be selected to prevent shear failure before developing the full flexural capacity. However, the experimental program assures selecting of proper slab thickness and width so that shear stress will not exceed in slab too.

5) Stiffener plates should be provided under the point load or over support to eliminate stress concentration

7.2 DESIGN STRESS IN CFRP

The stress in CFRP should be selected such that proper contribution of CFRP to the section capacity is involved. On the other hand, this assumption should be reasonable so that steel section could rotate to reach this level of stress. Beside those points, the stress in CFRP should be limited to a certain limit to prevent premature failure of CFRP. The premature failure could be de-bonding of epoxy adhesive or rupture of CFRP. In this work, de-bonding of CFRP was more critical and occurred for different girders.

Table 30 listed all the required girders with different modes of failure and stress in CFRP. The listed girders in this table are girders that reached yielding of steel section at interior support prior to reach the ultimate load. The ability of girder to allow yielding of steel section at interior support will be discussed later. All of these girders were developed stress in CFRP more than $0.31\sigma_u$. Stress in CFRP higher than ($0.41\ \sigma_u$) will be

avoided to eliminate de-bonding failure which occurred at this level of stress. So, it's recommended to use stress in CFRP at level of (0.35 σ_u).

Table 30 Level of CFRP stress in Different girder

Girder	Group	Stress in CFRP (MPa) (% of ultimate)	Mode of failure
G1	I	1067 (0.31 σ_u)	Shear-compression
G2		1250 (0.36 σ_u)	Shear-compression
G2R	II	1392 (0.41 σ_u)	De-bonding of CFRP
C1	C	1480 (0.43 σ_u)	Crushing of concrete
C2		1450 (0.42 σ_u)	Crushing of concrete
C3		1510 (0.44 σ_u)	Crushing of concrete

7.3 THICKNESS OF CFRP SHEETS AND SHEAR STUDS

The designed thickness of CFRP is the thickness that allows reaching the plastic moment capacity of steel section at interior support prior to reach the moment capacity at mid-span without de-bonding of CFRP sheets. Therefore, the maximum thickness of CFRP is limited to the de-bonding of CFRP and ability of this thickness to allow yielding of steel section at interior support. The designed thickness is used to calculate the required number of shear studs to form the composite action at negative moment region.

7.3.1 Selection of Maximum Thickness to avoid De-bonding of CFRP

The shear stress could be calculated according to Rosenboom and Rizkalla [34] using the following equation

$$\tau = \frac{d}{dx}[K_p(x)\varepsilon_p(x)] \qquad \text{Equ. (7-1)}$$

Where $\tau = \frac{d}{dx}[\varepsilon_p(x)]$ is the change in strain along the length of the beam x and K_p is the axial stiffness of the plating material per unit width. The value of K_p could be taken as n E_{CFRP} t_f since constant thickness is used along the beam where n is number of CFRP layers, t_f is the thickness of the matrix per layer, and E_{CFRP} is the elastic modulus of CFRP. The numerical results along with the experimental ones showed that the distribution of strain along the CFRP is approximately linear before de-bonding of CFRP sheets, so that, the change of strain along the length could be calculated as:

$$\tau = \frac{\varepsilon}{L/2} \qquad \text{Equ. (7-2)}$$

Where ε is the strain over the interior support and L is the length of CFRP sheet. According to equation (7-1) and (7-2), and assuming reasonable design value of strain ($0.35\sigma_u$), the thickness and number of layers could be calculated using the following equation:

n $t_f = \tau \, E_{CFRP} \, \frac{L/2}{\varepsilon}$ Equ. (7-3)

7.3.2 Selection of Maximum Thickness to avoid Partial Yielding of Steel Section at Interior Support

The experimental and numerical works showed reduction of ultimate capacity as the ratio of positive/negative moment capacity (α) is decreased. Different girders were listed in Table 31 along with the ratio α. This table shows that the capacity is increased by increasing thickness of CFRP as long as the ratio of positive to negative moment region capacity is higher than (1.1 – 1.2). Reduction of ultimate strength and partial yielding of steel section at interior support were recorded for all girders that have ratio α less than 1.1. According to this fact, the design of composite girders partially reinforced with CFRP will consider minimum value of the ratio α is 1.2 to allow full yielding of steel section at interior support. Therefore, the thickness of CFRP should be limited such that moment capacity at negative moment region is equal to the positive moment capacity divided by the ratio α.

Table 31 The effect of ratio α on the ultimate capacity of girder

Girder	Group	Thickness of CFRP (mm)	α	Ultimate capacity (KN)
G1	I	0.131	1.31	297
G2		0.262	1.22	319
G3		0.393	1.05	285
C1	C	0.131	1.48	341
C2		0.262	1.38	361
C3		0.393	1.20	388
C4		0.524	1.10	385
C5		0.655	1.01	375

Based on the ratio of positive to negative moment capacity, the maximum thickness of CFRP could be calculated as follows:

General assumption is to consider the location of the N.A in the steel web as shown in Fig. 7-3. The location of N.A could be calculated using the equilibrium equation (Equ. 7-4).

$$T_s = C_c + C_s + C_{sr} \qquad \text{Equ. (7-4)}$$

Generally, the moment capacity at positive moment region could be calculated using Equ. (7-5). Special case to have the N.A is in the concrete slab, then the compression in steel is zero

$$M = A'_{st} f_y d_1 + A''_{st} f_y d_4 + A_{sr} f_s d_3 + 0.85 f'_c b a d_2 \qquad \text{Equ. (7-5)}$$

Where

A'_{st} is the area of steel section in tension

A'st is the area of steel section in compression

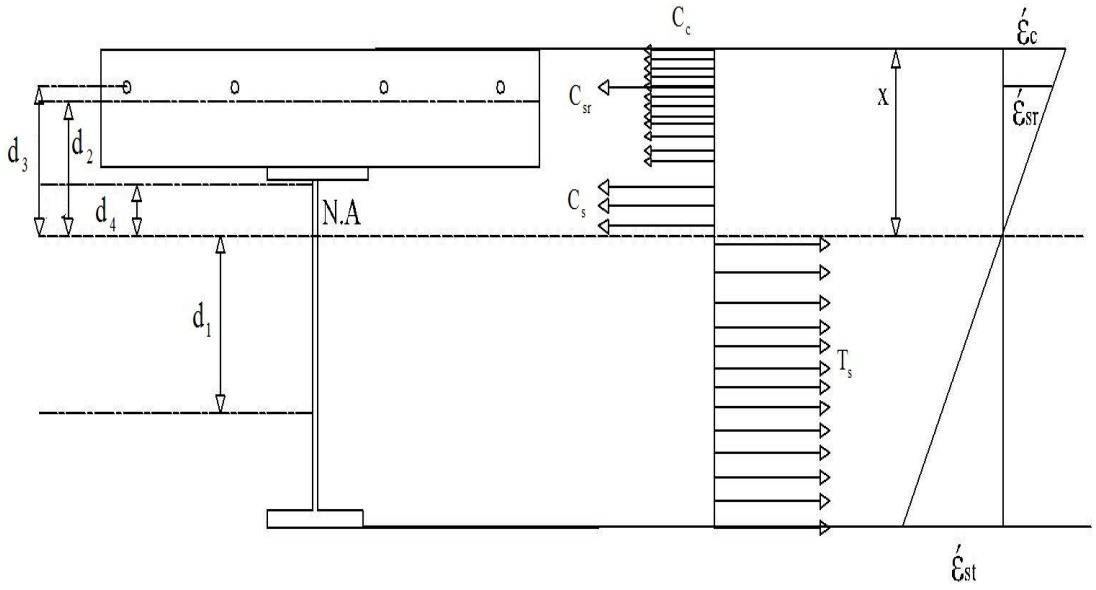

Fig. 7- 3 Distribution of stress and strain at positive moment region

The capacity at negative moment region could be calculated according to the mentioned design philosophy, and the stress distribution at ultimate load is presented in Fig. 7-4.

$$M^*_{-ve} = \frac{M_{+ve}}{\alpha} \qquad \text{Equ. (7-6)}$$

Where the ratio α is considered equal to 1.2 as discussed before.

Based on an assumed location of the N.A, the moment capacity at negative moment region is a given in Equ. (7-7). The tension in CFRP could be calculated using Equ. (7-8), and thickness of CFRP could calculated using Equ. (7-9). Finally, check the equilibrium equation (Equ. 7-10) and revise the location of N.A if needed accordingly.

$M^{*}_{-ve} = A''_{st}\, f_y\, (d_1) + T_{S.R}\, (d_4) + A'_{st}\, f_y\, (d_2) + T_{CFRP}\, (d_3)$ Equ. (7.7)

$$T_{CFRP} = \frac{M^{*}_{-ve} - A''_{st}\, f_y\, (d_1) - T_{S.R}\, (d_4) - A'_{st}\, f_y\, (d_2)}{d_3}$$ Equ. (7-8)

$$t_{CFRP} = \frac{T_{CFRP}}{0.3\, \sigma_{u\,CFRP}\, b_{CFRP}}$$ Equ. (7-9)

Where b_{CFRP} is the width of CFRP sheet

$T_{CFRP} + T_s + T_{S.R} = C_s$ Equ. (7-10)

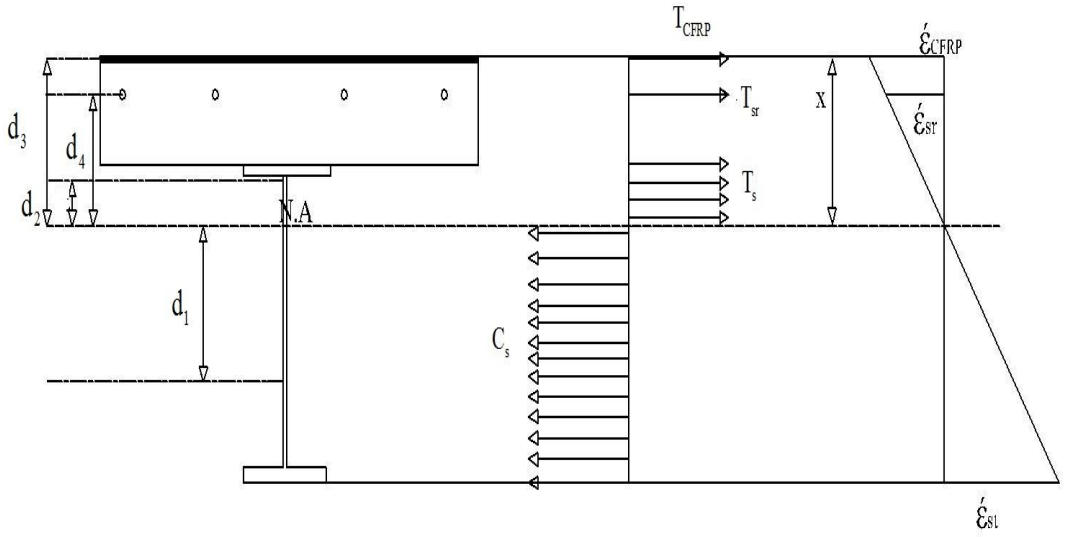

Fig. 7- 4 Strain and stress distribution over the interior support at ultimate load

The length of CFRP should cover the negative moment region in addition to at least 150 mm from each side as development length.

7.3.3 The Required Number of Shear Studs

The shear studs are needed to form the composite action between the steel section and concrete slab at mid-span. At negative moment region, the shear studs are needed to resist the tangential shear force due to steel reinforcement and CFRP sheets and form the composite action. Therefore, number of shear studs to resist the tangential force at each side is

$$N = \frac{T_{S.R} + T_{CFRP}}{Q} \qquad \text{Equ.(7-11)}$$

Where Q is the design shear strength of shear studs. The tension force in steel reinforcement $T_{S.R}$ is equal to $A_{S.R}\, f_y$, and T_{CFRP} is the design tensile force in CFRP. The design tensile force of CFRP could be calculated after determining thickness of CFRP as introduced in the last sections. So that, total number of shear studs at negative moment region is

$$N = \frac{(A_{S.R}\, f_y + n\ t_{CFRP} b_{CFRPf}\ 0.35\ \sigma_u) * 2}{Q} \qquad \text{Equ. (7-12)}$$

According to equation (7-12), shear studs of 19 mm diameter is needed at spacing of 120 mm to form the composite action between the steel section and 2 layers of CFRP sheets.

7.4 DESIGN STEPS FOR CONTINUOUS COMPOSITE GIRDER STRENGTHENED WITH CFRP AT NEGATIVE MOMENT REGION

For a continuous composite steel-concrete girder, the following design steps could be used to find the required CFRP thickness, and calculate the ultimate strength:

1) Calculate the capacity of steel-concrete section at mid-span. This could be calculated according to Equ's. (3-1) – (3-3).
2) Calculate the maximum allowed thickness to eliminate de-bonding of CFRP.
3) Calculate the maximum allowed thickness to allow full yielding of steel section at interior support prior to reach moment capacity at mid-span.
    3.1) Calculate the maximum allowed strength at negative moment region according to an assume value of positive/negative moment capacity (α).
    3.2) Assume the location of Neutral axis (N.A) for section at interior support.
    3.3) Find the forces in each component (compression steel, tension steel, steel reinforcement, and CFRP) and distance between the N.A and the centroid of each force.
    3.4) The force in CFRP should be calculated in term of thickness of CFRP (t_{CFRP}).
    3.5) Calculate the required thickness in CFRP and convert into number of layers depending in the available CFRP sheet.
    3.6) Check Equilibrium of forces.
    3.7) Find the new location of N.A and revise the calculated force accordingly.
4) Take the least value and convert it into number of CFRP layers according to the available type of CFRP.

7.5 ULTIMATE PLASTIC CAPACITY

The elastic capacity of continuous composite girder depends on the moment diagram. Usually, most of the girders under the distributed or point loads, the capacity of section over the interior support control. In this way, the use of CFRP increases the ultimate capacity of section over the interior support and therefor increases the capacity of composite girder. However, the full plastic capacity of girder could allow the girder to carry higher load. Formation of plastic hinge over the interior support, followed by rotation of the composite section over the interior support up to reach the full capacity at mid-span (failure load).

The design procedure in this chapter assumed certain value of capacity of section at positive moment to that at negative moment (α) to guarantee the ability of girder to develop the full plastic capacity. The full plastic capacity depends on loading condition and geometry of girder. For the design girder in this work, assume that the capacity of section over the interior support is M_p whereas at positive moment region is $\alpha\ M_p$ as shown in Fig. 7-5. The full plastic load is given in Equ's. (7-13) and (7-14).

$$P=\left(\frac{(8\alpha+4)Mp}{L}\right)$$ Equ. (7-13)

The value of α is 1.2, then the full plastic load is

$$P=\frac{13.6\,M_p}{L}$$ Equ. (7-14)

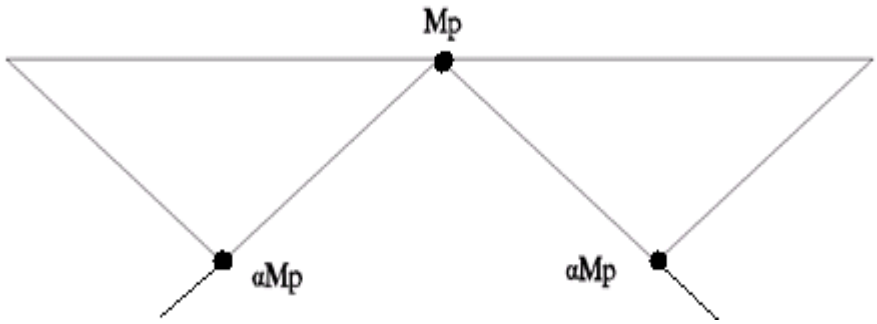

Fig. 7- 5 Failure mechanism of girder

7.6 ELASTIC DESIGN OF COMPOSITE GIRDER

The elastic capacity of composite girder is defined as the maximum load that could be applied to the composite girder before first yielding of steel section occurred. The first yielding point could be either one of two cases; yielding of bottom flange at mid-span or bottom flange at interior support. At the same time, this load could be taken as the load at which composite action is maintained at negative moment zone.

The maximum service load could be calculated as follows:

1) Calculate the location of N.A for mid-span section
2) The strain at bottom flange of steel section is yielding
3) Use the strain compatibility to find strain in top flange, steel reinforcement, and concrete
4) Find the corresponding forces based on the calculated strains
5) Calculate the elastic moment for mid-span section
6) Repeat all steps for section at interior support
7) Use the elastic moment diagram to find the force required to achieve yielding of steel for both section
8) The least of the two forces is the maximum applied force.

CHAPTER EIGHT

CONCLUSION AND FUTURE WORK

8.1 CONCLUSION

Experimental investigations of six continuous composite girders reinforced with CFRP were conducted in this research. The research included developing of FE model to simulate behavior of continuous composite girder. Finally, according to the experimental and numerical results, simplified design equations were developed to expect the ultimate capacity of girders. Based on the findings of the work, the following conclusions are drawn.

- The use of CFRP sheets at the top of concrete slab at negative moment region is capable of maintaining the composite action at higher load close to the service load.

- The capacity and stiffness of girders are increased by use of CFRP sheets bonded to the slab at negative moment region. The increase in ultimate capacity is directly proportional to the CFRP thickness up to certain thickness, when the negative moment capacity is close to the positive moment capacity.

- Tests have shown that the theoretical prediction of the failure load using plastic analysis yields value lower the actual failure load because of higher load carrying capacity of steel girders due to strain-hardening. Thus, plastic analysis can be used for a safer prediction of failure load.

- The proposed Finite Element model of the continuous composite girder bonded with CFRP at negative moment region has yielded satisfactory results comparable with the experimental data, lending confidence in the adoptability of the modeling.

- Selection of CFRP thickness should allow the composite girder to reach full yielding of steel section at interior support, followed by reaching the moment capacity at mid-span without de-bonding of CFRP sheets.

- The study agreed with the ACI specifications for the development length. It is required to cover to the negative moment region and to extend the CFRP sheets at least 150 mm from each side.

- Shear studs spacing had minimal effect on the ultimate capacity as long as it achieves the full composite action. The increase of spacing such that girder is partially composite, decreased the CFRP stress which resulted in slight reduction on the ultimate capacity.

- The stress in CFRP is function of; geometry of steel section, yielding of steel section at interior support, shear studs spacing, and thickness of concrete slab. The study suggested a designed stress of $0.35\sigma_u$.

- Simplified design equations were presented in the study. Equations were derived based on several assumptions. Those equations are able to predict the ultimate capacity of girder and guarantee that composite girder could develop this capacity.

- The study suggested specific ratio of positive to negative moment capacity. The suggested value (α=1.2) allows yielding of steel section at interior support followed by reaching the moment capacity at mid-span.

8.2 FUTURE WORK

Suggestions for the future research are:

1) Use of CFRP to maintain the composite action of continuous steel-concrete girder under cyclic and fatigue loading.

2) Experimental investigation of use of ultra-high performance concrete at negative moment zone.

3) Development of FE model to analyze continuous composite girder reinforced with CFRP with different construction method.

4) Testing continuous composite girder with different steel section shape.

REFERENCES

[1] B. Jurkiewiez, C. Meaud, and L. Michel, "Non linear behaviour of steel-concrete epoxy bonded composite beams," Journal of Constructional Steel Research, vol. 67, pp. 389–397, 2011.

[2] Aravind, N., Samanta, A. K., Roy, D. S., & Thanikal, J. V. (2013). Retrofitting Of Reinforced Concrete Beams Using Fibre Reinforced Polymer (Frp) Composites–A Review. Journal of Urban and Environmental Engineering (JUEE), 7(1).

[3] A. M. Ibrahim and M. S. Mahmood, "Finite Element Modeling of Reinforced Concrete Beams Strengthened With FRP Laminates," European Journal of Scientific Research, vol. 30, pp. 526-541, 2009.

[4] T. C. Miller, M. J. Chajes, D. R. Mertz, and J. N. Hastings, "Strengthening of a steel bridge girder using CFRP plates," Journal of bridge engineering, vol. 6, p. 514, 2001.

[5] Quantrill, R. J., & Hollaway, L. C. (1998). The flexural rehabilitation of reinforced concrete beams by the use of prestressed advanced composite plates. Composites Science and Technology, 58(8), 1259-1275.

[6] K. Lau, P. Dutta, L. Zhou, and D. Hui, "Mechanics of bonds in an FRP bonded concrete beam," Composites Part B: Engineering, vol. 32, pp. 491-502, 2001.

[7] Akbarzadeh, H., & Maghsoudi, A. A. (2011). Flexural Strengthening of RC Continuous Beams Using Hybrid FRP Sheets. In Advances in FRP Composites in Civil Engineering (pp. 739-743). Springer Berlin Heidelberg.

[8] Kasimzade, A., & Tuhta, S. (2012). Analytical, Numerical and Experimental Examination of Reinforced Composites Beams Covered with Carbon Fiber Reinforced Plastic. Journal of Theoretical and Applied Mechanics, 42(1), 55-70.

[9] Sobuz, H. R., Ahmed, E., Hasan, N. M. S., & Uddin, M. A. (2011). Use of carbon fiber laminates for strengthening reinforced concrete beams in bending. Int J Civil Struct Eng, 2(1), 67-84.

[10] Balamuralikrishnan, R., & Antony, J. C. (2009). Flexural Behavior of RC Beams Strengthened with Carbon Fiber Reinforced Polymer (CFRP) Fabrics.

[11] Siddiqui, N. A. (2010). Experimental investigation of RC beams strengthened with externally bonded FRP composites. Latin American Journal of Solids and Structures, an ABCM Journal, 6(4), 343-362.

[12] Kadhim, M. M. A. (2012). Effect of CFRP plate length strengthening continuous steel beam. Construction and Building Materials, 28(1), 648-652.

[13] Galal, K., Seif ElDin, H. M., & Tirca, L. (2011). Flexural performance of steel girders retrofitted using CFRP materials. Journal of Composites for Construction, 16(3), 265-276.

[14] Narmashiri, K., Ramli Sulong, N. H., & Jumaat, M. Z. (2011). Flexural strengthening of steel I-beams by using CFRP strips. International Journal of Physical Sciences, 6(7), 1620-1627.

[15] Liu, X., Nanni, A., Silva, P. F., & Laboube, R. A. (2001). Rehabilitation of steel bridge columns with FRP composite materials. Proc., CCC 2001, Composites in construction, 10-12.

[16] Sallam, H. E. M., Badawy, A. A. M., Saba, A. M., & Mikhail, F. A. (2010). Flexural behavior of strengthened steel–concrete composite beams by various plating methods. Journal of Constructional Steel Research, 66(8), 1081-1087.

[17] Tavakkolizadeh, M., & Saadatmanesh, H. (2003). Strengthening of steel-concrete composite girders using carbon fiber reinforced polymers sheets. Journal of Structural Engineering, 129(1), 30-40.

[18] Schnerch, D., Dawood, M., Sumner, E. A., & Rizkalla, S. (2005, May). Behavior of steel-concrete composite beams strengthened with unstressed and prestressed high-modulus CFRP strips. In Proceedings of the 4th Middle East Symposium on Structural Composites for Infrastructure Applications (MESC4)(Alexandria, Egypt, 2005),(CD-ROM, 13 pp).

[19] P. K. Basu, A. M. Sharif, and N. U. Ahmed, "Partially Prestressed Continuous Composite Beams. I," Journal of Structural Engineering, vol. 113, pp. 1909-1925, 1987.

[20] P. K. Basu, A. M. Sharif, and N. U. Ahmed, "Partially prestressed composite beams. II," Journal of Structural Engineering, vol. 113, pp. 1926-1938, 1987.

[21] A. Elremaily and S. Yehia, "Use of External Prestressing to Improve Load Capacity of Continuous Composite Steel Girders," 2006.

[22] S. Chen, X. Wang, and Y. Jia, "A comparative study of continuous steel-concrete composite beams prestressed with external tendons: Experimental investigation," Journal of Constructional Steel Research, vol. 65, pp. 1480-1489, 2009.

[23] J. Nie, M. Tao, and S. Li, "Analytical and Numerical Modeling of Prestressed Continuous Steel-Concrete Composite Beams," Journal of Structural Engineering, vol. 1, p. 305, 2011.

[24] D. H. Choi, Y. S. Kim, and H. Yoo, "External Post-tensioning of Composite Bridges by a Rating Equation Considering the Increment of a Tendon Force Due to Live Loads," International Journal of Steel Structures, vol. 8, pp. 109-118, 2008.

[25] Manual, S. C. (2005). American Institute of Steel Construction. Inc., Thirteenth Edition, First Print.

[26] American Society for Testing Materials. ASTM standards. American Society for Testing Materials

[27] Ziraba, Y. N., Baluch, M. H., Basunbul, I. A., Sharif, A. M., Azad, A. K., & Al-Sulaimani, G. J. (1994). Guidelines toward the design of reinforced concrete (RC) beams with external plates. ACI Structural Journal, 91(6).

[28] Ziraba, Y. N., Baluch, M. H., Basunbul, I. A., Azad, A. K., Al-Sulaimani, G. J., & Sharif, A. M. (1995). Combined experimental-numerical approach to characterization of steel-glue-concrete interface. Materials and Structures, 28(9), 518-525.

[29] ACI Committee, American Concrete Institute, and International Organization for Standardization. "Building code requirements for structural concrete (ACI 318-08) and commentary." American Concrete Institute, 2008.

[31] Lubliner, J., Oliver, J., Oller, S., & Onate, E. (1989). A plastic-damage model for concrete. International Journal of solids and structures, 25(3), 299-326.

[32] Lee, J., & Fenves, G. L. (1998). Plastic-damage model for cyclic loading of concrete structures. Journal of engineering mechanics, 124(8), 892-900.

[33] Prakash, A., Anandavalli, N., Madheswaran, C. K., Rajasankar, J., & Lakshmanan, N. (2011). Three dimensional FE model of stud connected steel-concrete composite girders subjected to monotonic loading. International Journal of Mechanics and Applications, 1(1), 1-11.

[34] Rosenboom, O., & Rizkalla, S. (2008). Modeling of IC debonding of FRP-strengthened concrete flexural members. Journal of Composites for Construction, 12(2), 168-179.

VITAE

NAME	MOHAMMAD A. SAMAANEH
PLACE OF BIRTH	NABLUS, PALESTINE
PERMANENT ADRESS	Beit Iba- Nablus - Palestine
E-mail	mohammad_samaaneh@yahoo.com
	samaaneh@kfupm.edu.sa
PHONE NUMBER	+970599355666

EDUCATIONAL QUALIFICATION

Ph.D (Civil Engineering - Structures)

King Fahd University of Petroleum and Minerals, Dhahran, Saudi Arabia

M.S (Civil Engineering - Structures)

King Fahd University of Petroleum and Minerals, Dhahran, Saudi Arabia

B.S (Civil Engineering)

An-Najah National University, Nablus, Palestine